Novel Synthesis Methods for High Purity Amorphous Boron

by

Selçuk Acar

A Thesis Submitted to the
Graduate School of Engineering
in Partial Fulfillment of the Requirements for
the Degree of

Doctor of Philosophy
in
Materials Science and Engineering

Koç University
September 2012

Koc University

Graduate School of Sciences and Engineering

This is to certify that I have examined this copy of a Ph.D. thesis by

Selçuk Acar

and have found that it is complete and satisfactory in all respects,
and that any and all revisions required by the final
examining committee have been made.

Committee Members:

Mehmet Suat Somer, Ph. D. (Advisor) _____

Mehmet Sabri Çelik, Ph. D. _____

Özgür Birer, Ph. D _____

Uğur Ünal, Ph. D. _____

Melis Şerefoğlu, Ph. D. _____

Date: _____

ABSTRACT

The present PhD thesis entitled as “Novel synthesis methods for high purity amorphous boron” is focusing on the synthesis and purification of high purity (>99% B) elemental boron both in amorphous and crystalline forms. The production route for the commercially available elemental boron in the first step is based on the reduction of B_2O_3 with magnesium, which is also known as metallothermal or Moissan method. The further purification of the products occurs via acid leaching. However, recent studies showed that during the reaction of B_2O_3 and Mg, poorly crystallized Mg_2B_{25} is formed as the major byproduct - besides some B_6O and B_7O - which cannot be removed by conventional acid treatment [1, 2]. According to the literature, the most suitable production methods for high purity elemental boron are the reduction of BCl_3 with hydrogen gas at elevated temperatures - yielding diborane gas (B_2H_6) as the intermediate - or pyrolysis of pure diborane gas [3-5]. As diborane consists of only boron and hydrogen, its thermal decomposition yields only boron in solid form and hydrogen gas. The problems with diborane gas are the availability, price and toxicity. High purity (>99.99%) diborane is commercially available for 1500 €/tank (28 g gas per tank) and requires 6 months for shipping. In addition, diborane is extremely toxic and explosive when exposed to atmospheric air. It burns rapidly when combined with oxygen and water forming boric acid [6, 7].

The novelty in our approach in obtaining high purity amorphous boron is the development of a synthesis technique for “*on-demand-diborane*“ which can be *in-situ* pyrolyzed to the elements at T>573 K. Beside the above mentioned reaction of BCl_3/H_2 gas, there are several methods for the preparation of B_2H_6 reported in the literature [3, 4, 8, 9]. A great majority of them are solvent based reactions requiring further purifications and removal of solvents. Solid state reactions are easier to handle and do mostly not need

additional refining. In the last ten years new B_2H_6 production methods were introduced one of which is the metathesis reaction of metal chlorides with alkaline metal boron hydrides via ball-milling [9-12]. In the present study, the time consuming ball milling process was replaced by “gentle heating” of the mixture of the solid reactants which were pressed to pellets beforehand. In our studies, the gas phase pyrolysis of B_2H_6 yielded 98.5% pure amorphous boron. The rest is oxygen impurity resulting from the surface oxidation of the very reactive sub-micron (<300 nm) boron particles, nitrogen as in the form of surface nitride and carbon in the form of thin boron carbide layer. The further purification from oxygen is done by employing Microwave Induced Plasma Furnace (MWIP) in which highly reactive hydrogen radicals and hydrogen ions are generated at relatively low temperatures.

ÖZET

"Yüksek saflıkta amorf bor üretimi için yeni yöntemler" isimli bu doktora tezi, %99 üzeri saflıkta elementel bor üretimi ve saflaştırılması üzerine odaklanmıştır. Ticari olarak satılan elementel bor üretimi B_2O_3'ün magnezyum ile indirgenmesi ile yapılır ve metalotermal veya Moissan metodu olarak isimlendirilir. Sentez sonrası saflaştırma işlemi asit yıkaması ile yapılır. Ancak, son dönemdeki araştırmalar ile yukarıda bahsedilen yöntem sonucunda çok az kristallenmiş Mg_2B_{25} fazının ve B_6O/B_7O gibi suboskitlerin malzeme içinde kaldığını ve kimyasal yöntemler ile uzaklaştırılamadığı bulunmuştur. Literature gore, yüksek saflıkta elementel bor üretimi için en uygun yöntem BCl_3'ün yüksek sıcaklıklarda hidrojen ile indirgenmesi ve bu esnada ara ürün olarak oluşan B_2H_6'nın piroliz edilmesidir. Diboran gazı bor ve hidrojenden oluştuğu için, termal bozunması sonucunda sadece katı ürün olarak bor ve hidrojen gazı oluşmaktadır. Diboran gazının dezavantajları tedarik, fiyat ve toksisitesidir. Yüksek saflıkta (>%99.99) diboran gazı ticari olarak satılmasına rağmen tedarik süresi oldukça uzun ve pahalıdır. Bunun yanısıra, diboran gazı oldukça toksiktir ve havayla temasında patlayıcıdır. Oksijen ile birleştiğinde su ve borik asit oluşturarak yanar.

Bu çalışmada getirilen yenilik, yüksek saflıkta bor üretimi için gerekli diboran gazının "ihtiyaç anında üretim" metoduyla elde edilmesi ve 573 K üzerinde piroliz edilmesidir. Yukarıda bahsedilen BCl_3/H_2 reaksiyonun yanında, literatürde B_2H_6 üretimi ile ilgili pek çok yöntem bulunmaktadır. Bunların büyük kısmı solvent tabanlı olup ilave saflaştırma işlemleri gerektiren zahmetli işlemlerdir. Katı hal reaksiyonları ise kontrol edilmesi görece daha kolay ve ilave saflaştırma gerektirmez. Son 10 yılda, B_2H_6 üretimi için metal klorürlerin ve alkali metal bor hidrürlerin bilyalı değirmen ile metatezine dayanan yöntemler keşfedilmiştir. Bu çalışmada, zaman alıcı bilyalı değirmen işlemi reaktanların

“hafif ısıtılması” ile değiştirilmiştir. Çalışmalarımızda, B_2H_6’nın gaz fazı pirolizi ile %98,5 üzeri saflıkta amorf bor sentezlenmiştir. Geri kalan kısmın ise oldukça reaktif ve mikron altı parçacıklardan oluşan küresel bor parçacıkları üzerinde oluşan oksit, nitrit ve karbürden ibaret olduğu bulunmuştur. Malzemelerin saflaştırılma işlemi “Mikrodalga İnüdklemeli Plazma Fırını” denilen ve yüksek reaktiviteye sahip hidrojen türlerinin kullanımı ile yapılmıştır.

ACKNOWLEDGEMENTS

I would like to thank my advisor Prof. Dr. Mehmet Somer for his support and guidance during my Ph.D. thesis studies and accepting me to be a member of his research group. Also, I would like thank to my committee members for their time and giving me valuable ideas during our technical discussions.

I also have to thank Dr. Peter Höhn, Dr. Gudrun Auffermann, Dr. Umut Aydemir and Yiğit Öztan at MPI – Dresden for their help in the measurements and interpretation of the results of my samples.

I want to thank to all of my professors and instructors at Koç University.

Thanks to all of my colleagues in the MASE program for their friendship, and also thanks to my friends in the laboratory; Burcu Uslu, Ahmet Topçu and Araz Bateni. This thesis would not even be possible without Muharrem Abi (The Glass Blower). Thanks to Raquel Lage, Müjde Yahyaoğlu, İrem Korucu and Monika Kazancıoğlu for their help in the experimental work. Thanks to Dr. Melis Şeerefoğlu, Dr. Barış Yağcı, İlkin Kokal, Hüseyin Enis Karahan and Deniz Şanlı for their help in the characterizations and interpretations.

Finally, I would like to thank my parents for their endless support and encouragement. I also want to thank all the people whom I could not mention one by one.

TABLE OF CONTENTS

LIST OF TABLES

LIST OF FIGURES

NOMENCLATURE

HSAB : Hard Soft Acid Base Principle

DTA : Differential Thermal Analysis

DSC : Differential Scanning Calorimetry

TGA : Thermogravimetric Analysis

MS : Mass Spectrometry

XRD : X-Ray Diffraction

EDX : Energy dispersive X-ray spectroscopy

TEM : Tranmission electron microscope

SEM : Scanning electon microscope

ICP – OES : Inductively Coupled Plasma – Optical Emission Spectrometer

MWIPF : Microwave Induced Plasma Furnace

DLS : Dynamic Light Scattering

BET : Brunaur – Emmet - Teller

λ : Wavelength of the incident beam

Chapter 1

INTRODUCTION AND LITERATURE REVIEW

1.1 Literature Review and Theoretical Concepts

Boron is a semiconducting 3A (E13) group element having 10.81 g/mol molar mass and atomic number 5 [5, 7, 13, 14]. It is the 51st most common element in the crust of earth at a concentration of 3 grams/ton. Its abundance is 10^{-9} times that of hydrogen and about 10^{-6} that of carbon, nitrogen, or oxygen. There are two stable isotopes of boron, ^{10}B and ^{11}B which have natural occurrence of 20 % and 80 %, respectively. Other boron isotopes (^{8}B, ^{12}B and ^{13}B) have half lives of less than 1 second. ^{10}B isotope is used for neutron absorption [5, 13, 15-17].

Boron cannot be found in the elemental form in nature, due to its high affinity to oxygen, boron ores always contain boron – oxygen compounds [18]. Highly concentrated, economically feasible deposits of boron minerals, always containing compounds of boron and oxygen, are found in regions with a history of volcanism or hydrothermal activity (Mojave desert in the southwest of USA, And Mountains Zone in South America and South-Center Asia-Alpine zone) [19]**.** According to 2010 data 71.3 % of the proven boron mineral deposits are placed in Turkey [20]. Table 1.1 shows the boron deposits distribution all over the world.

Table 1.1 Boron deposits in the world [20]

Country	**Total Reserve (1000 tonnes)**	**Total Reserve (% B_2O_3)**
Turkey	885.000	71.3
U.S.A	80.000	6.5
Russia	35.000	2.8
China	47.000	3.8
Argentina	9.000	0.7
Bolivia	19.000	1.5
Chili	41.000	3.3
Peru	22.000	1.8
Kazakhstan	102.000	8.2
Iran	1.000	0.1
Total	**1.241.000**	**100**

90 % of the boron mining activities in the world are performed by Turkey and USA [21]**.** List of commercially produced boron minerals are given in Table 1.2.

Table 1.2 Commercially Important Boron Minerals [16, 18, 21-26]

Mineral Name	**Formula**	**% B_2O_3**	**Location**
Sodium Borates			
Kernite	$Na_2B_4O_7{\cdot}4H_2O$	51.0	USA
Borax	$Na_2B_4O_7{\cdot}10H_2O$	36.5	Turkey, USA, Argentina, China
Tincal	$Na_2B_4O_7{\cdot}5H_2O$	47.8	Turkey, USA, Argentina, China
Calcium Borates			
Colemanite	$Ca_2B_6O_{11}{\cdot}5H_2O$	50.8	Turkey, USA, Argentina
Datolite	$CaBSiO_4(OH)$	21.8	Russia
Inyoite	$Ca_2B_6O_{11}{\cdot}13H_2O$	37.6	Argentina
Pandermite	$Ca_4B_{10}O_{19}{\cdot}7H_2O$	49.8	Turkey
Calcium-Sodium Borates			
Propertite	$NaCaB_5O_9{\cdot}5H_2O$	49.6	Turkey, USA
Ulexite	$NaCaB_5O_9{\cdot}8H_2O$	43.0	Turkey, USA, China, Peru, Chili, Bolivia, Argentina
Calcium – Magnesium Borates			
Hydroborasite	$CaMgB_6O_6(OH)_6{\cdot}3H_2O$	50.5	Argentina, China
Magnesium Borates			
Borasite	$Mg_6B_{14}O_{26}C_{12}$	62.2	Russia
Szaybelite	$MgBO_3(OH)$	41.4	China

Boron minerals are processed to obtain commercial boron products which find more than 250 application areas [26]. Boron products can be divided into two main groups: refined and special boron products. Table 1.3 and Table 1.4 contain the names and application areas of refined and respectively special boron products.

Table 1.3 Refined boron products and application areas [5, 13, 16, 18, 21-26]

Name	**Application Areas**
Boric Acid	Antiseptics, boron compounds, fire retarders, photography, textile, fertilizer, catalysts, glass, glass-fiber, glazing
Boron Oxide	Glass Industry (Pyrex), optic-fiber
Colemanite	Glass, metallurgy, nuclear technology, textile, glass-fiber
Ulexite	Paper, heat insulation, glass-fiber, nuclear technology, metallurgy
Anhydrous Borax	Fertilizer, glass, glass-fiber, metallurgy, glazing, fire retardant
Sodium Perborate	Detergents, textile
Sodium Metaborate	Adhesives, detergents, agricultural chemicals, photography, textile
Sodium Pentaborate	Fire retardant, fertilizer

Table 1.4 Special boron products (chemicals) and application areas [5, 13, 15, 18, 21-24, 27]

Name	Application Areas
Elemental Boron (amorphous and crystalline)	Military pyrotechnics, neutron absorbers, igniters in airbags, semiconductors, superhard materials (ReB_2, HfB_2), superconductors (MgB_2)
Boron Filaments	Aeorospace composites and engineering composites
Boron Halides	Medicine, catalysts, electronics, optics
Special Sodium Borates	Photography chemicals, adhesives, textile, detergents, fire retarders, fertilizers
Fluoroboric Acid	Coating solutions, fluoroborate salts, $NaBH_4$
Trimethyl Borate	Coating solutions, fluoroborate salts, $NaBH_4$
Sodium borohydride	Chemical purification, paper whitening, metal surface cleaning
Boron Esters	Catalyst in polymerization reactions, polymer stabilizers, fire retarders
Boron carbide	Surface treatment of machining tools, engineering ceramics, ultrasound devices, metallurgy, rocket nozzles
Boron nitride	Surface coating in high temperature machining, high temperature lubrication, engineering ceramics and composites, industrial abrasives, cutting tools (cubic BN)
Boron hydrides	p-type dopant in semiconductors, reducing agent in organic synthesis, high purity elemental boron synthesis

Elemental boron in amorphous form finds an important application area as being an additive in solid rocket propellants to achieve higher thrust force due to its very high heat of combustion. Boron and boron-rich compounds have gravimetric energy density of 58.5 MJ/kg, which is quite above than hydrocarbon fuels (Gasoline 47.3 MJ/kg, Kerosene 46.2 MJ/kg, and Methane 55.5 MJ/kg) and third one after hydrogen (141.8 MJ/kg) and beryllium (68 MJ/kg) [13, 28, 29]. However, boron's potential of being a rocket fuel is limited due to the formation of native oxide layer (0.5 - 2 nm thick B_2O_3) upon heating in oxygen atmosphere. Detailed procedures to overcome this oxide layer formation are described in the literature [28, 29]. And, it is well-known that having high surface area, small particle size (sub-micron) and spherical particle shape are directly related and have positive effects on combustion values [28, 29].

Elemental form of boron was discovered in 1808 simultaneously and independently by Joseph Gay Lussac and Louis Thenard through reduction of B_2O_3 with potassium and by Sir Humpry Davy through electrolysis of boric acid [5, 27]. However, purity of these elemental forms was well below 50 wt% boron [27]. In 1892, Henri Moissan obtained amorphous boron by reducing B_2O_3 with magnesium which was the most efficient reducing agent among other alkaline and earth alkaline metals [13, 30]. Purity of amorphous boron obtained with this method can be increased up to 95-97% by several chemical procedures which are mainly acid treatment of the reaction products [3-5, 8, 9]. Reduction of B_2O_3 with magnesium metal is named as metallothermal – or magnesiothermal – reaction and is so called "*Moissan Method*" on behalf of its inventor. Moissan method is still the widely used process for the commercial production of amorphous boron [3-5, 8, 9]. Figure 1.1 shows the timeline of elemental boron starting from its discovery in 1808 to 2000's by stating the change in its purity, and commercial production as well.

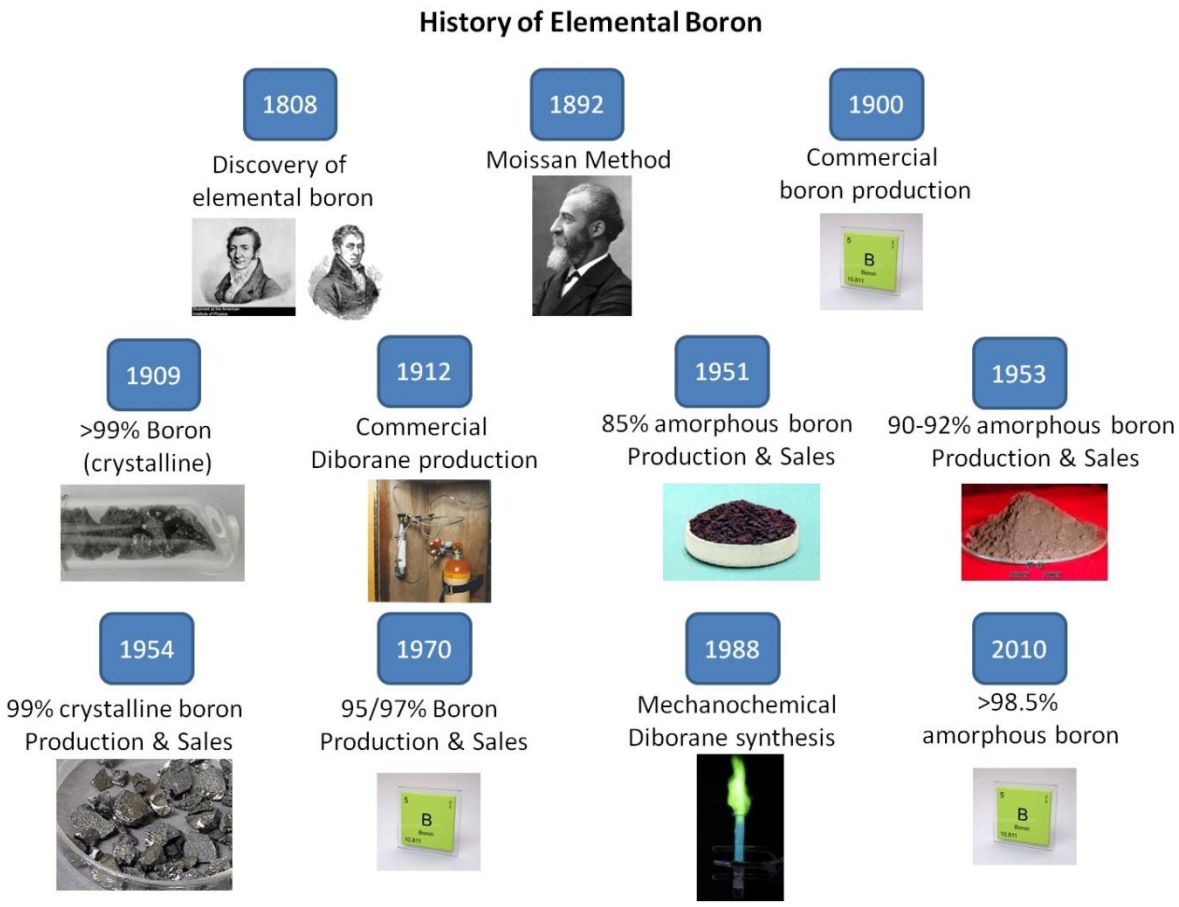

Figure 1.1 Timeline of elemental boron [5, 13, 27, 30]

Elemental boron exists in amorphous and crystalline forms, and so far 16 crystalline boron modifications were published [13, 14, 17, 31]. Among 16 crystalline polymorphs most of them were reported to be boron-rich compounds like YB_{66}, NaB_{15}, $B_{50}N_2$ etc. [13]. The preparation and conversion of pure boron are performed at elevated temperatures and it is well-known that contamination of the base element even in ppm level can have an influence on the electronic structure of inorganic solids and result dramatic changes in material properties. Two crystalline boron phases exist at ambient conditions: α – rhombohedral, β – rhombohedral, in which the latter one is thermodynamically stable at

high temperatures and α – rhombohedral boron is so called the low temperature phase [13, 17, 31, 32]. There are two more crystalline elemental modifications named α and β tetragonal boron which are both high temperature and metastable phases. However, these two modifications were reported to be stabilized by foreign atoms (N and C), therefore it is a subject of discussion whether they are real allotropes of boron or not [13]. γ – B_{28} form is recently published [17, 33]and is a high pressure modification of β-rhombohedral boron, which consists of partially positively and partially negatively charged structural units. Lastly, α- Ga modifications is reported to be the high temperature – high pressure phase showing metallic properties [13]. Figure 1.2 shows the phase diagram and crystalline modifications of elemental boron.

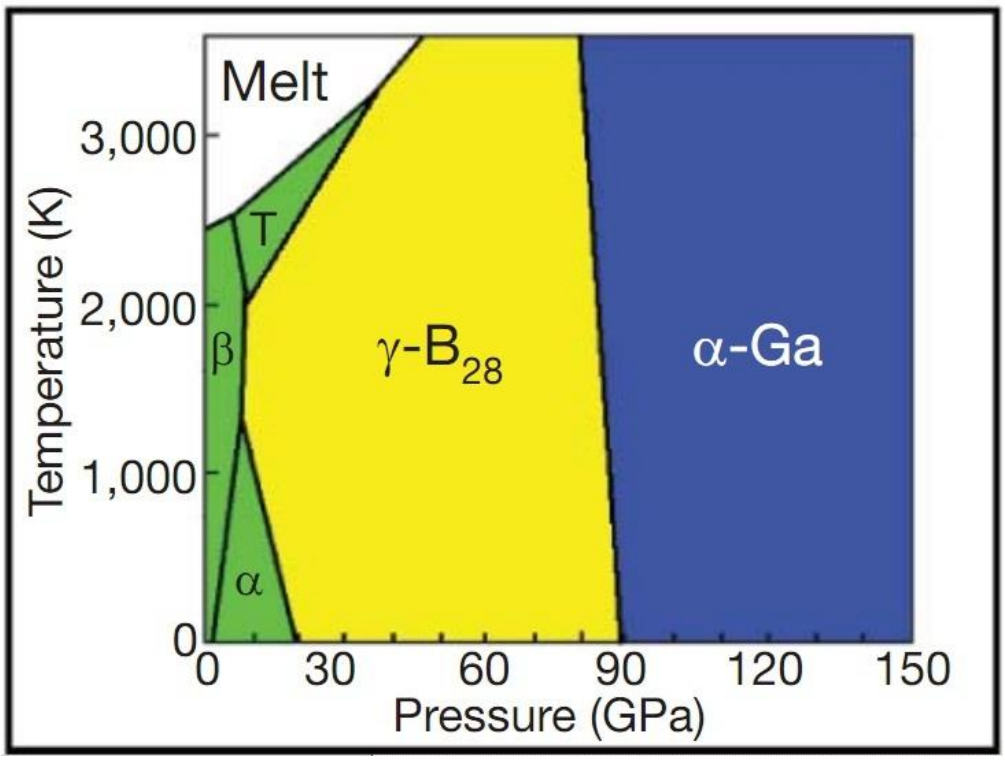

Figure 1.2 Phase diagram of crystalline boron [33]

Elemental boron has interesting bonding behavior mainly due to its electron deficiency with respect to carbon. Boron – nitrogen compounds are isoelectronic to carbon allotropes. When carbon atoms are substituted with boron in crystal lattice of diamond electron holes are formed. Boron's electron deficiency avoids formation of two center bonds and boron can form three-center bonds as observed in boron hydrides [5]. Three-center two-electron (3c-2e) bonds are electron deficient in which three atoms are held together by two electrons [34]. All known boron structures are dominated by B_{12} icosahedra with three-center bonds within the icosahedra and covalent two and three-center bonds between the icosahedra [17, 33]. For better understanding the bonding in crystalline boron, α-B_{12} is a good example. This modification is characterized by two nonequivalent sites identified as polar (B_p) and equatorial (B_e) (Figure 1.3). B_p and B_e atoms are linked through covalent bonds and three-center bonds, respectively. Each B_p atom has six covalent bonds in which five bonds link to nearest neighbors inside the icosahedron (intra-icosahedra) while the other one links to a B_p atom of another icosahedron (inter-icosahedra). B_p atoms form relatively strong two-center two-electron (2c-2e) covalent bonds with other B_p atoms of neighboring icosahedra. On the other hand, B_e atoms has five covalent bonds that are linked to boron atoms in the icosahedra [35].

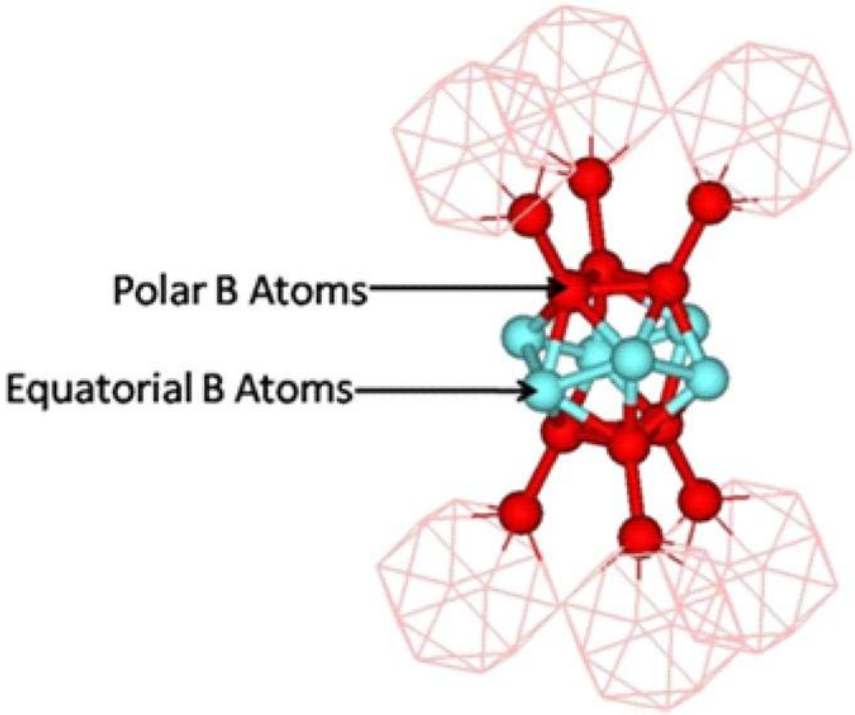

Figure 1.3 Bonding in crystalline boron [35]

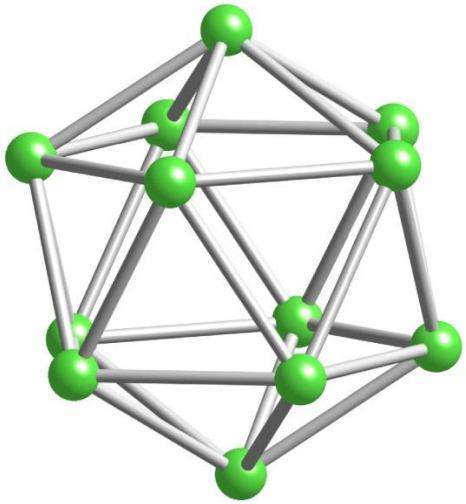

Figure 1.4 B_{12} icosahedra [35]

Rhombohedral modifications, α-B_{12} and β-B_{106} phases (12 and 106 atoms in the unit cell, respectively), correspond to the pure elemental form of boron. B_{106} phase is more stable at elevated temperatures and an irreversible phase transition was reported from B_{12} to B_{106} above 1400 K [13, 17, 36]. At high pressures (several gigapascals) and temperatures the very low packing efficiency (34% for α-B_{12}) of atoms in icosahedral structures lead to destruction of icosahedra and formation of denser metallic α-Ga phase for boron [13].

Amorphous form of elemental boron is comprising also B_{12} icosahedra. However, short range order of B_{12} icosahedra is dominant in this modification [37]. Short range order is well defined by observing the extremely broad reflections (halos) in X-ray or electron diffraction patterns [9, 38]. Amorphous boron is assumed to be an intermediate stage between the α and the β rhombohedral structures. According to literature, heating of amorphous boron above 1223 K, sharp reflections of β-rhombohedral boron emerges while broad reflections vanish. This indicates that amorphous boron is possibly a microcrystalline form of β-rhombohedral boron [9, 38, 39]. Table 1.5 summarizes the physical properties of amorphous and crystalline boron forms.

Table 1.5 Physical properties of elemental boron [3-5, 8, 9, 15]

	Amorphous	**α-rhombohedral**	**β-rhombohedral**	**γ-orthorhombic**
Melting Point(K)	2573	2453		-
Boiling Point – Sublimes (K)	2923	3923		-
Density (g/cm^3)	2.35	2.45	2.35	2.52
Appearance	Brown	Red-brown	Black	-
Z (atoms/unit cell)	-	12	106	28
		Irreversible phase transition above 1473 K		Theoretical High T and P phase

The aim of this study is to obtain elemental boron in amorphous form with a purity value that can only be achieved in crystalline modifications which require high temperature treatments [9]. As well-known from solid state reactions, amorphous materials are always more reactive than their crystalline forms. For boron case, amorphous boron is more preferred than the crystalline boron by chemists due to its higher reactivity which is closely related to its large surface area [28].

1.2 Synthesis Methods of Elemental Boron [3, 4, 8, 9]

Production of high purity elemental boron can be achieved by several methods. Boron production methods can be listed as:

- Chemical vapor deposition (CVD)

Massive amount of boron is deposited on the substrates and unreacted boron halide is recycled.

- Reduction of boron halides with hydrogen

$$BX_3 + 1.5H_2 \rightarrow B + 3HX,\ X = Cl, Br$$

$$BX_3 + 1.5H_2 + \text{Substrate} \rightarrow B(\text{on substrate}) + 3HX$$

Tungsten, tantalum, molybdenum wires and, graphite, BN, and also boron rods can be used as substrate materials. Substrate material should not react with boron at high reaction temperatures. Table 1.6 gives examples of deposition reactions.

Table 1.6 Boron production by reduction of boron halides [4, 9]

Boron Halide	**Substrate**	**Temperature**
$BCl_3 – H_2$	Graphite	1723 K
$BBr_3 – H_2$	Tungsten	1173 K
$BBr_3 – H_2$	Tantalum	1123 K
$BBr_3 – H_2$	Molybdenum	1223 K

Metal substrates can be used up to 1773 K where destruction of wires occurs.

- Reduction of boron halides with a metal

Elementary zinc is suitable for reduction of BCl_3 at temperatures 873 to 1123 K resulting 99.5% purity. The product contains amorphous and α-rhombohedral boron and a zinc-containing boron phase.

Sodium can be used in the gas phase reduction of boron halides around 753 K, resulting 98.8 % amorphous boron.

Tetragonal boron (98% B) is formed by the reduction of BCl_3 with tin at 1323 K which transforms to β-rhombohedral structure by annealing at 1273 K.

- Pyrolysis of boron halides

Gaseous boron halides decompose on hot substrate surface.

$$BX_3 + \text{substrate} \leftrightarrows B\ (\text{on substrate}) + 1.5\ X_2$$

273 to 1373 K region is used for the above reaction. Boron, tantalum, tungsten, molybdenum, vitreous BN and fused silica are suitable for substrate materials.

- Pyrolysis of boron hydrides

Amorphous boron in powder form is obtained by thermal decomposition of diborane, pentaborane or decaborane, usually diluted with hydrogen, by passing through a quartz tube which is heated at 573 to 1173 K, and by the pyrolysis of solid boron hydrides in a BN boat.

Massive amounts of high purity amorphous or crystalline boron is produced by the gas phase pyrolysis of diborane on wire form substrates according to the above reaction;

$$B_2H_6 + \text{substrate} \leftrightarrow 2B\ (\text{on substrate}) + 3H_2.$$

The substrate is a thin wire of tantalum or tungsten. Boron rods of 250 mm length and 10 mm diameter can be produced. Impurities, except carbon, can be easily removed by zone melting. Carbon free diborane is a key factor for avoiding the formation of stable, volatile carbonyl-borane according to:

$$B_2H_6 + CO \rightarrow 2BH_3CO$$

- Physical vapor deposition (PVD)

Boron films can be made by evaporation and condensation of elementary boron in vacuum on to a smooth substrate. Boron single crystals can be formed by the evaporation of elemental boron at 2373 K and 10^{-5} to 10^{-6} mbar.

- Chemical transport

This method simply consists of transportation of amorphous boron in a quartz ampoule via iodine or bromine at elevated temperatures (above 1073 K) and formation of crystalline boron.

- Reduction of boron – oxygen compounds with metals (Metalothermal method)

This technique is also known as Moissan method, which is the reduction of boron oxygen compounds with magnesium in the form of powder or turnings. Excess B_2O_3 is required in order to convert magnesium oxide into borates.

$$B_2O_3 + 3Mg \rightarrow 2B + 3MgO$$

$$2B_2O_3 + 3Mg \rightarrow 2B + Mg_3(BO_3)_2$$

$$4B_2O_3 + 3Mg \rightarrow 2B + 3Mg(BO_2)_2$$

After acid treatment of borates and oxides, MgB_2, MgB_4 and MgB_{12} are remaining in the product. The main impurity is reported as Mg_2B_{25} [2]. The final yield of the reactions is 86 to 88%.

The reduction of boron – oxygen compounds with aluminum yields aluminum borides such as AlB_{10} and AlB_{12}

- Electrolysis

Boron is deposited by the electrolysis of melts of metal borates and fluoroborates with metal or graphite electrodes as the cathode.

Among the methods described above, pyrolysis of boron hydrides and boron halides yield highest purity elemental boron in amorphous form. However, unlike boron halides, boron hydrides are composed of only boron and hydrogen, solid elemental boron and hydrogen gas are formed as thermal decomposition products. For example in BCl_3 case, HCl is formed as a reaction product which requires further purification procedures [9, 40].

Chemical analysis of elemental boron is performed by oxidizing to boric acid in hot concentrated nitric acid. Elemental boron is not soluble in HF or HCl. Boron is not reactive

to NaOH up to 773 K. At room temperature boron is reacting only with oxygen [5]. Analytical and instrumental methods that are commonly used for chemical analyses of boron are as follows:

- Acid – base titration (Boric acid with NaOH)
- ICP-OES (Inductively Coupled Plasma – Optical Emission Spectrometry)
- ICP-MS (ICP – Mass Spectrometry)
- AAS (Atomic Absorption Spectrometry)

Among the above methods, ICP – OES and ICP – MS are reported to give more accurate and reliable result in the chemical analyses of elemental boron [19, 25, 41].

1.3 Diborane (B_2H_6)

As mentioned in the previous section amorphous and crystalline boron of highest purity grade can be synthesized only by thermal decomposition of boron hydrides on suitable substrates. In our study we are proposing the *in-situ* thermal decomposition of diborane gas (B_2H_6) to produce > 99% pure elemental boron. To accomplish the thermal decomposition reactions, the precursor gas diborane has to be synthesized or purchased.

Diborane was first isolated and characterized by Stock in 1912 [42]. His process included the hydrolysis of metal borides to give a mixture of higher boron hydrides. However, the yield of the process was very low [43]. In 1931, Schlesinger et al, proposed a reaction mechanism that involves passing hydrogen and boron trichloride (BCl_3) through a silent electrical discharge which resulted B_2H_5Cl as the major product and by using fractional distillation B_2H_6 and BCl_3 were obtained [43-45]. In 1940's, $NaBH_4$ became commercial at a reasonable price and was used as the starting material for large scale production of diborane [43]. In 1950's Brown (former PhD student of Schlesinger) and

coworkers proposed the most convenient method to produce large scale diborane, the reaction of $NaBH_4$ with BF_3, which is still the major process used today [6].

Although diborane is commercially available in steel cylinders and can be handled safely by trained personnel, it is a very hazardous and toxic gas [46]. When large amount of diborane is required, on demand production is usually preferred.

Structure of diborane was the subject of prolonged discussions among structural chemists. The electron deficiency of boron itself does not permit a bonding behavior as observed in ethane (C_2H_6). Moreover, discussions on the bonding of diborane revealed a new concept called "three-center two-electron" bond, which is used to describe the structure of molecules that are consisted of electron deficient elements. According to recent views, the 1s orbital of hydrogen and four $2sp^3$ hybrid orbitals of boron are involved in a diborane molecule. Each boron atom forms two covalent B-H bonds, in which the two boron atoms and four hydrogen atoms being in the same plane. The remaining two hydrogen atoms are positioned at equal distances from this plane on a line perpendicular to it and bisecting the B-B line (Figure 1.6). These hydrogen atoms are called "bridge atoms" and join to boron atoms by three-center two-electron bonds [6, 34, 47-50]. Each B-H-B bridge is regarded as a filled three-center localized bonding orbital. Several theoretical studies have been completed for B_2H_6 [9, 51]. The results indicate that for each B-H-B bridge bond the boron atoms share less than 2 electrons and of these, 0.50 - 0.80 electrons are shared with one hydrogen atom, and 0.50 - 0.80 electrons with the other [9].

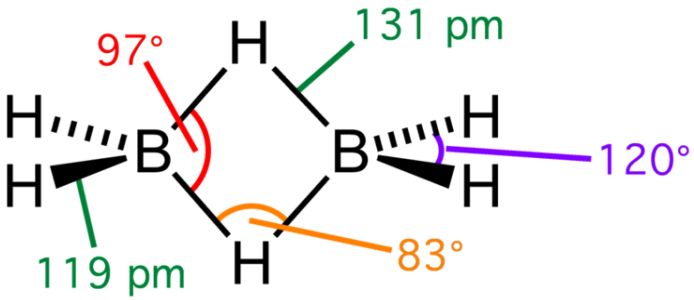

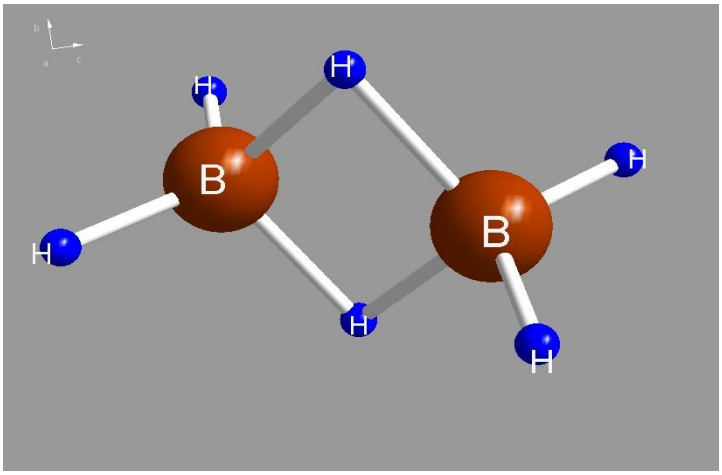

Figure 1.5 Structure of diborane [98, 99]

According to literature data, diborane gas can be synthesized by several methods [52-54]. These can be divided into two main categories: Solvent base and solid phase mechanochemical syntheses.

Solvent base preparation methods of B_2H_6 are:

- Reaction of $Li[BH_4]$ with organic acids. Reactions are conducted in dibutyl ether between 263 and 318 K.
- Dimethoxyborane ($HB(OCH_3)_2$), is considered to be rearranged to form B_2H_6 in the reaction:

$$6HB(OCH_3)_2 \rightarrow B_2H_6 + 4B(OCH_3)_3$$

- Hydride ion is abstracted from $[BH_4]^-$ to generate BH_3 units which combine to form the dimer, B_2H_6 according to

  $MBH_4 + BX_3 \rightarrow ½\ B_2H_6 + M[HBX_3]$; $M=[N(n\text{-}C_4H_9)_4]^+$,$[P(CH_3)(C_6H_5)_3]^+$; BX_3 = BBr_3, BCl_3. CH_2Cl_2 is used as solvent.

Solid phase reactions are as follows:

- $3Na[BH_4] + 4BF_3 \rightarrow 2B_2H_6 + 3Na[BF_4]$ at room temperature
- Mechanochemical activation of mixtures of alkali metal tetrahydridoborates and I_2, $SnCl_2$, $ZnCl_2$ or $CrCl_3$ at room temperature [10, 11]. Chlorides are better reagents than I_2 since the product does not require purification. B_2H_6 and H_2 are formed in these reactions, with the yield of B_2H_6 being 85 to 96% for I_2, $SnCl_2$ or $ZnCl_2$ and 60% for $CrCl_3$.

Solvent base methods include costly and time taking solvent preparation and purification, separation of the target substances from reaction media and by-products. Environmental problems due to waste products formed during the reactions are important issues.

Mechanochemical activation provides room temperature synthesis and avoids solvent problems. Besides, the reactants are cheaper and readily found in Turkey.

Reaction mechanism of diborane production by mechanochemical activation method is as follows:

$$MCl_2 + 2M_ABH_4 \rightarrow M(BH_4)_2 + 2NaCl \qquad (M : Sn, Zn, Cu\ ;\ M_A : Li, Na, K) \qquad (1)$$

$$M(BH_4)_2 \rightarrow M + B_2H_{6(g)} + H_{2(g)} \qquad (2)$$

The yield of B_2H_6 formation decreases in the series $LiBH_4 > NaBH_4 > KBH_4$. Because $LiBH_4$ is much more expensive than the latter two, it is reasonable to use $NaBH_4$ in the reactions.

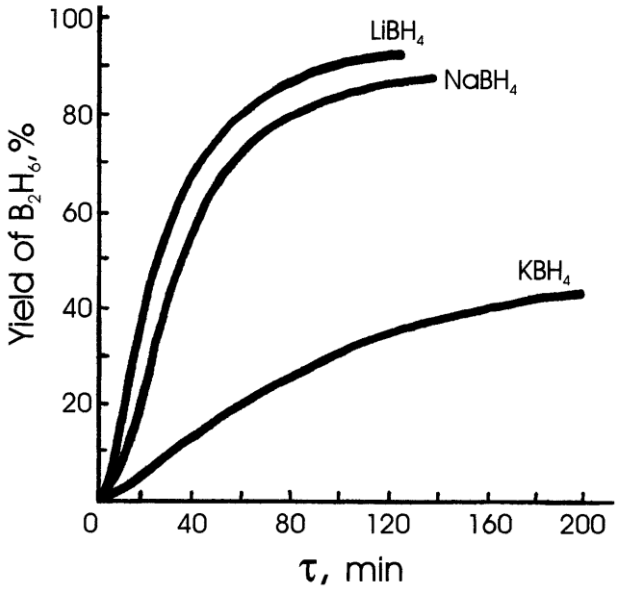

Figure 1.6 Dependencies of B_2H_6 yields in reaction 1 ($SnCl_2 + 2M_ABH_4$) on time and on the nature of M_ABH_4 [55].

When choosing the suitable metal chloride, one should take into account of the hygroscopic property, toxicity and possibility to recover metal from reaction products in the anhydrous form for repeated use. $SnCl_2$ is non-hygroscopic, tin is not toxic, readily available and easily transformed into $SnCl_2$ by reacting with HCl.

In $Zn(BH_4)_2$ case, $ZnCl_2$ is highly hygroscopic, even shows deliquescence behavior, and needs to vacuum dried at 473 K before reaction. Zinc is also cheap and easily transformed into $ZnCl_2$ by reacting with HCl.

$Sn(BH_4)_2$ and $Zn(BH_4)_2$ are the examples of complex metal hydrides that desorb hydrogen and diborane to elemental Sn and Zn due to instabilities of metal hydride and boride. According to Nakamori et al. [56], heat of formation of $Sn(BH_4)_2$ and $Zn(BH_4)_2$ are positive, and as Sn and Zn are highly electronegative metals (1.96 for Sn, 1.65 for Zn),

destabilizing $[BH_4]^-$ anion and leading to formation of BH_3 units at relatively low temperatures. In this trend $Sn(BH_4)_2$ decomposes at lower temperatures than $Zn(BH_4)_2$.

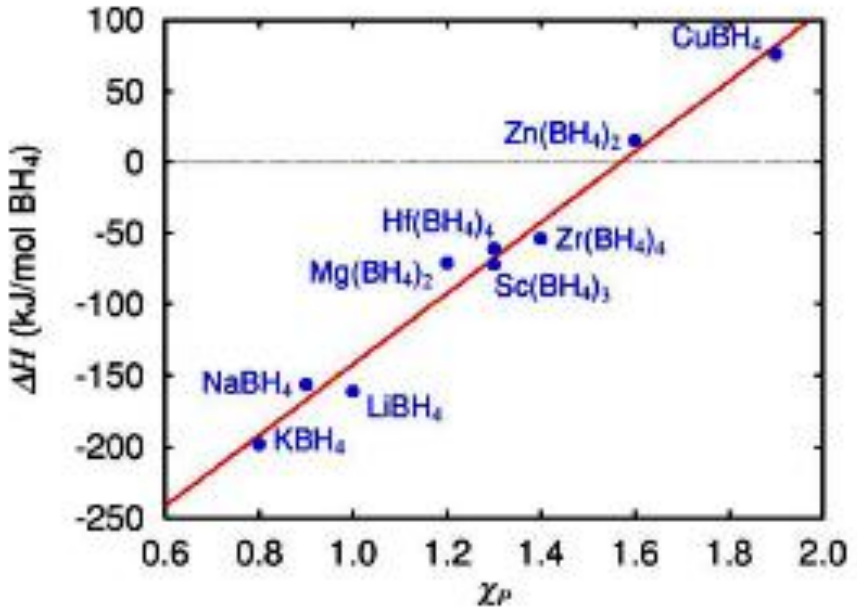

Figure 1.7 Relation between the heats of formation and the Pauling electronegativities of cations [56].

According to Figure 1.7, complex metal hydrides having heat of formations below zero line, are very stable up to 773 K (for KBH_4) and decomposes to metal hydride and hydrogen gas instead of B_2H_6. Those having positive $\Delta H_{formation}$ decomposes to diborane and hydrogen gas [56].

Thermal decomposition reactions of $Sn(BH_4)_2$ and $Zn(BH_4)_2$ are given below:

$$Sn(BH_4)_2 + 2NaCl \rightarrow B_2H_6 + Sn + H_2 + 2NaCl \text{ @ } 298 \text{ K}$$

$Zn(BH_4)_2 + 2NaCl \rightarrow B_2H_6 + Zn + H_2 + 2NaCl$ @ 358 - 413 K in molten state of $Zn(BH_4)_2$

Gas phase pyrolysis of diborane to yield amorphous boron is as follows;

$$B_2H_6 \rightarrow 2B + 3H_2 \text{ @ } 573 - 1273 \text{ K}$$

At low temperatures, around 573 K, during the Pyrolysis of diborane, formation of higher boranes and hydrogen gas was reported [53], which reduces the amorphous boron yield of the decomposition reaction. The formations of higher boranes are given as follows:

$$BH_{3(g)} + B_2H_{6(g)} \leftrightarrows B_3H_{9(s)}$$

$$2B_3H_{9(s)} \leftrightarrows 3B_2H_{6(g)}$$

$$B_3H_{9(s)} \leftrightarrows B_3H_{7(s)} + H_{2(g)}$$

$$BH_{3(g)} + B_3H_{7(s)} \leftrightarrows B_4H_{10(s)}$$

$$B_2H_{6(g)} + B_3H_{7(s)} \leftrightarrows BH_{3(g)} + B_4H_{10(s)} \leftrightarrows B_5H_{11(s)} + H_{2(g)}$$

Both BH_3 and B_2H_6 are thermodynamically unstable compounds and easily decomposed to their constituents [7, 57, 58].

Tens of US patents were published between 1940s and 1970s on the production and purification of diborane in which the main reaction mechanism of Brown et al [43] is utilized predominantly. All these processes were claimed to be used in industrial scale production of diborane. A list of the mostly proposed reaction mechanisms and reaction yields are given below.

Table 1.7 List of US Patents on the production and purification of diborane [59-64]

Patent No US#	**Company**	**Proposed Reaction Mechanism**	**Reaction Yield (%)**
2,658,815	General Electric	$6LiH + BF_3 \rightarrow B_2H_6 + 6LiF$	80
2,967,761	Thiokol Chem.	$NaBH_4 + (CH_3)_2SO_4 \rightarrow ½\ B_2H_6 + NaCH_3SO_4 + CH_4$	70
2,983,582	Matheson Chem.	$6LiH + 2BCl_3 \rightarrow B_2H_6 + 6LiCl$	85
3,024,091	Dow Chem.	$2BCl_3 + 3MgH_2 \rightarrow B_2H_6 + 3MgCl_2$	90
3,069,236	Aerojet-General	$MBH_4 + H_2SO_4 \rightarrow B_2H_6 + H_2 + M_xSO_4$	85

1.4 Microwave Induced Plasma

1.4.1 Definition of Plasma

The term “PLASMA” was first used by Langmuir in 1928 to describe the main body of a gas discharge. The word “PLASMA” originates from the Greek meaning “to mold” [65]. Basically, plasma can be defined as a state of matter in which a significant number of the atoms or molecules are electrically charged or ionized. In another words, it is the 4^{th} state of the matter [66]. Plasmas are ionized form of gases that contains ions, radicals, electrons and neutral species. Most of the visible matter (> 90%) in the whole universe is in the plasma state. In plasma, negative and positive charges are equal in number and plasma is assumed to be neutral [67]. The ionization degrees vary from 100% to very low degrees (i.e. fully and partially ionized) [65].

The natural or artificially produced plasmas have found application areas since the late 1950s. Although solids and liquids can be transformed to plasma state, gaseous state is the most commonly used in plasma technology. These solid state and liquid state systems are called “condensed matter plasmas” [68].

Plasma technology is mainly utilized in the following areas of material processing[69]:

- Surface modification
- Plasma phase chemical reactions (so called “Plasma Chemistry”)
- Destruction of toxic and harmful substances
- Plasma welding and cutting (plasma torches etc.)

Plasmas provide three main features that are attractive for applications in chemistry and related fields:

- Temperatures and energy densities of plasma components exceed those in conventional chemical technologies
- Plasmas are able to produce very high concentrations of energetic and chemically active species (electrons, ions, radicals, excited states and different wavelength photons)
- Plasma systems can be far from thermodynamic equilibrium, meaning that they contain high concentrations of chemically active species and keeping bulk temperature as low as room temperature.

These plasma properties allow noticeable increase in the efficiencies of traditional chemical processes and also stimulation of chemical reactions which are impossible in conventional chemistry [67, 70-72].

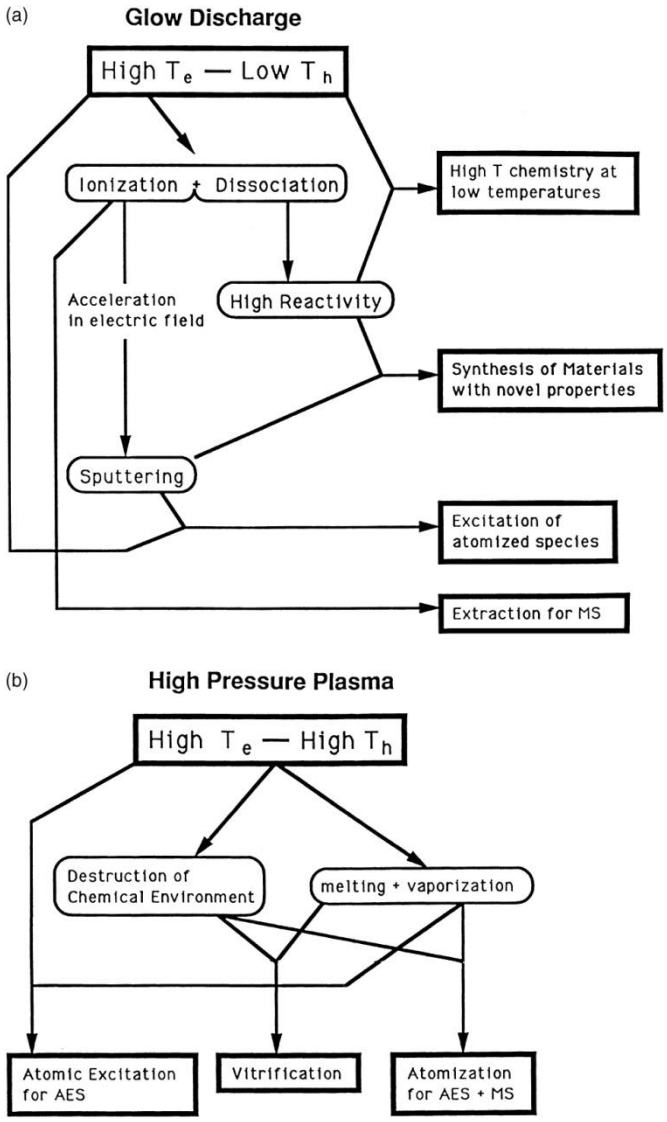

Figure 1.8 Schematic of applications of thermal and cold plasmas (T_e : electron temperature, T_h : heavy particle temperature) [65]

1.4.2 Plasma Types

Plasma can be obtained when sufficient energy, higher than the ionization energy, is given to atoms of a gas, resulting ionization and production of electrons and ions. Parallel

to the ionization process recombination of electrons with ions to form neutral species occurs simultaneously. In gases, plasma is excited and sustained by providing energy to the gas by combustion, flames, electrically heated furnaces, direct current, radio frequency, and microwaves etc [65, 66, 68, 73-76].

Due to cosmic radiation, there are always a few free electrons in a gas. The electrons are very light and can accumulate sufficient kinetic energy through acceleration in an electric field to sustain gas ionization. The electrons reach much higher temperatures than other particles in the gas. The high electron temperatures allow inelastic collisions of electrons with neutrals (impact ionization) and sustain plasma [71, 77].

Plasmas can be divided into two main categories:

- Low – Pressure (Glow discharge) Plasmas
- High Pressure Plasmas

Or

- Low – Temperature (Cold) plasmas
- High – Temperature (Thermal) plasmas

Gaseous plasmas are sometimes classified as equilibrium or non-equilibrium referring to the electron temperature as compared to the gas temperature. Low pressure glow discharges area generally classified as non-equilibrium plasmas because the electron temperature is significantly greater than the gas temperature (heavy particles). Commonly, glow discharges have electron temperatures in the $10^4 – 10^5$ K (1-10eV) range, whereas the gas temperature is generally less than 5×10^2 K or near ambient. As a consequence of the high mass differences ($m_{Heavy}/m_{electron} > 2000$) between heavy particles and electrons, the energy transfer in elastic collisions is very inefficient and equilibrium is not established between the species. This leads to thermal isolation of electron from the atoms and the molecules [69, 71, 78].

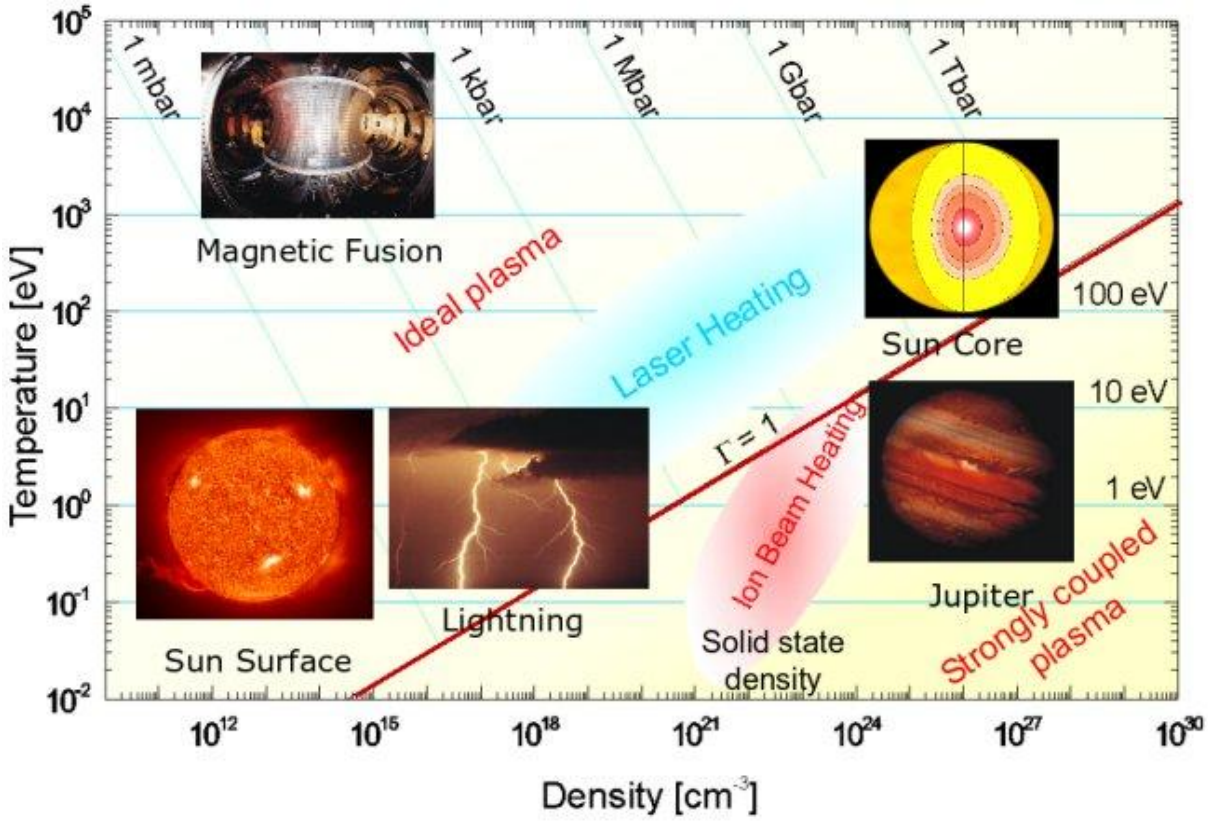

Figure 1.9 Temperature range of various plasma types [100]

One of the fundamental properties of both types of plasmas is their high electron temperature, which causes excitation, ionization and dissociation of gaseous species. In low pressure plasmas, homolytic dissociation of gases produces radicals, which readily react at much lower temperatures than molecular species. As a result, the relatively low temperature of ions, atoms or molecules present in low pressure plasmas allows the performance of high temperature chemistry at low temperatures. At higher pressure the plasma state can be initiated at very high temperatures, which results in the destruction of chemical bonds [68].

The high reactivity of low pressure plasmas is due to high electron temperatures and very low neutral gas temperatures. The concentrations of radicals in these systems are typically 100 to 1000 times higher than that of the ions. The high energy of active species greatly reduces activation energy barriers of chemical reactions and the plasma exhibits a kinetic "factor effect". The low pressure plasmas can be used as powerful tools in materials science where low temperature processing of materials is required [71].

The degree of ionization is an important factor in the application of plasmas. When the degree of ionization is close to unity, it is called completely ionized plasma, which is seen in thermonuclear plasma systems. When the ionization degree is low (10^{-7} to 10^{-4}) the plasma is called weakly or partially ionized and mainly used in plasma chemistry applications [73].

1.4.3 Microwave Induced Plasmas

The plasmas that are ignited or created by the injection of microwave power, electromagnetic radiation in the range of 300 MHz to 10 GHz, are called "*Microwave Induced Plasmas (MWIP)*". This plasma type operates over a wide range of conditions, i.e. pressures less than 0.1 Pa to a few atmospheres, power values between a few W to several hundreds of kW and sustained in both noble and molecular gases [73, 79].

Laboratory scale plasma generation systems are mainly based on three energy sources; DC, RF and MW. Microwave Induced Plasma Systems have several advantages over other two. These are [78, 80]:

- Microwave systems are cheaper and simple methods for obtaining sustainable plasmas
- The main disadvantage of DC discharges is the use of electrodes. Electrodes are quickly deformed and need to be replaced in plasma applications

- MW plasmas have higher degree of ionization (7% more than RF systems) and high ion concentrations (up to 10^{13} cm^{-3})

Microwave induced plasma systems for chemical purposes are usually utilized at low pressures (<10 mbars) and temperatures to avoid destruction of chemical bonds. In these conditions gas phase recombination of ionized species is negligible. The main loss in the concentration of active species is the recombination on the walls of plasma discharge chamber. The probability of recombination is expressed with recombination coefficient which is the ratio of number of atoms recombined at a surface in unit time and flux of atoms towards the surface. Ceramics and silica glass have lowest recombination coefficients (~10^{-4}) while metals have the highest values. Also, ceramics and silica are transparent to microwaves, so they are the most suitable chamber materials in microwave plasma operations [75, 81].

Chapter 2

EXPERIMENTAL PROCEDURES AND CHARACTERIZATION METHODS

As explained in the previous chapter, the aim of this study is to obtain high purity (>99 %B) elemental boron in amorphous form. Thermal pyrolysis of diborane (B_2H_6) was chosen as the main synthesis route. B_2H_6 was produced "on demand" via thermal decomposition of a $M(BH_4)_2$ (*M* : Sn, Zn, Cu etc.). Pyrolysis of B_2H_6 yields elemental boron as the solid product. A novel technique which is based on hydrogen plasma treatment of powder materials was utilized for the oxygen removal of solid product as the purification step. Hydrogen plasma purification process was optimized and converted into a semi-continuous system. SEM, TEM, EDX, DLS, BET, Powder XRD, DTA/TGA/MS, emission spectrometer, ICP-OES and elemental analysis devices were used in the characterization of intermediate and final products. Details of these experimental procedures and characterization methods are explained in this chapter.

Below, main topics of the experimental work are listed with subcategories:

- Synthesis of elemental boron
    - Synthesis of B_2H_6
        - Obtaining $M(BH_4)_2$ (*M*:Sn,Zn,Cu etc.) via ball-milling method and thermal decomposition of these complex metal borohydrides to yield B_2H_6
        - Storage of B_2H_6 in lecture bottle
    - Pyrolysis of B_2H_6

        - Building pyrolysis setup
        - Optimization of the reaction conditions
- Hydrogen plasma aided oxygen removal and purification
    - Microwave Induced Plasma Furnace (MWIPF)
        - Building plasma furnace
        - Optimizing plasma formation conditions
    - Continuous Microwave Induced Plasma Furnace (cMWIPF)
    - Investigation of plasma medium
        - Temperature & Pressure measurements
    - Spectral characterization of reactive species
        - Emission Spectra
- Characterization of the materials
    - Chemical analysis of elemental boron
        - Boron content determination (ICP-OES)
        - Oxygen content determination (Elemental Analysis)
    - Structural analyses, particle size and surface area determination
        - Powder XRD
        - SEM, TEM, EDX

- DLS and BET

2.1 Synthesis of B_2H_6

Thermal decomposition of B_2H_6 yields solid elemental boron and hydrogen gas above 573 K according to following reaction:

$$B_2H_6 \rightarrow 2B + 3H_2 \quad T > 573K$$

Amorphous form can be obtained in the temperature range 573 to 1373 K. Above 1373 K with sufficient annealing time crystalline phase formation (β-rhombohedral) occurs [3]. B_2H_6 is a commercially available gas which is mainly used in electronics industry and in CVD processes. However, it is quite expensive (1 mole B_2H_6 in a lecture bottle is sold for 1500€), highly toxic and explosive. So, on demand production of B_2H_6 is preferable for laboratory purposes as it is safer and cheaper. As described in the previous chapter, B_2H_6 can be obtained by thermal decomposition of transition metal borohydrides, such as $Sn(BH_4)_2$, $Zn(BH_4)_2$ and $Cu(BH_4)_2$, at moderate temperatures.

$$Sn(BH_4)_{2(s)} \rightarrow Sn_{(s)} + B_2H_{6(g)} + H_{2(g)} \quad T > 298K$$

$$Zn(BH_4)_{2(s)} \rightarrow Zn_{(s)} + B_2H_{6(g)} + H_{2(g)} \quad T > 353K$$

$$Cu(BH_4)_{2(s)} \rightarrow Cu_{(s)} + B_2H_{6(g)} + H_{2(g)} \quad T > 353K$$

Synthesis of metal borohydrides can be achieved via ball milling method as it provides milder reaction conditions. The formation occurs as a result of a metathesis reaction between chlorides of metals (MCl_2 : $SnCl_2$, $ZnCl_2$, $CuCl_2$, etc.) and alkaline metal

borohydrides ($M_A BH_4$: $LiBH_4$, $NaBH_4$ and KBH_4) by mechanochemical activation. In mechanochemical activation, reactions occur during the action of deformation and friction of solid materials. In our experiments Fritsch Pulverisette P7 Premium planetary ball milling device with stainless steel grinding bowls and balls was used. Reactants were weighed and filled into grinding cups with calculated number of balls inside the glove box (under Argon gas) and sealed with inert atmosphere lids. Details of ball milling reactions and results are given in the next chapter.

Synthesis conditions for obtaining almost pure $M(BH_4)_2$ are given in the literature [6,10-12]. The formations of these complex metal borohydrides are intermediate steps in the synthesis of B_2H_6 and elemental boron. Thus, instead trying to obtain pure $M(BH_4)_2$, our studies were directly focused on the optimization of reaction conditions for the highest B_2H_6 yield employing TGA/MS measurements. In this manner, reactants were well ground according to stoichiometric ratio ($1MCl_2$: $2M_ABH_4$) in ball-milling device for different milling times and speeds. The resulting powder mixtures were pressed into pellet form (10 mm stainless steel die) with a hydraulic press to enhance solid state interaction. The following systems were investigated with respect to their B_2H_6 evolution rates and temperatures. Details of these studies are given in the next chapter.

- $SnCl_2$ – $LiBH_4$/$NaBH_4$/KBH_4
- $ZnCl_2$ – $LiBH_4$/$NaBH_4$/KBH_4
- $CuCl_2$ - $LiBH_4$/$NaBH_4$/KBH_4
- $NiCl_2$ - $LiBH_4$/$NaBH_4$/KBH_4

Figure 2.1 Pressed reactant mixture pellets

2.2 Pyrolysis of B_2H_6 and Synthesis of elemental boron

Pyrolysis of B_2H_6 and formation of elemental boron was the main reaction in the syntheses. On demand B_2H_6 generation was achieved by thermal decomposition of $M(BH_4)_2$. Figures 2.2 and 2.3 show the schematic and the actual experimental setup, in which $M(BH_4)_2$ decomposes to diborane which pyrolyzes further to yield solid amorphous boron simultaneously.

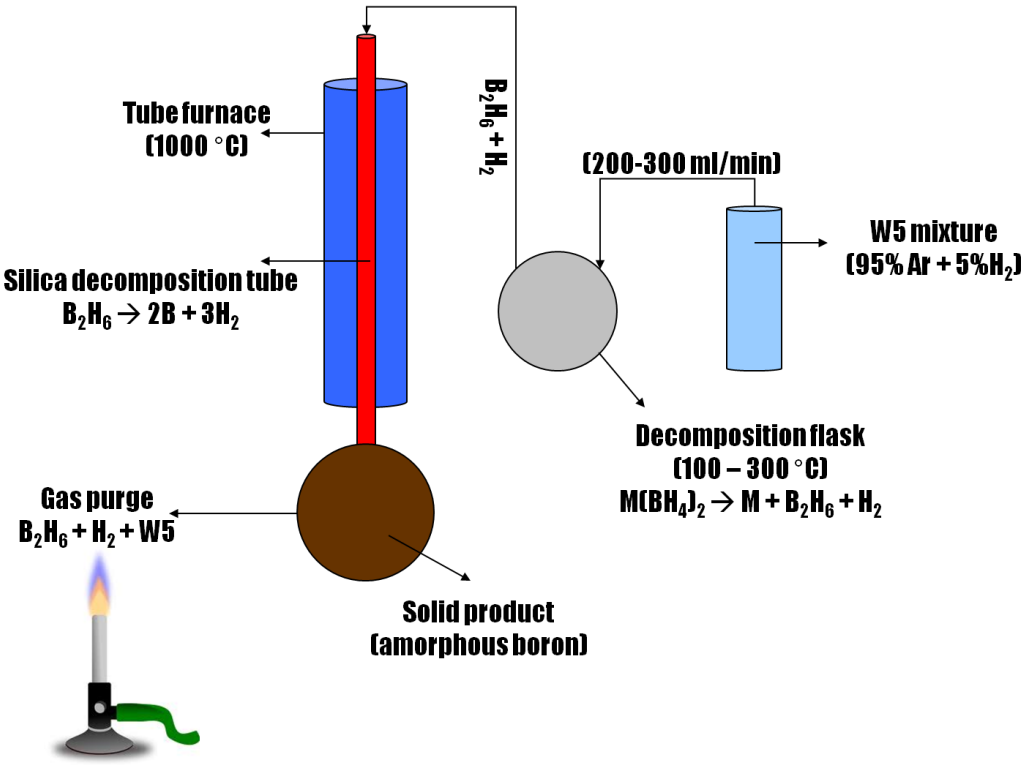

Figure 2.2 Schematic of elemental boron synthesis setup

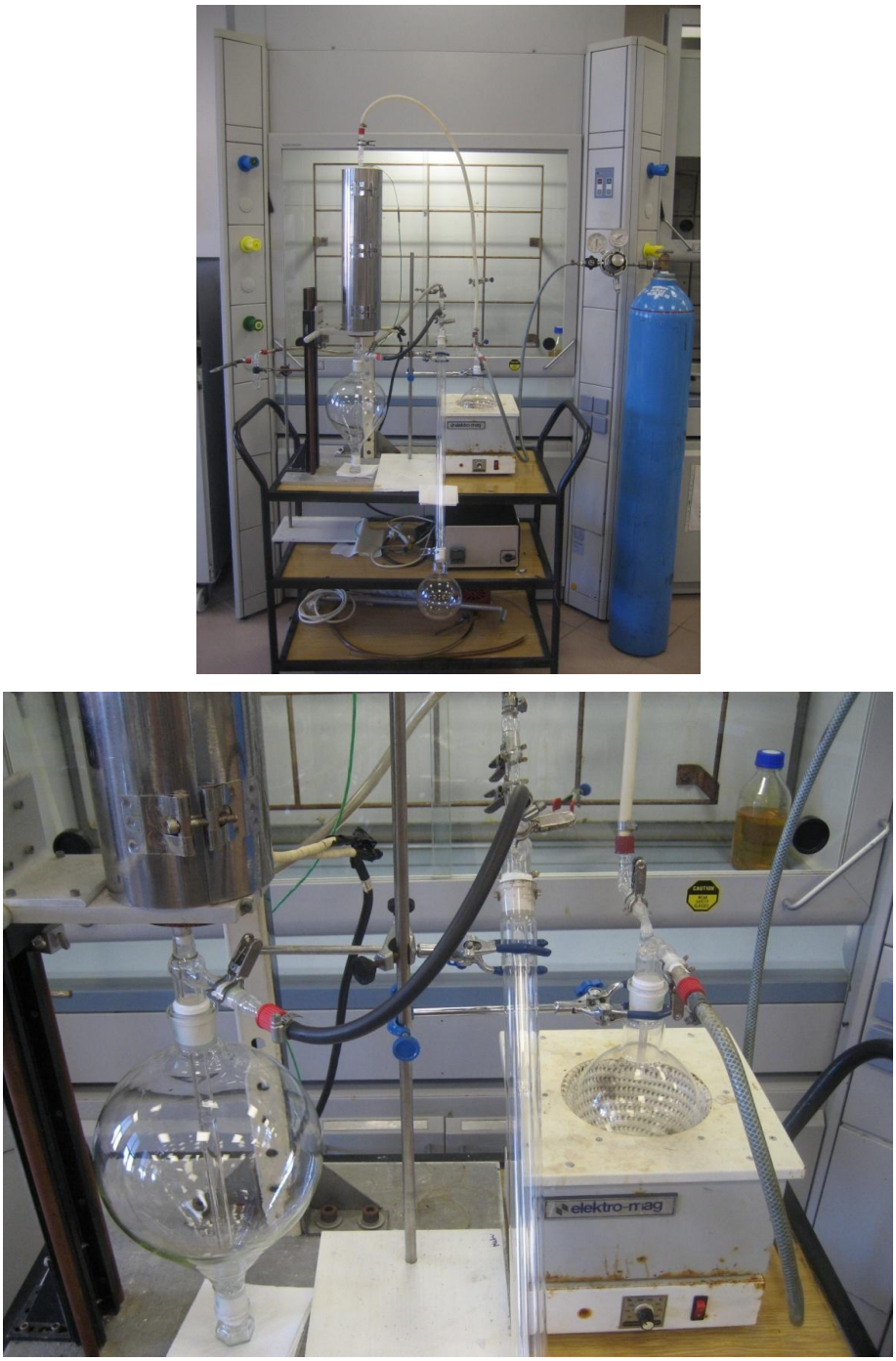

Figure 2.3 Pictures of elemental boron synthesis setup

As shown in Figure 2.3, the decomposition setup contains one vertical tube furnace (50 cm heating zone with 20 mm diameter), 50 cm long 14 mm diameter silica glass tube for B_2H_6 pyrolysis, one round bottom flask heater (up to 650 K) and 1 liter flask, 3 liters rotavap flask under tube furnace for collecting solid product, 1 meter long glass tube powder collector, one bubbler connected to exhaust flame and Viton® plastic tubing for gas transport.

Experimental conditions were optimized for obtaining the highest yield possible in the decomposition process. Previously prepared pellets (MCl_2 + $2M_ABH_4$ mixture) were transferred into a one liter round bottom flask and the flask placed in a heating mantle. The flask was further connected via plastic tubing to the silica tube positioned in the vertical furnace. At the other end of silica tube, a three liter rotavap flask was used as powder collector. The exit of rotavap flask was attached to a second pyrex tube of 1 m length providing a trap for the "escaped" powder. In this manner ca. 85 % of the theoretical yield could be collected. Having closed all the connections, W5 gas mixture (95% Ar, 5% H_2) was flushed for about 30 minutes (flow rate = 500 mL/min) through the line to obtain an inert and reducing atmosphere. In the meantime, vertical furnace temperature was annealed to 1273 K which is the optimized temperature for our experimental procedure. The round bottom flask containing the gray white reaction pellets was slowly heated and when temperature exceeded 373 K (measured on surface of the flusk), a decomposition reaction took place generating diborane and hydrogen gas while the pellets turned to grey. By employing W5 mixture as the carrier gas, the generated gas mixture was transported to the silica tube (at 1273 K) inside the vertical furnace where B_2H_6 pyrolyzed to its constituents: amorphous boron and the hydrogen gas. Solid product was collected both in the three liter rotavap flask and the second pyrex tube while hydrogen and the unreacted diborane leave the system through the exhaust line which was connected to a Bunsen burner. The excess

hazardous and toxic diborane and the explosive hydrogen were burned in propane flame to yield harmless B_2O_3 and water. Hence, the process is environmentally friendly. It is worth mentioning, that the presence of hydrogen gas in the process is important and necessary to create a reducing atmosphere preventing the oxidation of the reactive amorphous boron powder formed in the furnace and deposited in the collectors.

2.3 Storage of B_2H_6 in lecture bottle

To store pure B_2H_6 gas in a lecture bottle for further uses was one of our targets. The experimental setup for transport and storage of B_2H_6 in a lecture bottle is depicted in Figures 2.4 and 2.5.

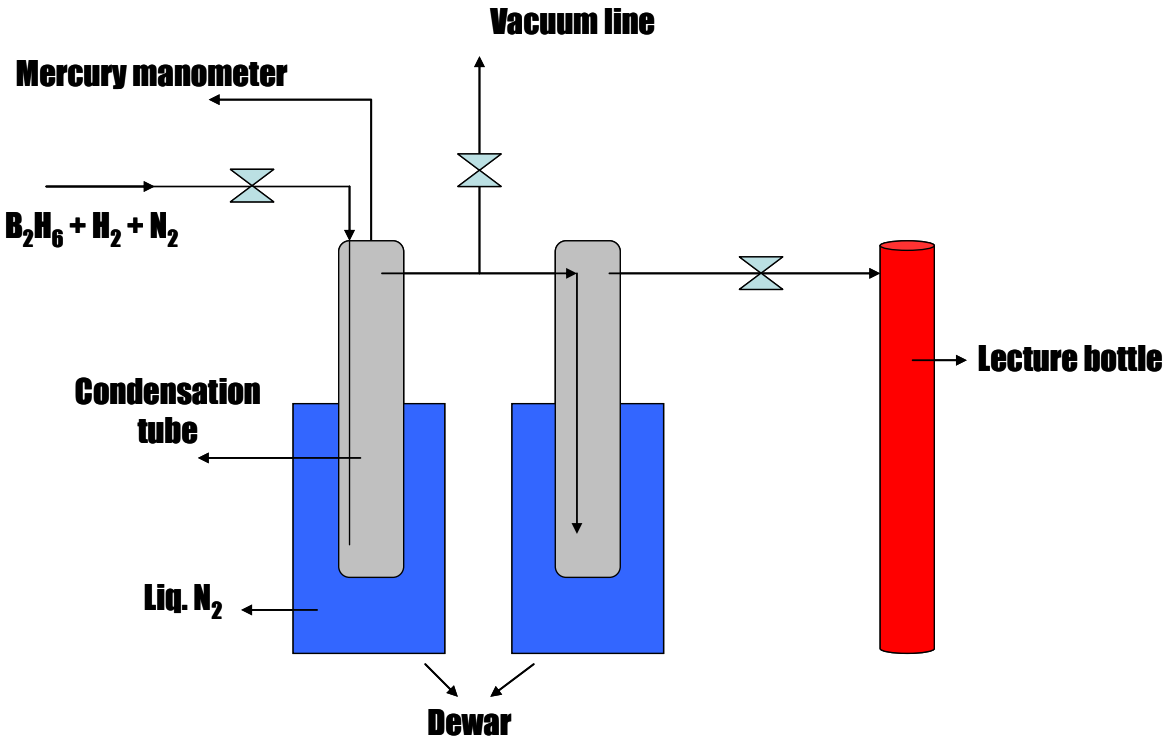

Figure 2.4 Schematic of B_2H_6 transfer into a lecture bottle

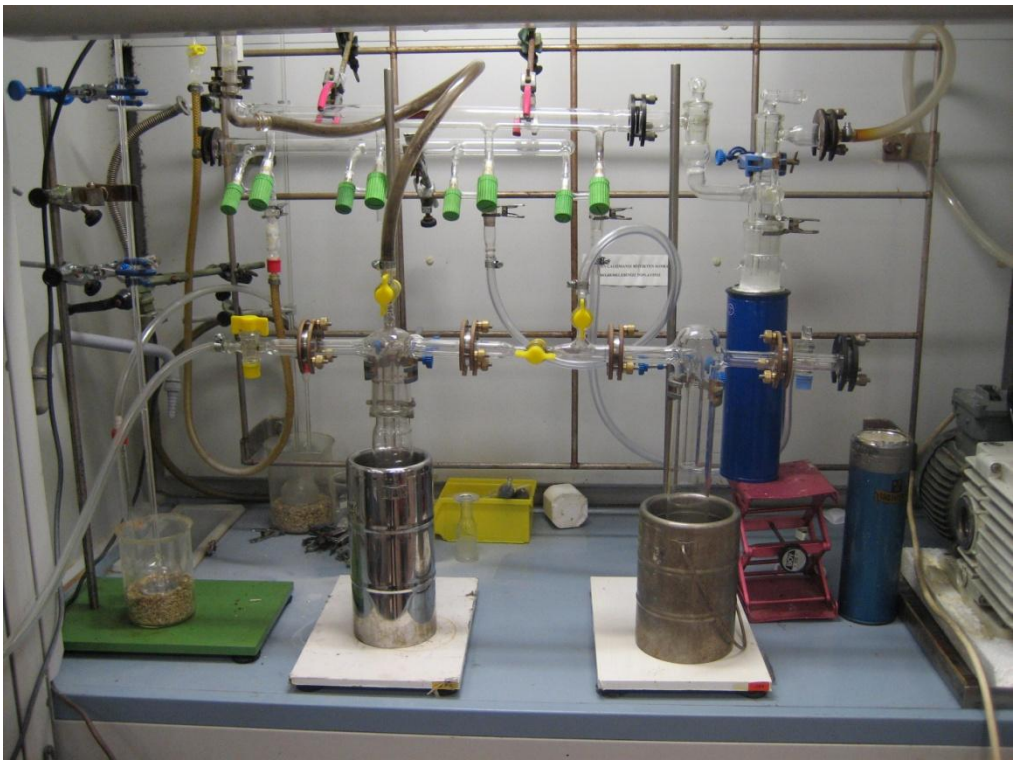

Figure 2.5 Picture of B_2H_6 storage setup

The principles of storage of B_2H_6 gas in a lecture bottle is based on the condensation of gas inside the bottle with the aid of liquid nitrogen (77 K) whose temperature is considerably lower than the melting point of B_2H_6 (108 K). The temperature difference is expected to create a driving force for the gas to be transported into the lecture bottle. The line must be evacuated ($<10^{-3}$ mbar) to avoid the presence of oxygen and water and to enhance the condensation process. B_2H_6 is highly sensitive to both oxygen and water converting it into boric acid (H_3BO_3) according to following reactions [7];

$$B_2H_{6(g)} + 3O_{2(g)} \rightarrow 2B(OH)_{3(s)}$$

$$B_2H_{6(g)} + 6H_2O_{(l)} \rightarrow 2B(OH)_{3(aq)} + 6H_{2(g)}$$

B_2H_6 was generated in another setup and transferred to gas condensation system. The latter was connected to mercury column manometers for emergency purge. Pure nitrogen was used as purge gas. B_2H_6 was first condensed into Pyrex containers with the help of liquid nitrogen and then transferred to lecture bottle. The total yield of diborane storage was quite low due to the possible reasons given below:

- The system was not fully evacuated or there was a leakage of air and it condensed with B_2H_6 inside the lecture bottle and oxygen and water in the air converted B_2H_6 into boric acid.
- B_2H_6 gas decomposed to boron and hydrogen inside the lecture bottle at room temperature.

A consequent literature search showed that storing B_2H_6 in a lecture bottle had several technical problems. Patent authors describing the B_2H_6 storage claimed that B_2H_6 should be kept at dry ice temperatures (195 K) to avoid a self-decomposition. Also, commercial B_2H_6 is filled with 10 % H_2 or He gas, in which H_2 or He pressure prevent B_2H_6 to decompose into boron and hydrogen by changing the direction of reaction to the reactants side.

2.4 Crystallization with Induction Furnace

According to literature data[4,5], conversion of amorphous boron to crystalline form occurs above 1373 K via direct heating in a crucible. Boron rods, boron nitride, tungsten, tantalum and glassy carbon crucibles are suitable containers/substrates for this purpose. Tantalum and glassy carbon can be used up to 2373 K, as further heating may lead to

formation of tantalum boride and boron carbides, respectively [3,4,9]. High temperature treatments of amorphous boron were conducted in 6 kW MTI EQ – SPG – 6A Induction Furnace. Experimental setup is shown in Figure 2.6.

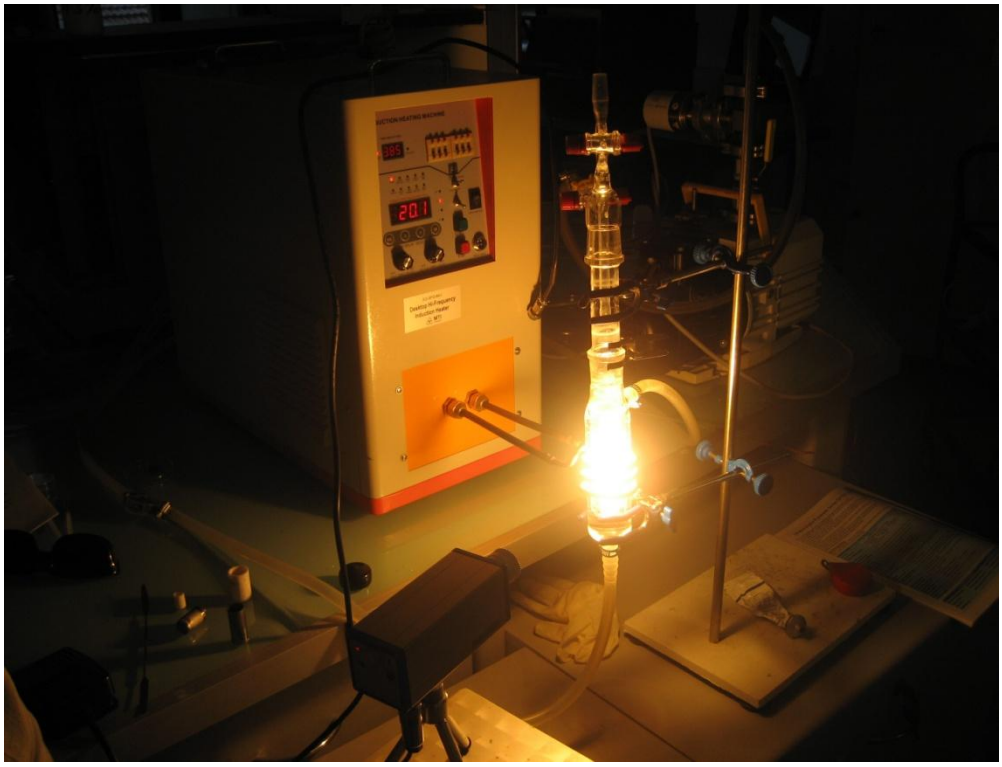

Figure 2.6 Induction furnace setup

Induction furnace is based on the rapid heating of conductive materials up to several thousand degrees Kelvin, depending on the material, due to the generation of eddy currents via fast oscillating electric field created in a circular copper coil [82]. In the experimental setup, tantalum crucible (10 mm radius, 25 mm height) is placed in a protective silica outer tube which can be evacuated up to $3 \cdot 10^{-2}$ mbar and cooled with cold water. To avoid the direct contact between the very hot Ta crucible and silica tube a piece of alumina rod was

use as distant holder. Temperature values of 2573 K and above are accessible within a few minutes and crucible can be kept at these temperatures up to 1 hour. Temperature of glowing materials was recorded by MAURER QKTRD-1085-2 two color infrared pyrometer (Spectral range 1: 0.85 – 1.1 μm, Spectral Range 2: 0.95 – 1.1μ, measuring range: 1173 – 3273 K) which can detect infrared emission independent of emissivity values of materials. Results of crystallization experiments with induction heating are given in the next chapter.

2.5 Microwave Induced Plasma Furnace (MWIPF)

The MWIPF system used in our experiments was patented by Max Planck Institute of Chemical Physics of Solids in Dresden/Germany in 2006 with the International Publication Number "WO 2006/122794 A2", "*Materials purification by treatment with hydrogen-based plasma*" [14].

Oxygen contamination of materials is a major problem for a wide range of materials in science and industry. The oxygen impurities are caused by adsorption and/or reaction with naturally abundant O_2. Conventional oxygen removal procedures are based on the reduction of corresponding oxides at high temperatures with a suitable reducing agent and often lead to contamination of material and to crucial microstructure changes. The claim of the invention is to provide a purification method for removing oxygen by avoiding a thermal treatment which causes microstructure changes and leaves reducing agents as impurities.

The promising way for the removal of oxygen is the application of non-equilibrium processes (cold plasmas). The hydrogen-based microwave induced plasma treatment is used for the purification of the wide range of temperature stable materials (materials which do not evaporate at temperature below 1773 K). $H^{\cdot}$ radicals and H^{+} ions are generated in the

MWIP are very active, so in principle, any kind of material may be purified by this procedure [14].

The authors of the invention prefer to use the method for removing oxygen from amorphous boron. Large scale amorphous boron production is based on reduction of B_2O_3 by a suitable reducing agent (Moissan method). In such a method, amorphous boron contains up to 4 wt % oxygen. Attempts to purify amorphous boron by any kind of thermal treatment lead to boron oxide evaporation and result crystallization of boron. Amorphous boron is desired in chemical reactions because it shows higher chemical reactivity compared to crystalline boron.

The main advantages of MWIP method are;

- It allows removing the oxygen from amorphous boron up to level, which is known only for crystalline boron (<0.1 mass %) in hydrogen plasma by using an oxygen getter material (Zr, Ti, etc)
- No additional reagents are in direct contact with the material and avoids further contamination
- XRD analyses show that plasma-treated product is in amorphous state like starting material is.

2.5.1 Experimental Setup

MWIPF system consists of 5 main parts:

- High purity (>99.9%) plasma gas cylinders (H_2, Ar, N_2 etc.)
- 2 digital mass flow meters with 100 sccm capacity with 0.1 sccm precision and digital mass flow meter controller
- 2.45 GHz, 1200 W, MKS Pyro – Special model microwave oven
- Quartz reaction tube, alumina and platinum crucibles
- Vacuum pump (<10^{-2} mbar) and digital vacuum gauge

Figure 2.7 MWIP System setup

The working principle of MWIP is based on cold plasma generation of high purity gases. The energy for excitation and ionization of gas is supplied from microwave source. The reaction tube and crucibles that are used during the procedure are high temperature resistant, chemically inert and transparent to microwaves. Quartz tube's surface has relatively lower recombination coefficient (for electrons and ions), which enhances ionization. 10 to 100 mg powdered sample can be treated in a single run. After all parts are connected as shown in Figure 2.7, vacuum pump is started to achieve a pressure of at least

$3x10^{-2}$ mbar. Vacuum is necessary, since the plasma generated in this system is low-pressure type cold plasma. Plasma generation depends on microwave power and gas flow rate. In our attempts hydrogen, argon, nitrogen and methane plasmas were successfully generated by the MWIP system.

Amorphous boron which is produced by Moissan method (reduction of B_2O_3 with Mg) contains oxygen impurities in three forms;

- Magnesium borates and magnesium oxide
- Amorphous B_6O and B_7O (boron sub-oxides)
- Passivating native oxide layers (B_2O_3) on the surface

Magnesium borates and oxide can be removed by acid leaching. According to a recent paper [15, 16], a passivating native surface oxide layer on amorphous boron particles is formed when exposed to air. The oxide layer has 0.5 – 2 nm thickness and reaches 20% of the powder volume in nanoparticle (~50 nm) amorphous boron. Surface oxide of amorphous boron is also called "water soluble boron" and can easily be analyzed quantitatively as boron oxide is soluble in water.

MWIP method is thought to be very effective in removing of surface layer oxides and boron sub-oxides. Boron sub-oxides are formed in the reaction during the Moissan process:

$$16B + B_2O_3 \rightarrow 3B_6O$$

$$19B + B_2O_3 \rightarrow 3B_7O$$

In these sub-oxides, oxygen is weakly bonded to B_{12} icosahedrons as shown in Figure 2.8. Hydrogen radicals and ions are thought to react with this weakly bonded oxygen and

leave the material as H_2O form. Removal of oxygen atoms increases the purity of amorphous boron samples.

$$2H^+ + B_6O + 2e^- \rightarrow 6B + H_2O$$

$$2H^+ + B_7O + 2e^- \rightarrow 7B + H_2O$$

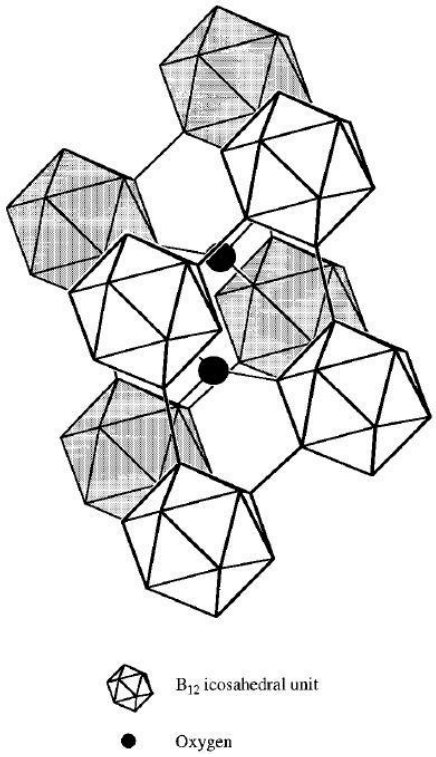

Figure 2.8 Structure of B_6O [17]

Surface oxide layers have 0.5-2 nm thickness and can easily be removed from the surface by highly energetic particles ($H^{\cdot}$ radicals and H^+ ions) either with sputtering effect or by reacting with very thin B_2O_3 layer and removing oxygen as H_2O.

2.6 Continuous Microwave Induced Plasma Furnace (c-MWIPF)

MWIPF system is a batch type process as described in the patent. It is designed for laboratory scale purposes and the amount of material that can be treated is limited to 50 – 100 mg per hour. Our aim was to scale-up the system to increase the amount of material that can be purified (oxygen removal), i.e. up to 50 – 100 g/day. Our knowledge and experience from batch type MWIP was transferred to continuous system and optimized plasma conditions were set in that way that the oxygen removal performance was at maximum.

A new plasma chamber, gas connections and powder dosing system are combined to form a continuous line. Plasma chamber is made up of a silica glass (l = 1000 mm, ∅ = with 40 mm) which is placed inside the microwave furnace and further connected to a one liter round bottom flask. Above the furnace, a commercial powder dosing system (Lambda Instruments Powder Doser) with one liter glass container is attached to upper end of silica plasma chamber. The powder dosing device was modified by using a special vacuum o-ring that acts as a mechanical feed-through and made the device vacuum tight ($P > 3x10^{-2}$ mbar). Figure 2.9 shows the picture of experimental setup for continuous plasma system.

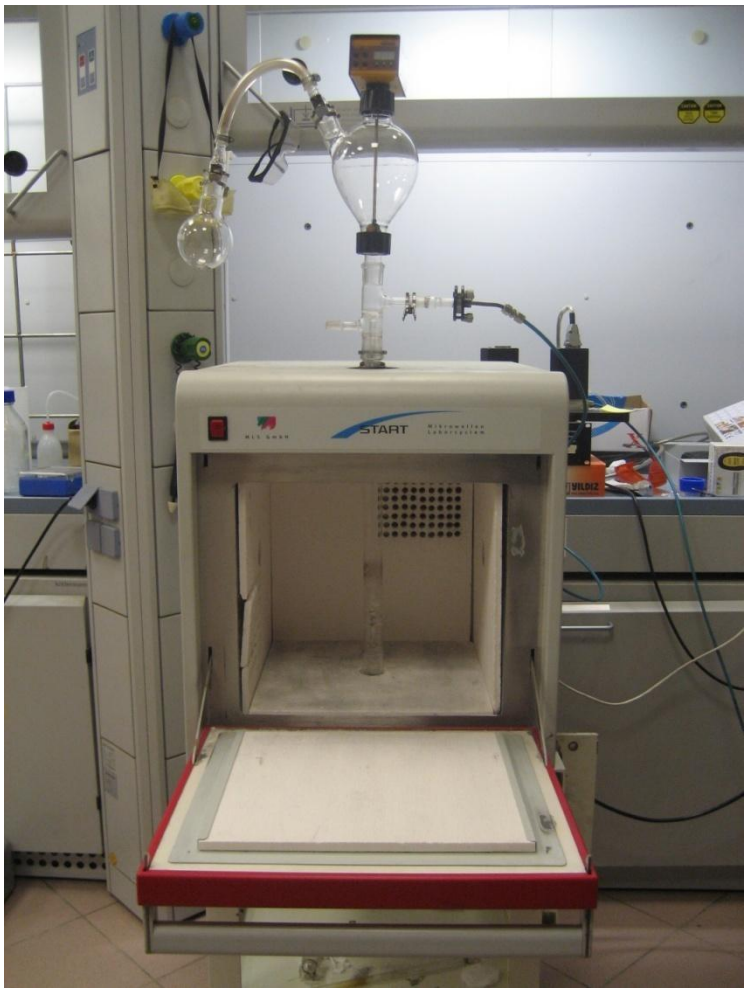

Figure 2.9 Picture of continuous plasma system

Principle of operation in c-MWIP is as follows:

- All connections are fastened and whole system is evacuated to $P>2x10^{-2}$ mbar
- Boron powder is transferred to main powder dosing flask from external container
- System is purged with hydrogen with the highest flow rate (110 sccm) for 15 minutes

- Plasma is ignited by inducing gas molecules via microwave power at different values
- Powder dosing device transfers boron powder to plasma chamber at the desired rate
- Powder is treated in hydrogen plasma while passing through the silica glass plasma chamber
- Plasma treated powder is collected in 1 lt flask placed at the bottom end of silica tube.

This procedure can be repeated several times for better oxygen removal performance. Results of cMWIPF experiments are given in the next chamber.

2.7 Plasma Diagnostics

According to literature [73-76], sophisticated measurement techniques (Langmuir probes etc.) are employed for the diagnostics of plasma environment to monitor ion concentrations, temperatures of ion and electrons, magnetic fields etc. Since we are not interested in such extended investigations, only temperature of plasma medium, pressure of the chamber and determination of species (ions and radicals) formed during the plasma treatment by emission spectrometer were studied for better understanding of plasma conditions. By using the data obtained here were used to find the optimum conditions for best oxygen removal conditions. Results of plasma diagnostics are given in the next chapter.

A K-Type thermocouple was used for temperature measurements. Thermocouple wire was fitted in a silica tube and placed inside the plasma tube. The temperature of the plasma medium was monitored which is assumed to represent the temperature of the heavy particle (ions, radicals). Figure 2.10 shows the equipment used for temperature measurements.

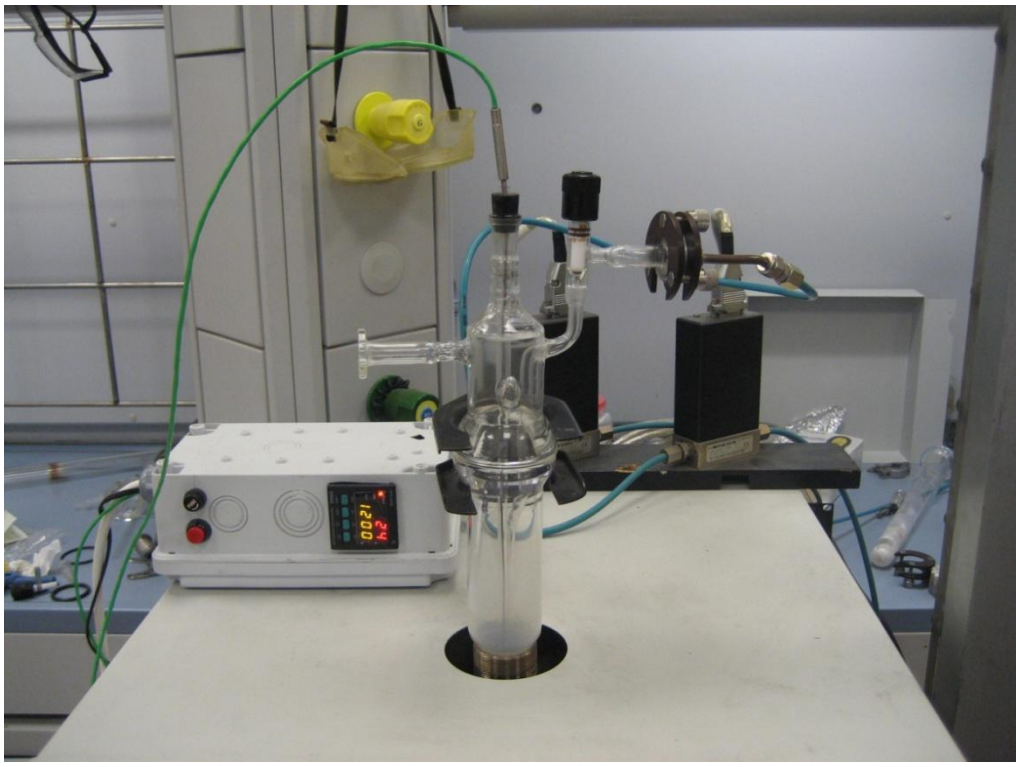

Figure 2.10 Equipment for temperature measurement

In MWIPF system, plasma generation occurs under atmospheric pressure which was measured and monitored by using a PFEIFFER PKR - 261 vacuum gauge and PFEIFFER TPG - 262 digital display. Data were taken by using the driver program of vacuum gauge for Labview® 8 software.

Optical emission spectrum of hydrogen plasma was investigated to observe which reactive species were present during the plasma process. Ocean optics MAYA 2000 UV-Visible spectrometer was employed for these measurements. Figure 2.11 shows experimental setup used for emission spectrum measurements.

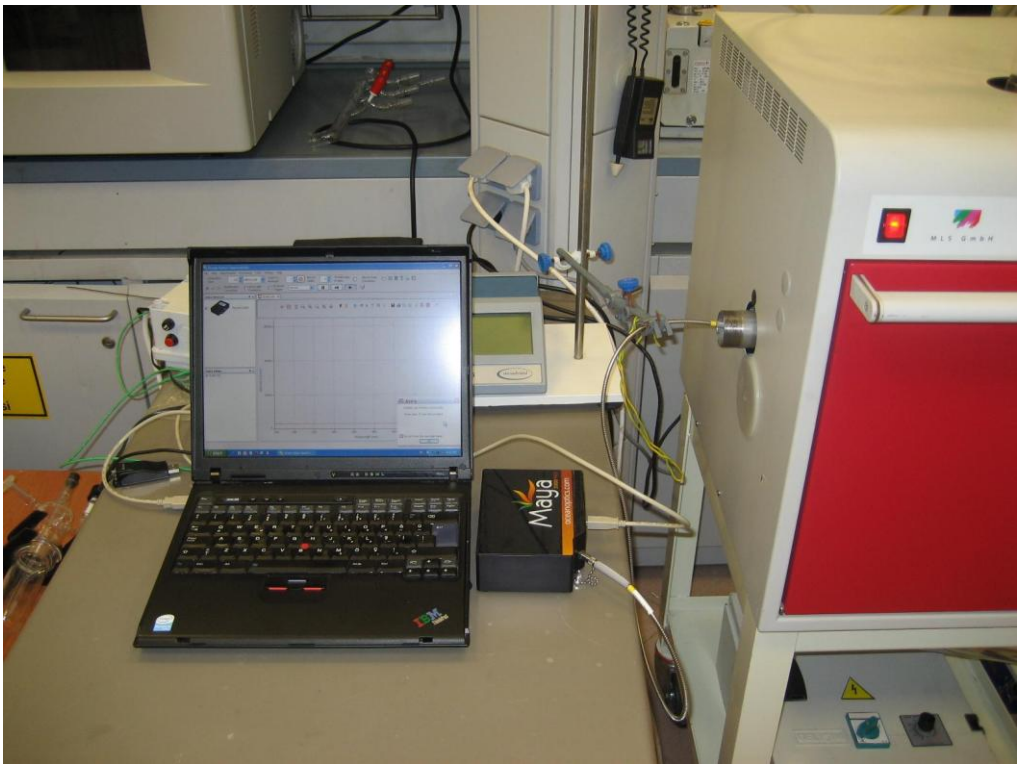

Figure 2.11 Emission spectrum measurement of hydrogen plasma

2.8 Chemical analysis of elemental boron

Quantitative analysis of boron was performed by using ICP – OES technique (Spectro Genesis ICP – OES). ICP – OES system basically measures the optical emission spectrum of the analyte solution and converts it to a quantitative result (in ppm, ppb or mg/L), by using a regression curve of known standards. The linearity of this curve, given by the R value, determines the accuracy of the measurement and must be ≥ 0.9999 for a reliable result. A method should be created for the element(s) of choice with measurements of calibration curve taken at least from three different concentrations.

The Spectro Genesis ICP – OES device was calibrated for quantitative analysis of boron in close collaboration with Dr. Gudrun Auffermann from MPI – CPfs / Dresden who is an

expert in this field. As ICP – OES is based on the optical emission spectrum measurement of elements, wavelength selection is an important issue. 4 recommended wavelengths (182.641, 208.959, 249.677 and 249.773 nm) of boron were employed in the preparation of standard calibration curve measurements.

The method generation for boron analysis was performed as follows;

- Standard stock solution of boron (1000 mg/L, Merck) was diluted to obtain in the range 0 and 100 mg/L
- All dilutions were prepared volumetrically by using a precise micropipette (1000 μL max.)
- 100 mL flasks were used for method solutions
- 5 – 10 mg of analyte was dissolved with 5 mL of concentrated $HNO_{3(aq)}$ for boron analysis in a 100 mL volumetric flask
- Same amount of concentrated HNO_3 was added to method solutions
- Method solutions were measured by ICP-OES and a regression curve having 0.99999 R value was obtained for each wavelength
- For obtaining reliable results, every time ICP – OES device is operated, all internal calibrations and method solutions should be remeasured

Elemental boron samples were acid digested in CEM Mars Xpress model microwave furnace for chemical analysis. 5 – 10 mg of sample was weighed in a 5 digit analytical laboratory scale (Precisa ES 225SM – DR) and poured in a Teflon vessel of acid digestion oven. 5 ml of concentrated nitric acid and 5 ml of distilled water mixture was added to vessel and placed into the oven. Samples were acid digested at 150 °C for 30 minutes (with 20 minutes ramp time) and cooled down to room temperature. After digestion, content of Teflon vessels were diluted to 100 ml Polypropylene flasks and measured in ICP-OES.

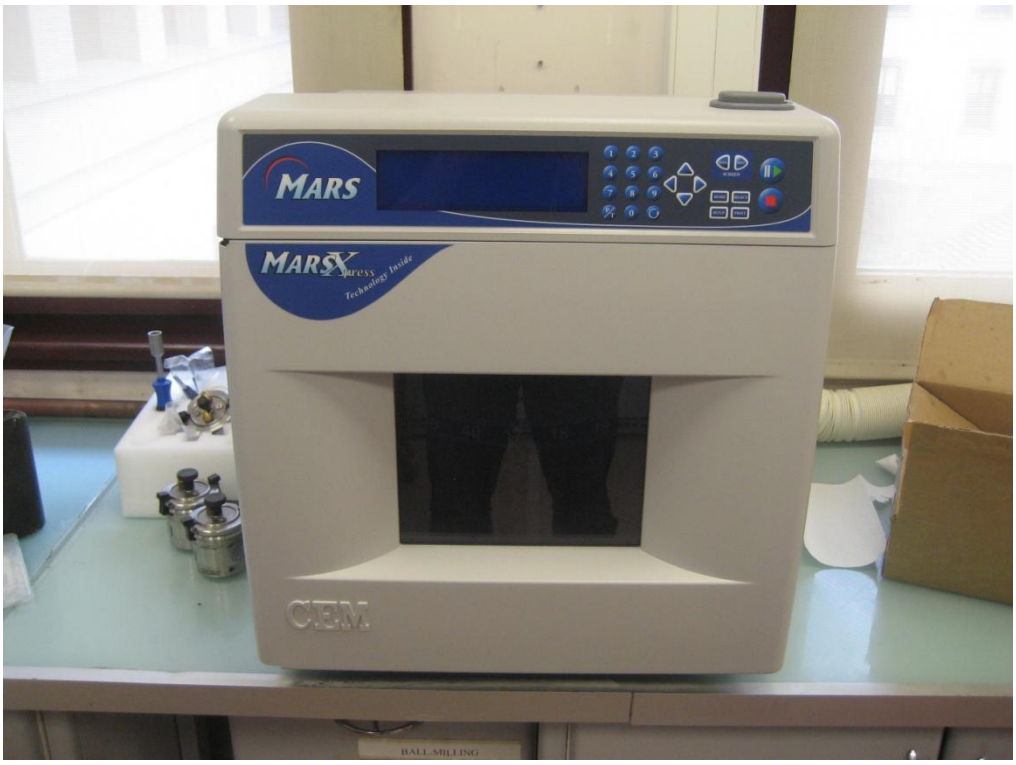

Figure 2.12 CEM Mars Xpress Model microwave acid digestion furnace

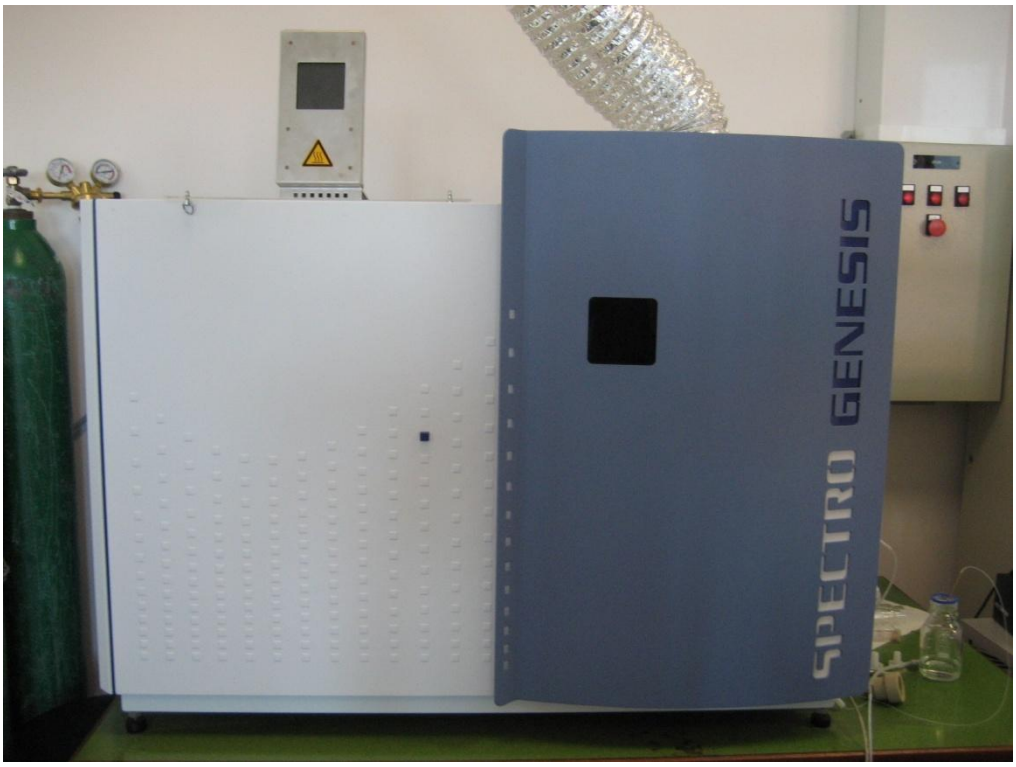

Figure 2.13 Spectro Genesis ICP - OES

2.9 p-XRD

The samples which will be measured in powder XRD must be grinded to a very fine powder. For this purpose a set of agate mortar and pestle was used to grind samples for maximum uniformity. To avoid the decomposition of the air and moisture sensitive samples during the measurement, special Polyimide films were used for XRD experiments. These films can be protective up to 2 hours. For the preparation of the XRD samples, 2-3 spatula tips of the well ground powder was distributed evenly on a Polyimide film that was placed on an aluminum sample holder. A second film was placed over the powder layer and the films were stretched and fixed with an aluminum ring. Entire sample preparations were performed in the glove-box under argon atmosphere.

X-ray diffraction analysis was performed by using HUBER G670 diffractometer with a germanium monochromator and CuKα_1 radiation (λ = 1.5405929 Å). The data collections were made in the range of $5° < 2\theta < 100°$ with 0.05° increments. Data manipulations were done by using STOE WinXPOW software [34].

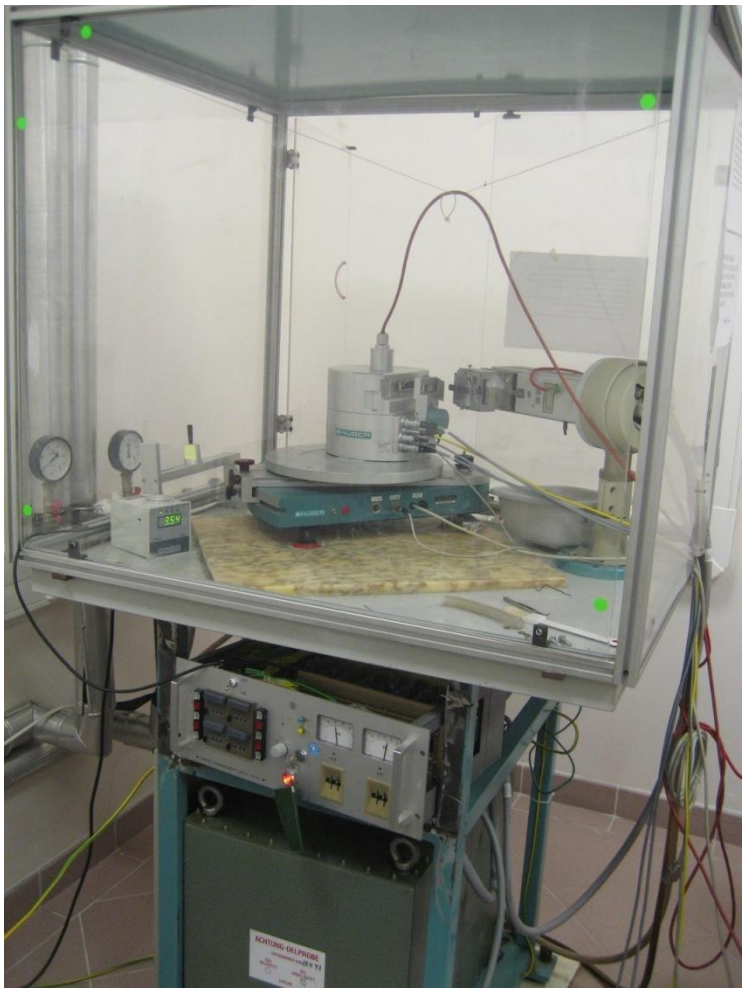

Figure 2.14 Huber G670 Powder XRD device

2.10 DSC – DTA/TGA – MS

Thermal characterizations of samples were performed by using DTA/TGA and mass spectrometer. For all measurements 15 – 20 mg sample weight was kept constant. Samples were well crushed and mixed in agate mortar under argon glove box to enhance uniformity and to enhance the surface area of powdered material touching the measurement pans.

Seiko SSC6300 DTA/TGA thermal analyzer, which can reach up to 1773 K under inert gas or synthetic air, was used for high temperature measurements. As all of our samples were air and moisture sensitive, the measurements were conducted under high purity argon gas which was also filtered through an oxygen absorber cartridge. Heating rate and argon flow were adjusted to 10 K/min and 400 ml/min, respectively. Aluminum or aluminum oxide crucibles were used depending on the upper temperature limit of the measurements. All data manipulations were done in MUSE® software.

Figure 2.15 Seiko SSC6300 DTA/TGA and Pfeiffer Thermostar 220 Mass spectrometer

Pfeiffer Thermostar 220 mass spectrometer was connected to the exhaust line of Seiko SSC6300 thermal analyzer. The Mass spectrometer is equipped with a Prisma detector that can monitor masses from 1 to 300 amu. Data manipulations were done in QUADSTAR software.

2.11 LECO Elemental Analysis Device

LECO TCH600 elemental analysis device was used to determine oxygen, nitrogen and hydrogen content of elemental boron samples. Instrument can detect oxygen between 0.05 ppm to 5.0%, for nitrogen 0.05 ppm to 3.0% and for hydrogen 0.1 ppm to 0.25.

The TCH600 measures nitrogen, oxygen, and hydrogen in a wide variety of metals, refractory, and other inorganic materials employing the inert gas fusion principle. A weighed sample, placed in a high-purity graphite crucible, is fused under a flowing helium gas stream (450 ml/min) at temperatures sufficient ($T > 2273$ K) to release oxygen, nitrogen, and hydrogen. The oxygen in the sample, in whatever form present, combines with the carbon from the crucible to form carbon monoxide. The nitrogen present in the sample releases as molecular nitrogen, and any hydrogen present is released as hydrogen gas [83].

Oxygen is measured by infrared (IR) absorption. Sample gases first enter the IR module and pass through CO and CO_2 detectors where oxygen is detected. Following this, sample gas is passed through heated copper oxide to convert CO to CO_2 and any hydrogen to water. Gases then re-enter the IR module and pass through a separate CO_2 detector for total oxygen measurement to maximize performance and accuracy for both low and high range. The instrument automatically chooses the optimum detection range [83].

Nitrogen is measured by thermal conductivity (TC). Sample gases pass through heated copper oxide which converts CO to CO_2 and hydrogen to water, which are then removed

with a trap to prevent detection by the TC cell. Gas flow then passes through the TC cell for nitrogen detection [83].

Hydrogen is measured by infrared absorption. Gases enter the IR module and pass through an H_2O detector for total hydrogen measurement [83].

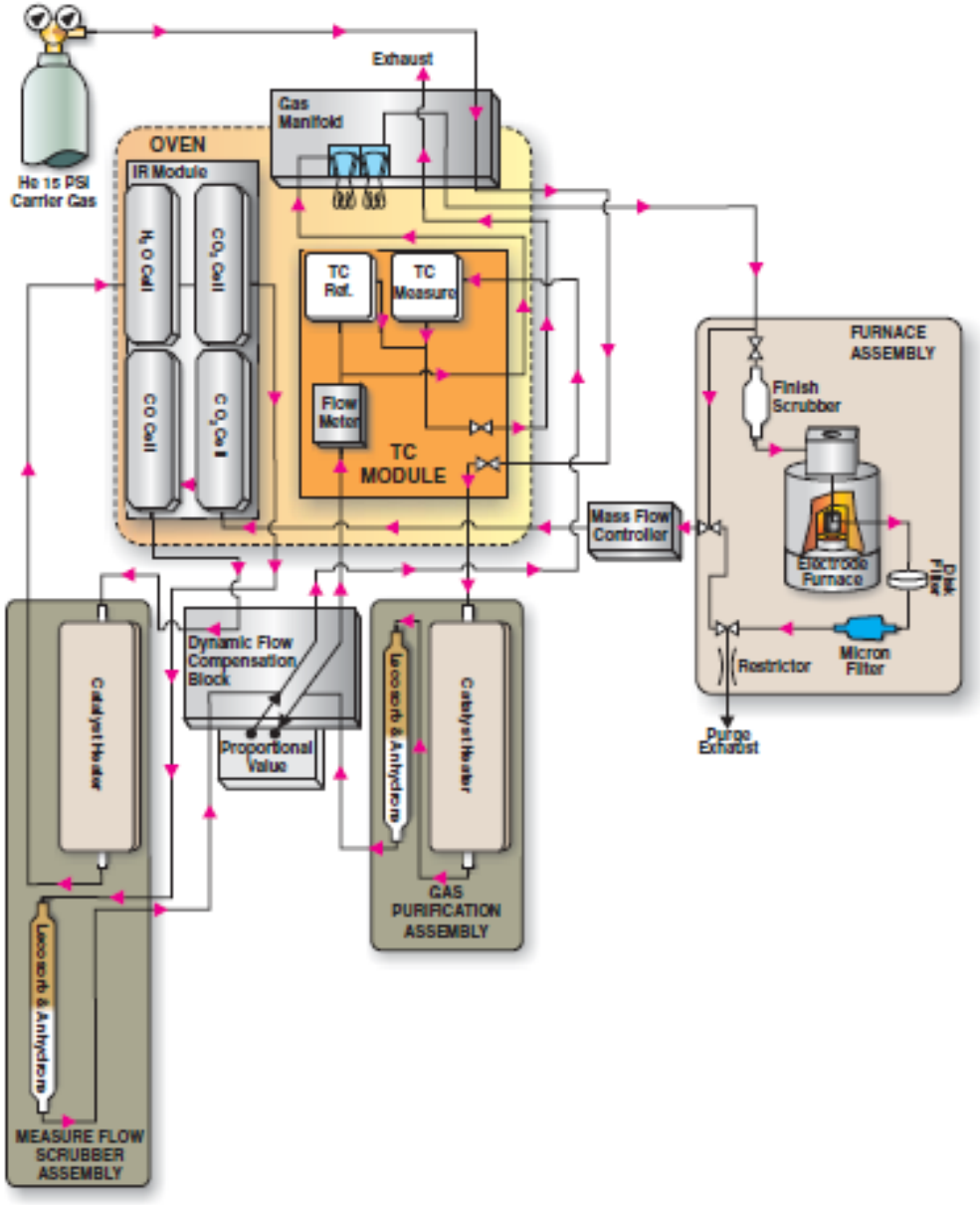

Figure 2.16 Flow diagram of TCH600 operation [83]

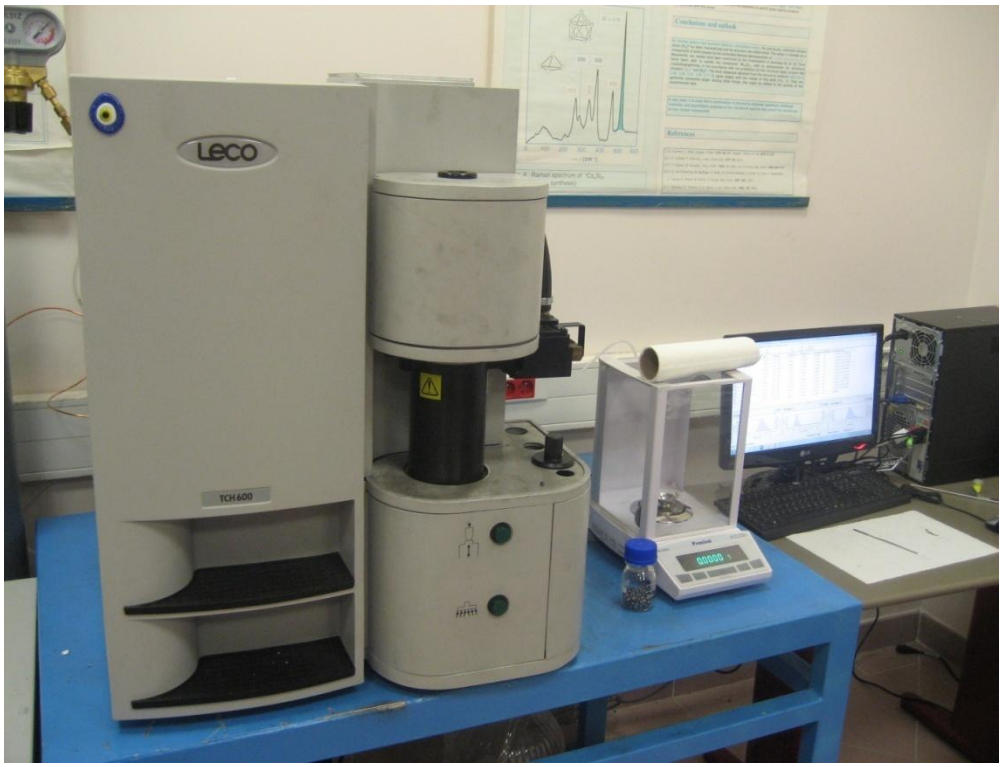

Figure 2.17 LECO TCH600 elemental analysis device

A special sample preparation method was employed for the analysis of boron samples. This technique was developed by Dr. Gudrun Auffermann in MPI-CPfS / Dresden for O/N determination in powdered inorganic materials.

The device is calibrated with reference metal pins in which oxygen and nitrogen values are known exactly. Our method is capable of measuring up to 5 wt% oxygen and 7.5 wt% nitrogen in 10 mg of sample. All sample preparations were done in the argon filled glove box to avoid further oxidation of samples. Weighed sample is filled in a tin capsule and placed in a nickel capsule with additional tin flux pellets. It is thought that catalytic effect of nickel enhances the reaction of oxygen with carbon crucible to form CO and CO_2, while

powder sample is dissolved homogenously in tin flux. By these improvements all oxygen and nitrogen content can be monitored with small deviations.

2.12 Planetary Ball – Milling

Fritsch Pulverisette Premium line 7 model planetary ball milling device was used in our experiments. Stainless steel coated grinding bowls with inert atmosphere lids and grinding balls were employed. The reason it is called planetary comes from the planet-like motion of grinding bowls. The bowls and the disk carrying them are simultaneously and separately rotating around their own axis at high speeds. The centrifugal force due to the motion of rotating bowls and grinding ball as well causes friction and impact effects that create a thermal load on the grinding material and makes chemical reactions possible.

Figure 2.18 Fritsch Pulverisette Premium Line 7 planetary ball milling device with stainless steel grinding equipments.

The ball milling experiments consists of two steps: loading powder mixture and grinding balls in a stainless steel bowl under an inert gas atmosphere and milling for the desired length of time and milling speed.

2.13 Glove box

Glove box is a device that is designed for handling of air and moisture sensitive materials in inert atmosphere. Usually, two gloves are attached to the device to perform experiments inside the box without breaking the seal or allowing potential damage to a worker's hands. An inert atmosphere is desired for working with oxygen and/or moisture sensitive materials. All glove box systems have at least one evacuable antechamber for transferring materials from outside to inside or vice versa. The evacuation for removal of moisture and air takes about 20-30 minutes. In our experiments, a glove box system with a high purity argon atmosphere, MBraun UniLAB model device was used. The box is equipped with an automatic regeneration system to recover the capabilities of oxygen and moisture filters. Amorphous copper is used in a column for oxygen removal. This column can be regenerated by passing a hydrogen/argon mixture through it while it is heated. The water formed is passed out of the column with the excess of gas mixture. Molecular sieves are used for removal of water by adsorption.

Values of oxygen and water levels can be checked by sensors that are connected to the working area of the system. Acceptable working conditions are less than 1 ppm of both oxygen and water in the working chamber.

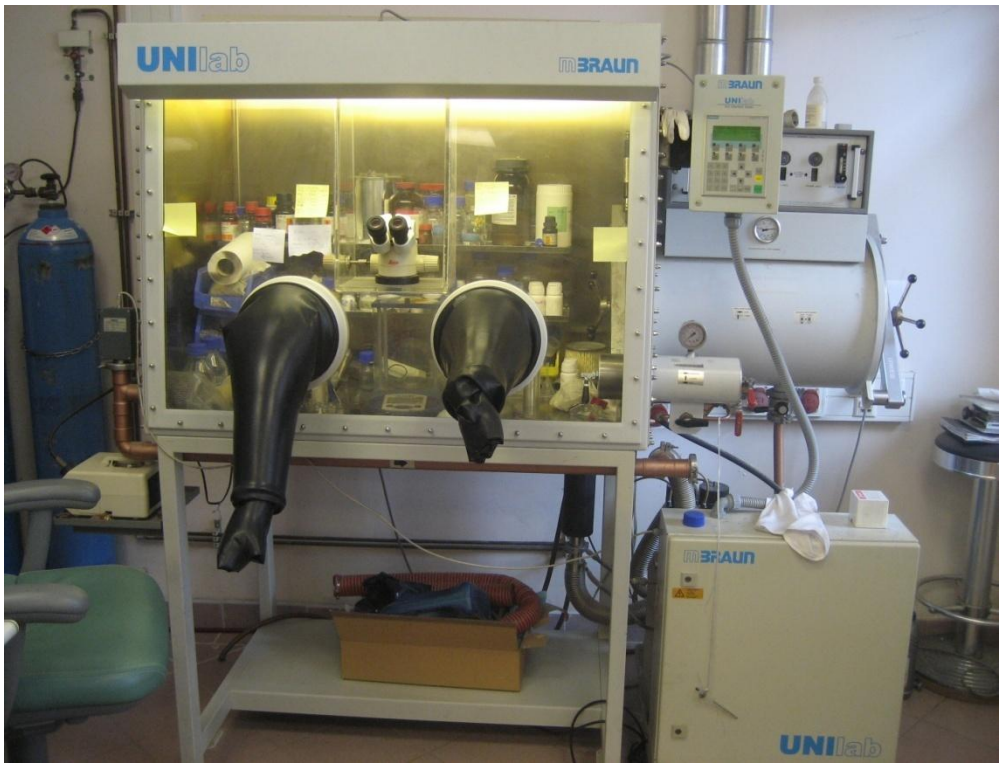

Figure2.19 MBraun UniLab model glove box system

2.14 SEM – TEM – EDX

SEM images were taken with Zeiss Ultra Plus FE-SEM device under 5 keV acceleration voltage in KUYTAM/Koç University. Powdered samples were dispersed in ethanol with ultrasonic bath for 5 minutes and dropped on aluminum stabs and left dry in the ambient conditions.

TEM, electron diffraction and EDX measurements were taken in MPI – CPfS Dresden/Germany by Yiğit Öztan. TEM images were taken with FEI TECNAI 10 device under 100 kV acceleration voltage. Powdered material was suspended in ethanol and dropped on a regular Cu TEM grid with 2 nm carbon foil and left for drying before introduction to TEM.

2.15 BET – DLS

Surface area measurements were performed in Koç University Energy technologies & Supercritical fluids research group. Micromeritics ASAP2020 BET Instrument was used. Specific surface area, porosity and pore size distribution data were taken for our samples. Results are given in the next chapter.

DLS measurements and data manipulations were done by Hüseyin Enis Karahan in Koç University Surface Physical Chemistry Research Laboratory. Malvern Instruments Nano – S Zetasizer device was used.

2.16 Preparation of metal chlorides

$SnCl_2$ and $ZnCl_2$ are commercially purchased in dehydrated form. To be sure, that the starting metal chlorides were completely anhydrous, both salts were vacuum dried ($<10^{-2}$ mbar) at 473 K for 2 hours before using in reactions. $CuCl_2$ and $NiCl_2$ were purchased as $CuCl_2 \cdot 2H_2O$ and $NiCl_2 \cdot 6H_2O$. When vacuum dried at 373 K for 2 hours, $CuCl_2 \cdot 2H_2O$ loses its crystal water and converts to $CuCl_2$. However, $NiCl_2$ is not accessible via vacuum heating of the hydrated salt. The problem is nickel chloride's readiness to hydrolyize to form undesired by-products such as oxides, hydroxides, oxohalides or the so-called basic salts [84]. Commonly, the anhydrous halides are made by passing $SOCl_2$ at moderate temperatures or using hydrogen halide gas at elevated temperatures. To avoid usage of gaseous hydrogen halides solid NH_4X (X = Cl, Br, I) was utilized [84] which decomposes around 573 K to yield:

$$NH_4Cl_{(s)} \rightarrow HCl_{(g)} + NH_{3(g)} \quad @\ 573\ K$$

$$NiCl_2 \cdot 6H_2O_{(s)} + 6NH_4Cl_{(s)} \rightarrow NiCl_{2(s)} + 6H_2O_{(g)} + 6NH_{3(g)} + 6HCl_{(g)}$$

Excess NH_4Cl is required to convert metal oxides or hydroxides which may form during the heating process into the corresponding halide.

The procedure of drying $NiCl_2 \cdot 6H_2O$ is as follows:

$NiCl_2 \cdot 6H_2O$ is mixed with NH_4Cl in molar ratio 1:8 and ground in mortar to have a fine homogenous powder. Mixture is placed into a pyrex ampoule and the ampoule in a second protective pyrex tube. While purging N_2/Ar through, the mixture is heated to 498 K in 2 h and then successively (in 6h) to 703 K and dwell for 2 hours. To remove the last traces of NH_4Cl, the cooled pyrex tube is connected to the vacuum line and heated to 773 K in 1 hour and annealed for 2 hours.

Chapter 3

RESULTS AND DISCUSSION

In Chapter 2, experimental procedures and details of characterization methods were described. In this chapter, results of the experiments will be given with further discussions.

3.1 Synthesis of amorphous boron

As repeatedly explained, thermal decomposition of diborane, B_2H_6 , to its constituent elements (B and H) is the main route for high purity elemental boron synthesis. Besides the high price of commercial B_2H_6, on demand production technique of B_2H_6 was chosen due to its toxicity, storage problems and explosive behavior.

Mechanochemical activation is a relatively novel method in the solid state syntheses and provides milder reaction conditions for obtaining thermodynamically metastable materials. B_2H_6 is accessible through gentle heating of certain transition metal borohydrides such as $Sn(BH_4)_2$, $Zn(BH_4)_2$ and $Cu(BH_4)_2$. These complex borohydrides can be obtained via metathesis reaction of alkali metal borohydrides ($LiBH_4$, $NaBH_4$ and KBH_4) with metal chlorides (e.g. $SnCl_2$, $ZnCl_2$, $CuCl_2$) at ambient conditions. Reactions occur as follows:

$$MCl_2 + 2M_ABH_4 \rightarrow M(BH_4)_2 + 2M_ACl, (M = Sn, Zn, Cu; M_A = Li, Na, K) @ RT \quad (1)$$

$$M(BH_4)_{2(S)} \rightarrow M_{(s)} + B_2H_{6(g)} + H_{2(g)}, (M = Sn, Zn, Cu) \quad (2)$$

The theory behind this reaction is the usage of a metal chloride in which the metal has a high electronegativity. As the result of metathesis reaction (1), the anions are mutually substituted to form alkali metal chloride and the metal borohydride (2). The tetrahedral complex anion $[BH_4]^-$ is stabilized by one delocalized electron. If the $[BH_4]^-$ group is combined with electron withdrawing counter ions, i.e. highly electronegative metal cations such as Sn^{2+}, Zn^{2+}, Cu^{2+}, etc, the electronic structure of the tetrahydridoborate group $[BH_4]^-$ will be markedly destabilized decomposing to metal, elemental boron and hydrogen or metal, "BH_3" and hydrogen. The monomer BH_3 molecules dimerize at low temperatures and form B_2H_6. Due to the high Pauling electronegativity of Sn^{2+}, Zn^{2+} and Cu^{2+} (1.96, 1.65 and 1.90), complex borohydrides of these metals are regarded as metastable and can easily be decomposed to generate B_2H_6 and H_2 as gaseous products.

One can obtain B_2H_6 "on demand" by using the above solid state reactions. When heated above 573 K, B_2H_6 is pyrolyzed to yield solid elemental boron and hydrogen gas (3).

$$B_2H_{6(g)} \rightarrow 2B_{(s)} + 3H_{2(g)} \ (T > 573 \ K) \qquad (3)$$

Pyrolysis of B_2H_6 produces elemental boron through a gas phase nucleation mechanism in the reducing hydrogen atmosphere and yields the high purity (>98.5 % B) boron in amorphous form.

According to the theoretical background given above, B_2H_6 formation is originated from the metathesis reactions (1 and 2), $SnCl_2$, $ZnCl_2$, $CuCl_2$ and $NiCl_2$ were chosen as candidate metal chlorides as the metal cations have high electronegativity values (Sn^{2+}: 1.96, Zn^{2+}: 1.65, Cu^{2+}: 1.90, Ni^{2+}: 1.91). The complex metal borohydrides that are formed through these reactions have positive heat of formations [56] meaning that they are not

thermodynamically stable and decompose to generate B_2H_6 at relatively low temperatures (between RT to 373 K).

Table 3.1 Metal chloride and alkaline metal borohydride systems for promising B_2H_6 generation

$SnCl_2 + 2LiBH_4$	$ZnCl_2 + 2LiBH_4$	$NiCl_2 + 2LiBH_4$	$CuCl_2 + 2LiBH_4$
$SnCl_2 + 2NaBH_4$	$ZnCl_2 + 2NaBH_4$	$NiCl_2 + 2NaBH_4$	$CuCl_2 + 2NaBH_4$
$SnCl_2 + 2KBH_4$	$ZnCl_2 + 2KBH_4$	$NiCl_2 + 2KBH_4$	$CuCl_2 + 2KBH_4$

Solid mixtures of $SnCl_2$, $ZnCl_2$, $CuCl_2$ and $NiCl_2$ with alkaline metal borohydrides were investigated with respect to their gas evolution characteristics and were analyzed using TG/MS spectroscopy. Table 3.2 depicts the results of these measurements and experimental conditions that were followed.

Table 3.2 TG/MS measurements for $MCl_2 - M_ABH_4$ systems

Reaction	**Total mass loss (%)**	**Decomposition Start Temp. (K)**	**Theoretical B_2H_6 (% mass)**	**Measured B_2H_6 (% mass)**	**Conversion (%)**
$SnCl_2 + 2LiBH_4$	9,61	500 (B_2H_6 + H_2)	11,87	9,41	79,2
$SnCl_2$ + $2NaBH_4$	10,30	460 (B_2H_6 + H_2)	10,43	10,10	96,8
$SnCl_2 + 2KBH_4$	8,61	455 (B_2H_6 + H_2)	9,30	8,44	90,8
$ZnCl_2 + 2LiBH_4$	12,7	390 (B_2H_6 + H_2)	15,38	12,45	80,9

$ZnCl_2$ + $2NaBH_4$	11,8	385 (B_2H_6 + H_2)	13,05	11,56	88,6
$ZnCl_2$ + $2KBH_4$	5,1	400 (B_2H_6 + H_2)	11,33	4,99	44,1
$NiCl_2$ + $2LiBH_4$	10,1	450 (H_2) 550 (B_2H_6)	15,99	-	-
$NiCl_2$ + $2NaBH_4$	***36,2***	450 (H_2)	13,49	-	-
$NiCl_2$ + $2KBH_4$	***33,7***	450 (H_2)	11,66	-	-
$CuCl_2$ + $2LiBH_4$	***46,4***	470 (B_2H_6 + H_2)	15,54	-	-
$CuCl_2$ + $2NaBH_4$	***29,1***	560 (B_2H_6 + H_2)	13,17	-	-
$CuCl_2$ + $2KBH_4$	***15,76***	460 (B_2H_6 + H_2)	11,42	-	-

Reactants given in Table 3.1 were mixed and pre-reacted with ball-milling device. It is important to note that it is possible to synthesize these complex metal borohydrides via ball-milling method by adjusting the exact reaction conditions (molar ratio, ball-milling time, rotation speed, etc.). However, in our case, these complex borohydrides are intermediate products. So, instead of trying to reach the optimum ball-milling conditions for the syntheses, we were focused on monitoring the gas evolution rates of B_2H_6 and hydrogen generated during the thermal decomposition process. Table 3.3 gives the preparation conditions of the mixtures via ball-milling device.

Table 3.3 Ball-milling parameters for $MCl_2 - M_ABH_4$ mixtures

$MCl_2 - M_ABH_4$	Time (min)	Rotation Speed (rpm)	Ball : Powder Ratio
$SnCl_2 - M_ABH_4$	10	150	30:1
$ZnCl_2$ - M_ABH_4	15	300	30:1
$CuCl_2$ - M_ABH_4	10	150	30:1
$NiCl_2$ - M_ABH_4	10	150	30:1

As Sn, Cu and Ni have higher Pauling electronegativities than Zn, they undergo a faster decomposition already during the ball-milling procedure for which a shorter milling time and lower speed were employed, as reported in literature [55,56]. The following figures show the results TG/MS measurements of the metal chloride – alkaline metal borohydride mixtures given in Table 3.1. Mass spectra signals of B_2H_6 and H_2 were set as $2(H_2^+)$, $10(^{10}B^+)$, $11(^{11}B^+)(^{10}BH^+)$, $12(^{11}BH^+)$, $13(^{11}BH_2^+)(^{10}BH_3^+)$, $14(^{11}BH_3^+)$, $21(^{10}B^{11}B^+)$, $22(^{11}B_2^+)$, $23(^{11}B_2H^+)$, $24(^{11}B_2H_2^+)$, $25(^{10}B_2H_5^+)$, $26(^{11}B_2H_4^+)$ and $27(^{11}B_2H_5^+)$ amu [85]. Mass spectra are given in the TG graphs without any scale, since they were not measured quantitatively, but only for the purpose of demonstration that the signals of both B_2H_6 and H_2 were observed.

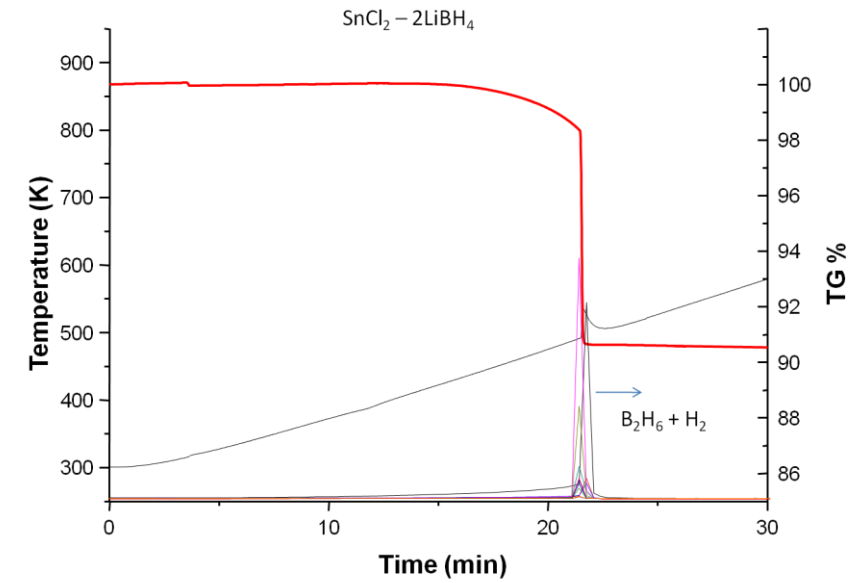
SnCl2 – 2LiBH4
Temperature (K)
TG %
Time (min)
B2H6 + H2

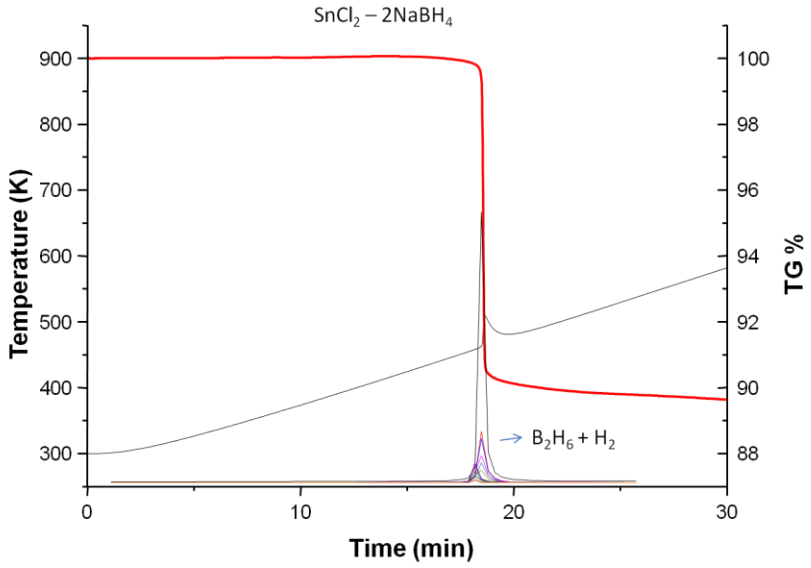
SnCl2 – 2NaBH4
Temperature (K)
TG %
Time (min)
B2H6 + H2

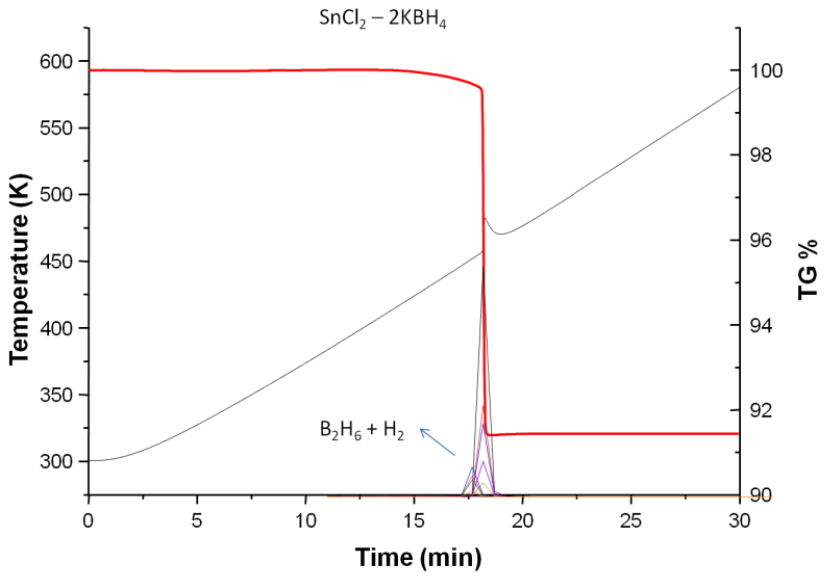

Figure 3.1 TG/DTA/MS diagrams of $SnCl_2 – MBH_4$ (M = Li, Na, K) mixtures

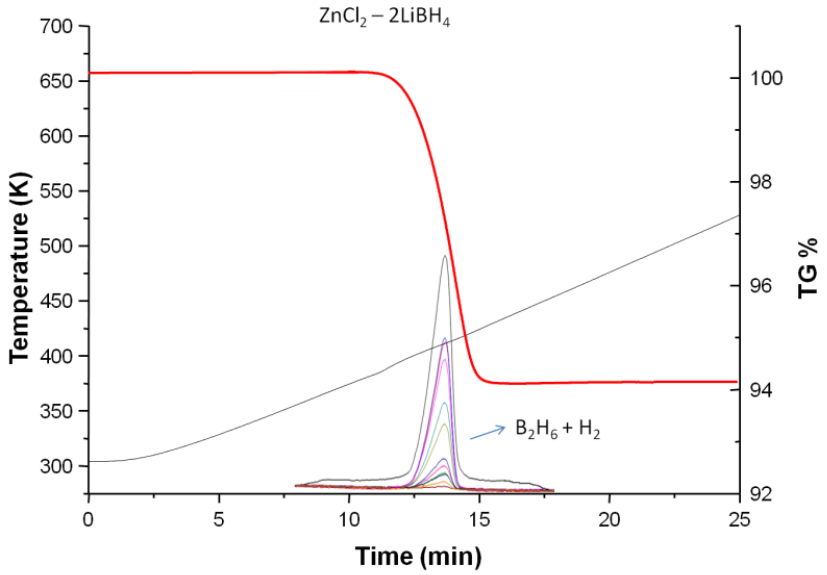

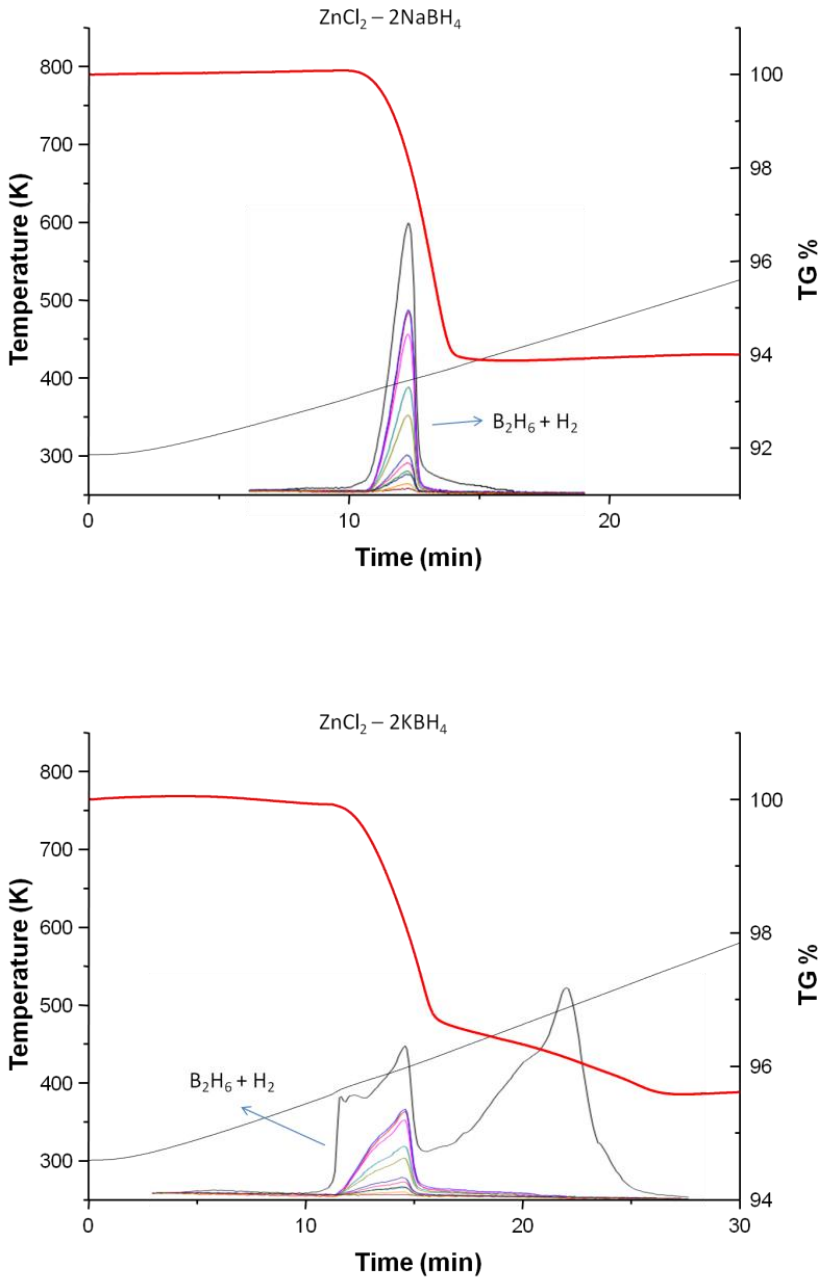

Figure 3.2 TG/DTA/MS diagrams of $ZnCl_2 – MBH_4$ (M = Li, Na, K) mixtures

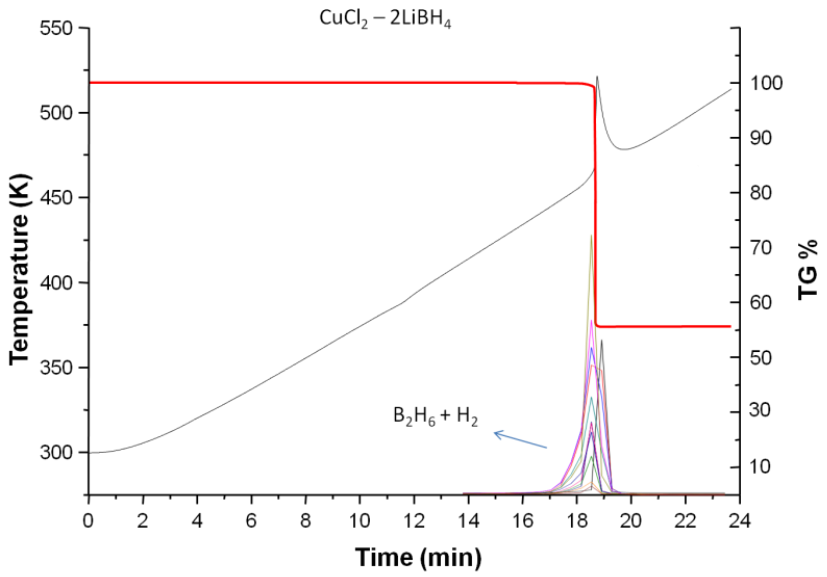
CuCl2 – 2LiBH4
Temperature (K)
TG %
Time (min)
B2H6 + H2
550
500
450
400
350
300
100
90
80
70
60
50
30
10
0
2
4
6
8
10
12
14
16
18
20
22
24

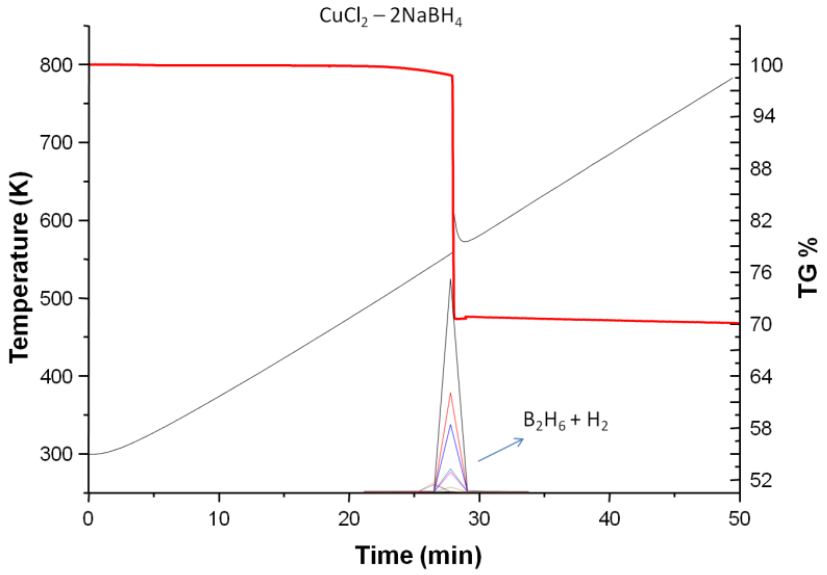
CuCl2 – 2NaBH4
Temperature (K)
TG %
Time (min)
B2H6 + H2
800
700
600
500
400
300
100
94
88
82
76
70
64
58
52
0
10
20
30
40
50

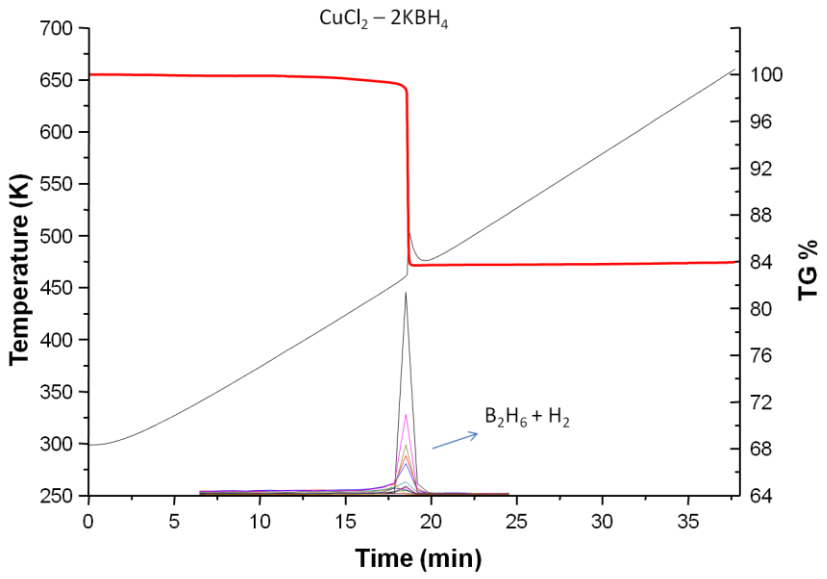

Figure 3.3 TG/DTA/MS diagrams of $CuCl_2$ – MBH_4 (M = Li, Na, K) mixtures

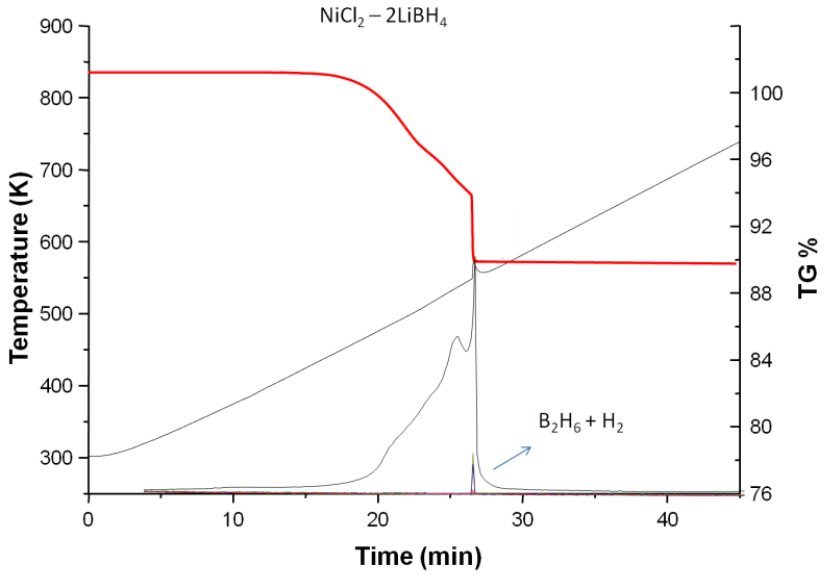

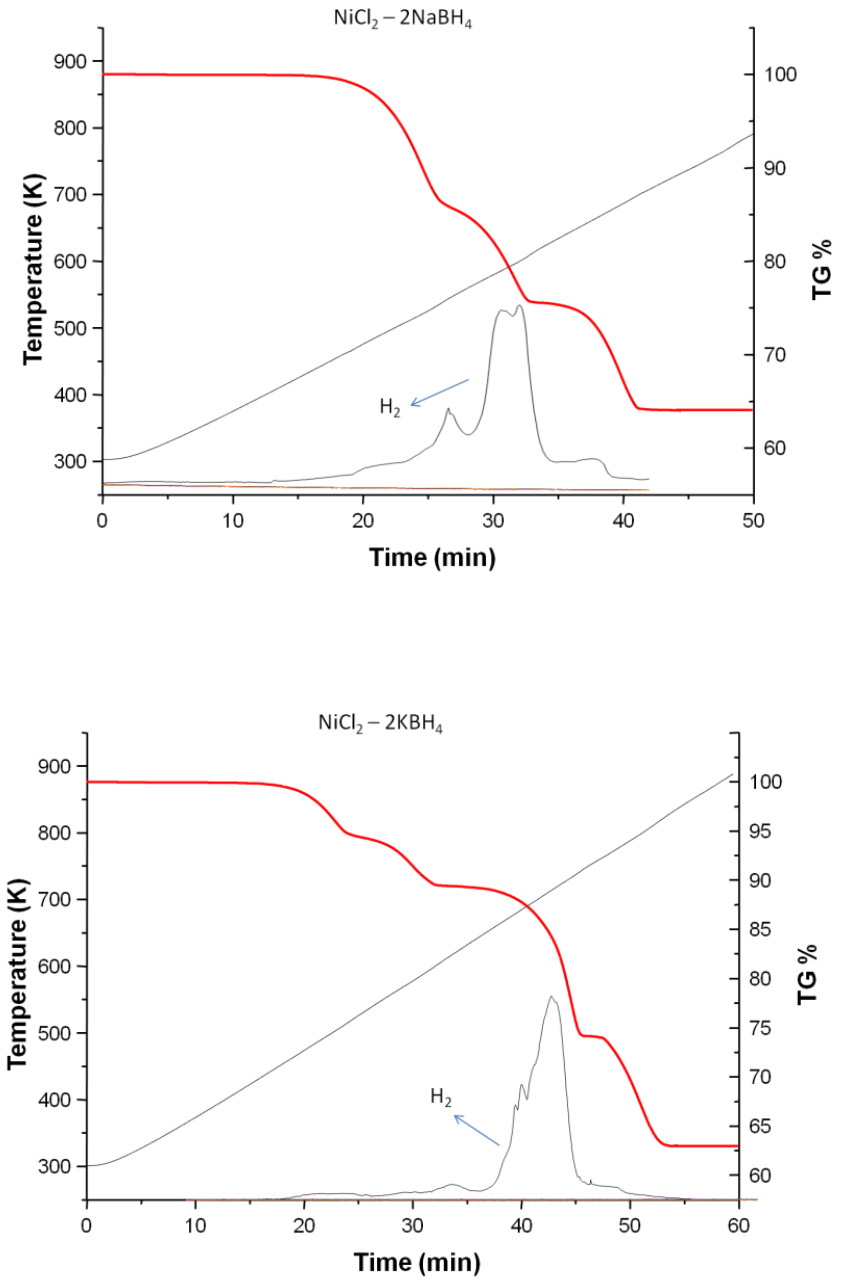

Figure 3.4 TG/DTA/MS diagrams of $NiCl_2 – MBH_4$ (M = Li, Na, K) mixtures

According to TG/MS studies, $CuCl_2$ and $NiCl_2$ mixtures showed vigorous and excessive mass losses upon heating. In the $CuCl_2$ case, MS measurements proved the formation of B_2H_6 while the experimental mass loss (46 %) detected was clearly above the theoretical value for B_2H_6 evolution (15 %). The difference between calculated and experimental values cannot be explained by means of decomposition reactions. For a better understanding following experiment was performed. A 10 g pellet of $CuCl_2 - 2NaBH_4$ mixture was heated under argon flow in a silica tube - equipped with a ground pyrex valve cap with gas inlet and outlet - and above 400 K, a sudden gas evolution took place. The gas evolution was so vigorous that the pyrex cap blew off, together with part of the sample content. The vehemence of the reaction explained the reason of extra mass loss in TG diagrams, as some of the solid product (Cu and M_ACl) erupts from the sample pan during the decomposition process. After this result, It was clear that the gas liberation in the $CuCl_2$ mixtures was hard to control , and thus, not suitable to diborane generation. The XRD diagram of the residue showed peaks of copper and NaCl (Figure 3.5).

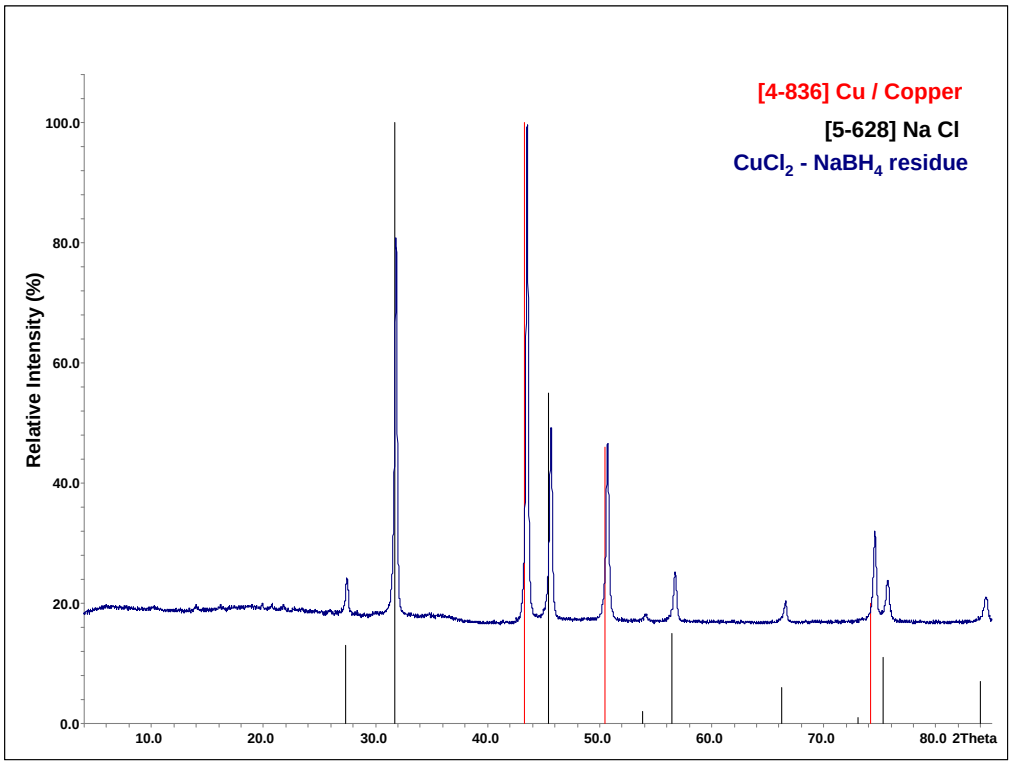

Figure 3.5 XRD diagram of $CuCl_2$ – $2NaBH_4$ mixture after decomposition

Although $NiCl_2$ blends seemed to be a quite promising source for B_2H_6, only reaction of $NiCl_2$ with $LiBH_4$ yielded B_2H_6 in very small amounts. The reason can be explained as Li is harder acid than Na and K according to HSAB (Hard and Soft Acid Base) theory. In addition $[BH_4]^-$ is the softer base with respect to the chloride anion. So, the combination of Li^+ and Cl^- ions to form LiCl is more favored than for all the other alkali metals. In this sense, the blends of $NiCl_2$ with $LiBH_4$ will be generating higher amounts of the intermediate compound $Ni(BH_4)_2$.

$$NiCl_2 + 2LiBH_4 \rightarrow Ni(BH_4)_2 + 2LiCl \rightarrow Ni + B_2H_6 + H_2 + 2LiCl \rightarrow 2B + 3H_2 + Ni + 2LiCl \quad (4)$$

Unlike the predictions, all combinations of $NiCl_2$ with other than lithium borohydrides were decomposed to yield only nickel and hydrogen gas. It is very likely that the catalytic effect of Ni converts $Ni(BH_4)_2$ directly to nickel, boron and hydrogen, so that B_2H_6 is completely missing in the mass spectra. In $LiBH_4$ case we assume that either Ni amount is not enough to catalyze the decomposition of the $Ni(BH_4)_2$ to its constituents, and/or that the formation of diborane occurs in the Li case at lower temperature at which Ni is catalytically not fully active, so that some amounts of B_2H_6 could be detected in mass spectra.

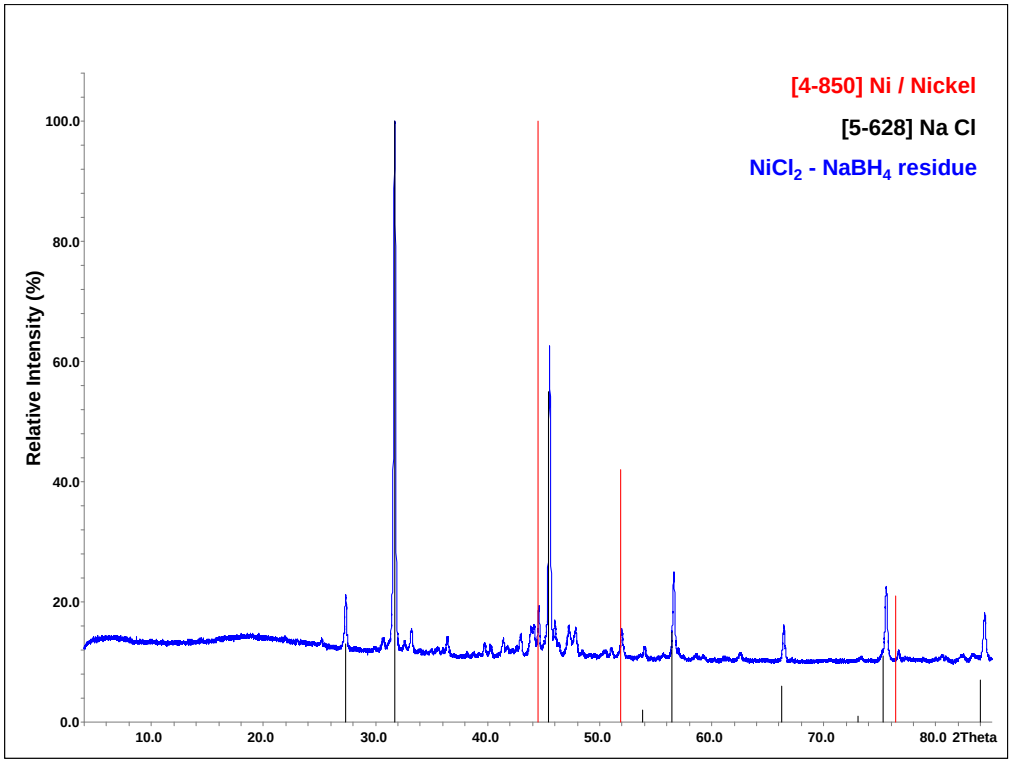

Figure 3.6 XRD diagram of $NiCl_2$ – $2NaBH_4$ mixture after decomposition

TG/MS measurements of the complex borohydrides show that only $SnCl_2$ and $ZnCl_2$ systems, that were prepared under these conditions, can be considered as possible

candidates for "on demand" B_2H_6 production. However, if one compares the amount of B_2H_6 formation for $SnCl_2$ and $ZnCl_2$ blends, due to the higher electronegativity of Sn (X=1.96), the absolute amount of B_2H_6 evolution is 10 % higher according to the following calculations:

$SnCl_2 + 2NaBH_4$: 189,62 g/mol + 75,66 g/mol = 265,28 g
Calculated B_2H_6 amount: 10,43 % of initial mixture (265,28 g) = 27,66 g
Experimental B_2H_6 amount: 10,10 % of initial mixture (265,28 g) = 26,79 g
$ZnCl_2 + 2NaBH_4$: 136,30 g/mol + 75,66 g/mol = 211,96 g
Calculated B_2H_6 amount: 13,05 % of initial mixture (211,96 g) = 27,66 g
Experimental B_2H_6 amount: 11,56 % of initial mixture (211,96 g) = 24,50 g

In another experimental study, we investigated the effect of ball-milling conditions on the gas evolution amounts of $SnCl_2$ and $ZnCl_2$ blends. Table 3.4 shows the results of time and milling speed dependences of B_2H_6 evolution.

Table 3.4 Effect of ball-milling conditions on B_2H_6 evolution

@ 150 rpm	5 min	10 min	15 min	20 min	30 min
$SnCl_2$ – $2NaBH_4$	10.3 %	10.6 %	9.4 %	8.6 %	7.3 %
@ 300 rpm	15 min	30 min	60 min	90 min	105 min
$ZnCl_2$ – $2NaBH_4$	11.8 %	12.1 %	12.3 %	12.3 %	12.4 %

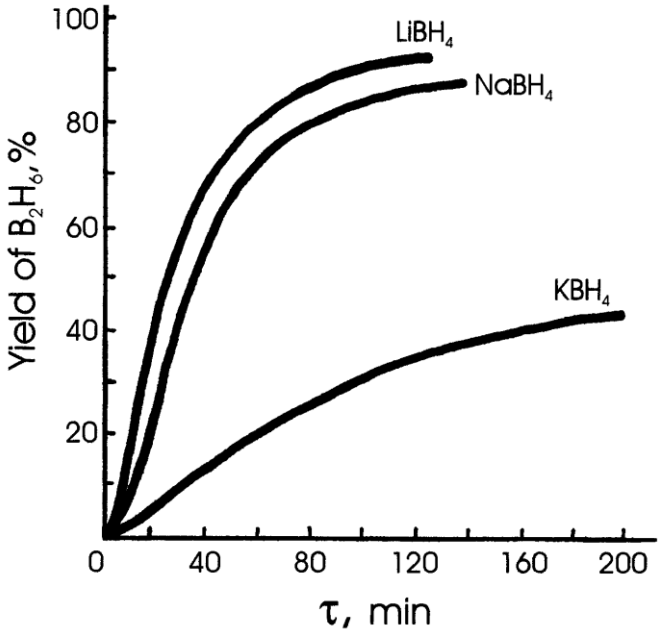

Figure 3.7 Dependencies of B_2H_6 yields in reaction 1 ($SnCl_2 + 2M_ABH_4$) on time and on the nature of MBH_4 [55].

The choice of $NaBH_4$ as the "borohydride precursor" is due to two facts: it gives comparable yield to $LiBH_4$ (and considerably more than KBH_4 (Figure 3.7)) and more importantly it is the cheapest one among alkaline metal borohydrides. $SnCl_2$ has several advantages on $ZnCl_2$ like:

- Sn^{2+} cation has higher electronegativity than Zn^{2+}, and $Sn(BH_4)_2$ is more unstable than $Zn(BH_4)_2$ so it decomposes at lower temperatures
- $SnCl_2$ – $2NaBH_4$ blend yields higher amount of B_2H_6 with respect to $ZnCl_2$ – $2NaBH_4$
- $SnCl_2$ – $2NaBH_4$ can yield up to 96% of theoretical B_2H_6 evolution with 10 minutes of ball-milling at 150 rpm, whereas $ZnCl_2$ – $NaBH_4$ blends reaches these values more than 2 hours of ball-milling process at 300 rpm (Table 3.4).

- $ZnCl_2$ is highly hygroscopic and shows deliquescence behavior whereas $SnCl_2$ is solid and can be kept dry at open atmosphere for a longer time. $ZnCl_2$ needs overnight vacuum drying (at 200 °C) before reactions.

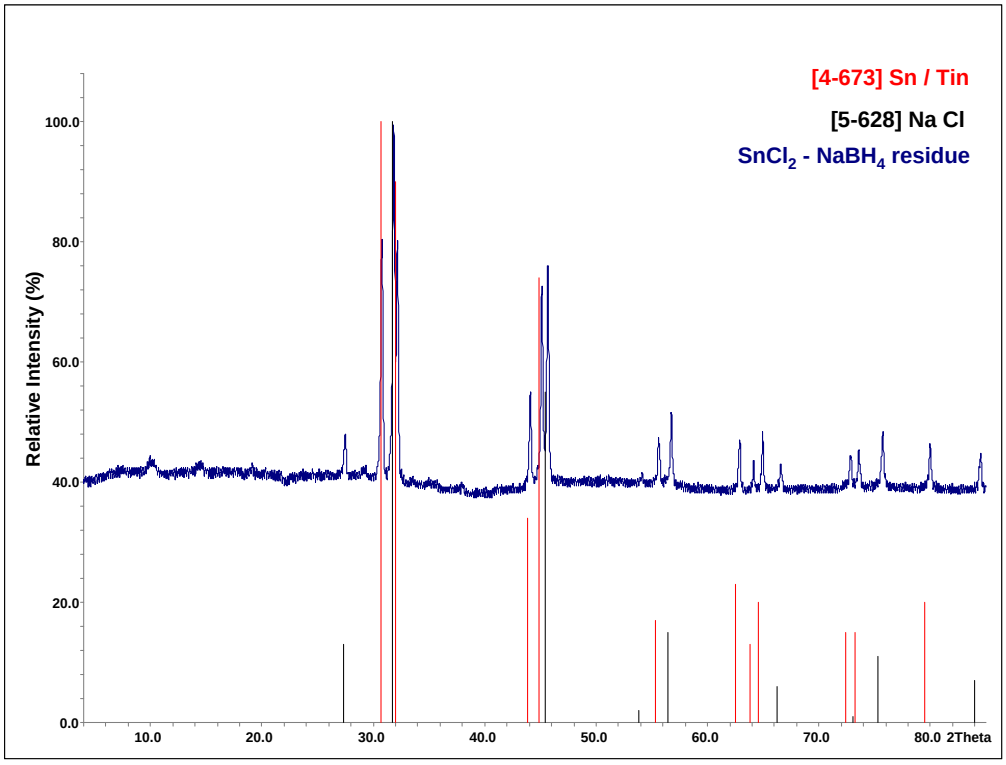

Figure 3.8 XRD diagram of $SnCl_2$ – $2NaBH_4$ mixture after decomposition

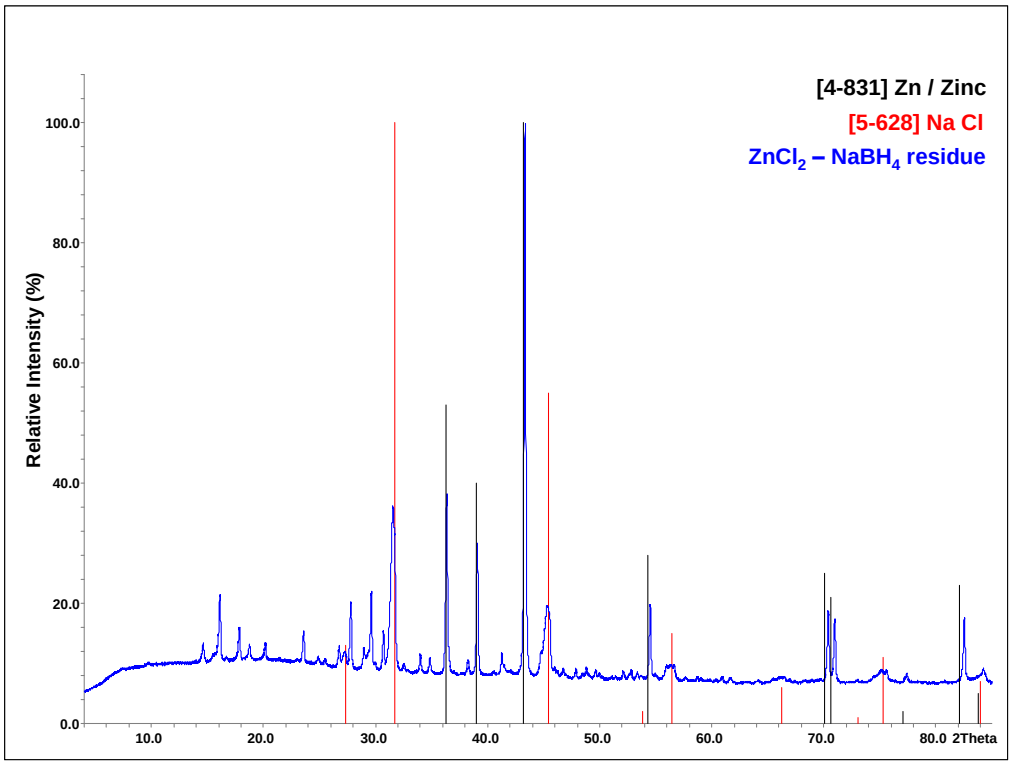

Figure 3.9 XRD diagram of $ZnCl_2$ – $2NaBH_4$ mixture after decomposition

3.2 Optimization of decomposition setup

Details of the decomposition setup were given in the previous chapter. The system was reached after several optimizations on furnace, silica tube dimensions, gas flow rates, powder collection and introduction of reactants into the line. In the below figures former versions of the experimental setup are given.

Figure 3.10 First experimental setup with total yield of less than 10 % of calculated boron amount

Figure 3.11 Second experimental setup with total yield of around 30 % of calculated boron amount

Figure 3.12 Third experimental setup with total yield of around 50 % of calculated boron amount

Figure 3.13 Fourth experimental setup with total yield of less than 10 % of calculated boron amount

Amorphous boron synthesis via pyrolysis of diborane is based on the decomposition of the gas on a suitable substrate at high temperatures. So, it is important to enhance the contact area and retention time of the gas with the substrate, which in our case is a silica tube. It is misleading to use a large diameter silica tube since it creates a temperature gradient inside the tube and does not ensure contact of the gas molecules with the walls. Now we know that longer tubes with smaller diameters show better results than longer and larger diameter tubes. However, one can do further improvements on the latter by changing the geometry of the tube and the direction of the flow so that higher surface contact and

longer retention time can be achieved. Also, independently of the decomposition setup, the gas pyrolysis yield increases with increasing substrate temperature (Table 3.5).

Table 3.5 Temperature dependency of pyrolysis yield for $SnCl_2 – 2NaBH_4$ blend

Pyrolysis Temperature (K)	**Reaction Yield (%)**
973	~71
1073	~76
1173	~80
1273	~85

Vertical tube furnace was the correct configuration as gas flows vertically while decomposing to its components and it was easier to collect the powder material. It was difficult to control the gas evolution rate of the reactant blend; however adjustment of carrier gas (W5 mixture) flow was possible. Optimum gas flow was found 500 ml/min for this experimental setup.

Pyrolysis of B_2H_6 yielded solid amorphous boron in very fine powder form, so it was mandatory to use multistage powder collector arrangement. We used a 3 liters rotavap flask and a long glass tube that increases the retention time of powders inside the collector.
Reactant blend was heated in a round bottom flask heater. Rapid heating to 373 K was used for starting gas evolution and temperature was raised to 573 K gradually as gas flow decreased. As a result of all these optimizations final version of the decomposition setup was reached (Figure 3.14) with 85 % yield of calculated boron amount.

Figure 3.14 Final version of the experimental setup with total yield of around 85 % of calculated boron amount

In the final version of the decomposition setup, total efficiency was calculated by using the results obtained from four experiments with different reactant loadings. Table 3.6 shows the summary of these experiments.

Table 3.6 Yields of $SnCl_2$ – $NaBH_4$ systems at 1273 K pyrolysis temperature

Experiment #	Blend amount	Calculated Boron	Experimental Boron	Yield (%)
DBE001	26.5 g	2.16 g	1.81 g	83.8
DBE002	13.2 g	1.08 g	0.95 g	87.9
DBE003	39.8 g	3.22 g	2.67 g	82.9
DBE004	59.7 g	4.86 g	4.10 g	84.3
Average yield				84.7 (±2.2)

3.3 Characterization of amorphous boron

Amorphous boron synthesized via pyrolysis of B_2H_6 was characterized using the following instrumental techniques:

- Structural analysis : p-XRD, electron diffraction
- Elemental analysis : ICP – OES for Boron content, LECO for O/N, EDX
- Thermal analysis : TG/DTA/MS
- Particle size and surface area analysis : DLS, BET

Powder XRD and electron diffraction analyses of boron samples revealed that no long-range order was formed during the synthesis and they were in amorphous state. This observation is in good agreement with the reports [3] in that synthesis was achieved below the crystallization temperature of amorphous boron. In both p-XRD and electron diffraction, characteristic halos of amorphous state were clearly observed.

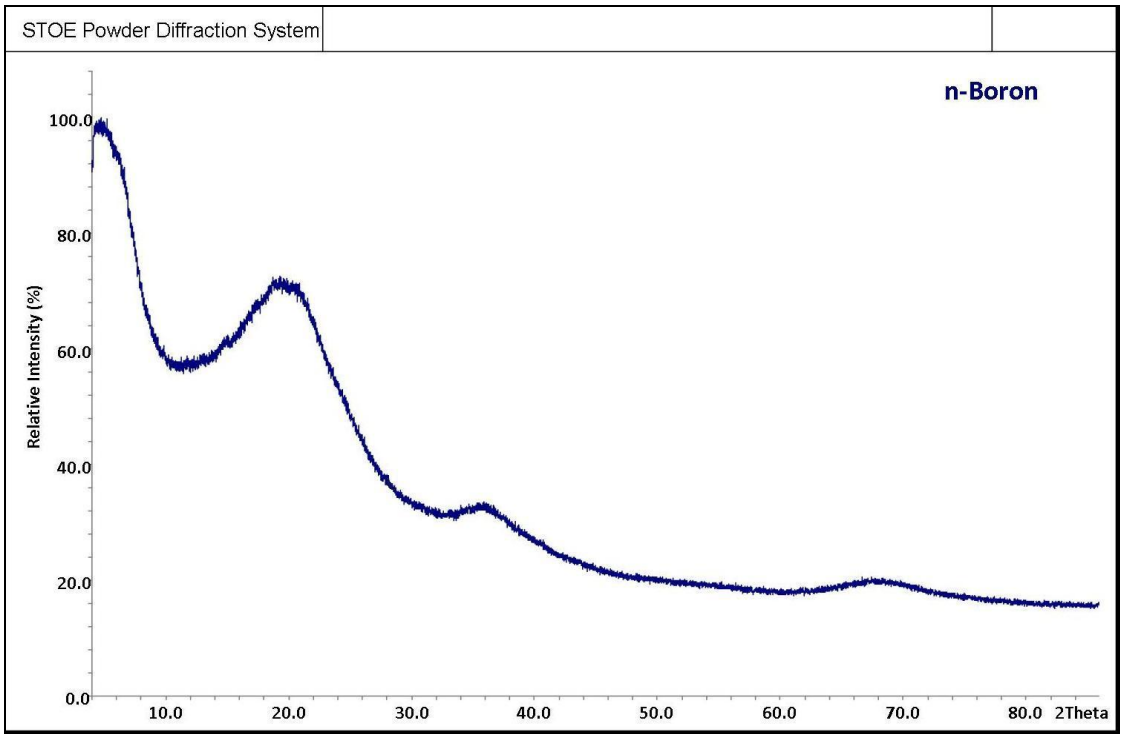

Figure 3.15 Powder XRD diagram of amorphous boron

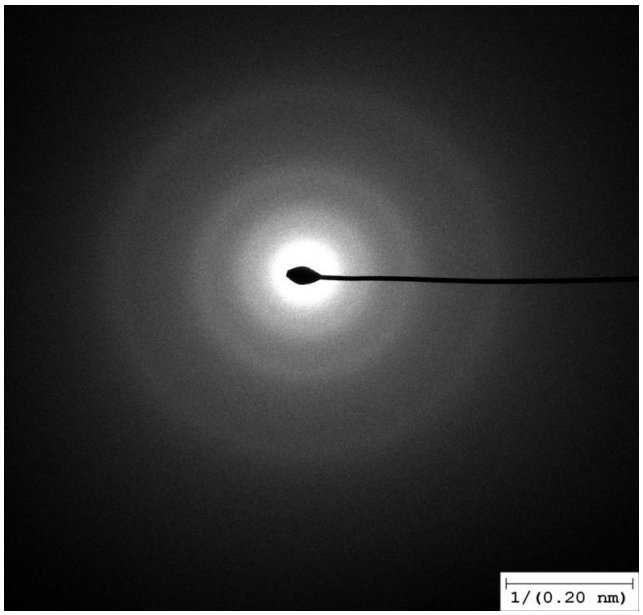

Figure 3.16 Electron diffraction pattern of amorphous boron

Elemental analyses were carried out to investigate the chemical content of amorphous boron. As described previously, the synthesis method based on the pyrolysis of B_2H_6, so in theory the only solid product should be the amorphous boron. However, any possible leakages from ambient atmosphere into the reaction medium might cause formation of oxide and nitride layer on the surface of amorphous boron. It is well known that boron has very high affinity to oxygen and it is almost inevitable to avoid native oxide layer formation when the material is exposed to oxygen atmosphere. On the other hand, boron nitride formation occurs at elevated temperature in the presence of nitrogen. Oxygen and nitrogen are the main possible impurities in boron samples. Also, carbon may be found in the chemical analysis which is assumed to be originated from the impurities of reactants ($NaBH_4$).

Boron content was measured with ICP – OES and confirmed by conventional acid – base titration. Oxygen and nitrogen contents were measured with LECO TCH600 elemental analysis device. Carbon analysis was done by Prof. René Flükiger in University of Geneva - Switzerland with LECO C/S/H (CS230) analyzer. Also, EDX measurements confirm the results obtained in chemical analyses.

The following results were obtained from the amorphous boron samples that were prepared from the decomposition of $SnCl_2 – 2NaBH_4$ blends and the resulting B_2H_6 was pyrolyzed at 1273 K. Three sets of experiments were performed. In the first one, solid product was collected in the open air and sent to analyses. In the second one, powder collector flask was transferred into argon filled glove box and all sample preparations and handling were done under controlled atmosphere. In the third one, pyrolysis setup was evacuated and purged with W5 mixture several times to make sure that oxygen and nitrogen presence were minimized and after the reaction, the same procedure was employed for the second time. EDX analysis was performed only for the first sample.

Table 3.7 Chemical analyses results of amorphous boron samples

Component	**1st set**	**2nd set**	**3rd set**
Boron (wt%)	97.3 (±0.1)	98.5 (±0.1)	99.0 (±0.1)
Oxygen (wt%)	1.38 (±0.05)	0.66 (±0.05)	0.45 (±0.05)
Nitrogen (wt%)	1.21 (±0.03)	0.73 (±0.03)	0.42 (±0.03)
Carbon (wt%)	0.18(±0.03)	0.15 (±0.03)	0.08 (±0.03)
BET Surface Area (m^2/g)	35.0 (±0.5)		

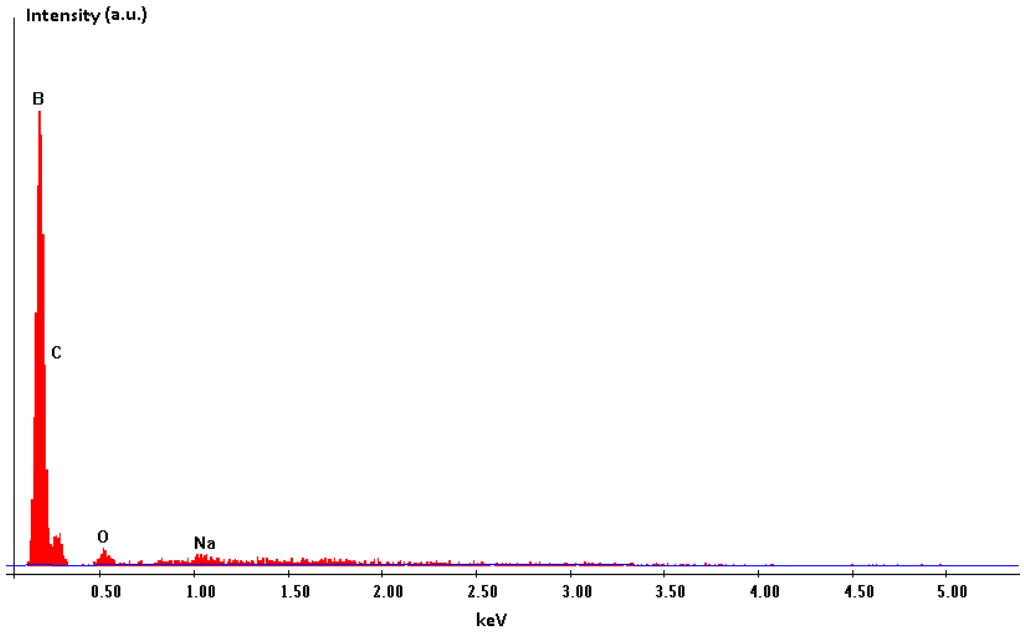

Figure 3.17 EDX analysis of amorphous boron

3.4 Particle Size Determination

Particle size distribution of amorphous boron samples were measured with Malvern Instruments Nano – S Zetasizer device. To monitor the dependency of particle size on the reaction conditions, four systematic pyrolysis experiments were conducted by varying the decomposition temperature of B_2H_6 in the tube furnace while carrier gas flow rate (500 ml/min) and reactant ($SnCl_2$ + $2NaBH_4$) mass of the mixture were kept constant (10 g). Table 3.8 shows the result of the experiments.

Table 3.8 Particle size dependency of amorphous boron on the pyrolysis temperature

Temperature (K)	Intensity mean (nm)	Polydispersity Index
973	188.9 ± 10.8	0.102 ± 0.037
1073	222.4 ± 37.2	0.141 ± 0.033
1173	253.7 ± 36.4	0.144 ± 0.035
1273	268.9 ± 34.2	0.132 ± 0.039

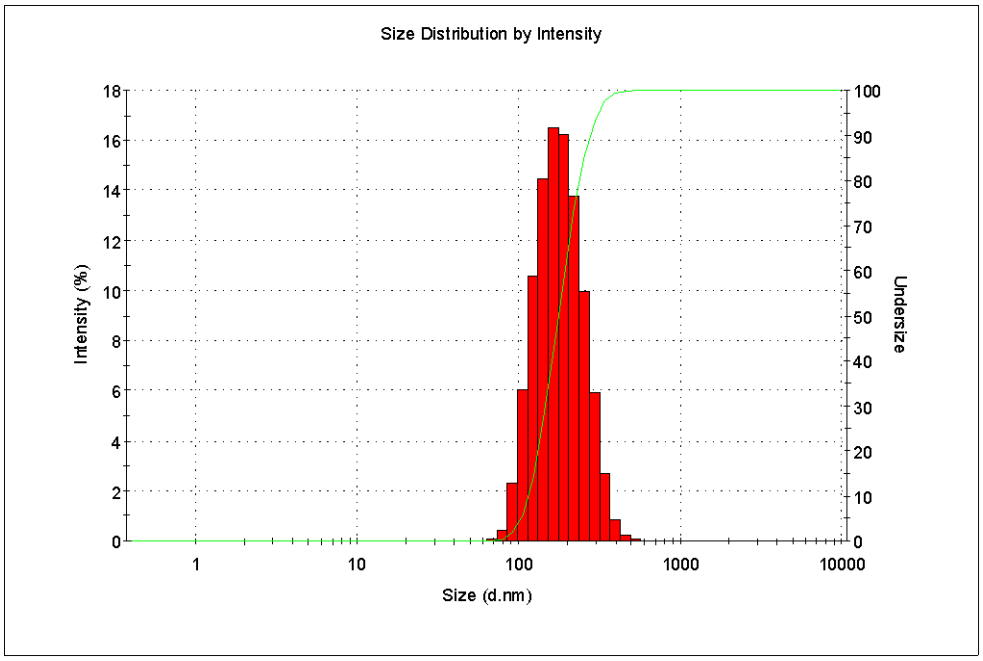

a. Amorphous nano boron (*n*-boron) – pyrolysis temperature 973 K

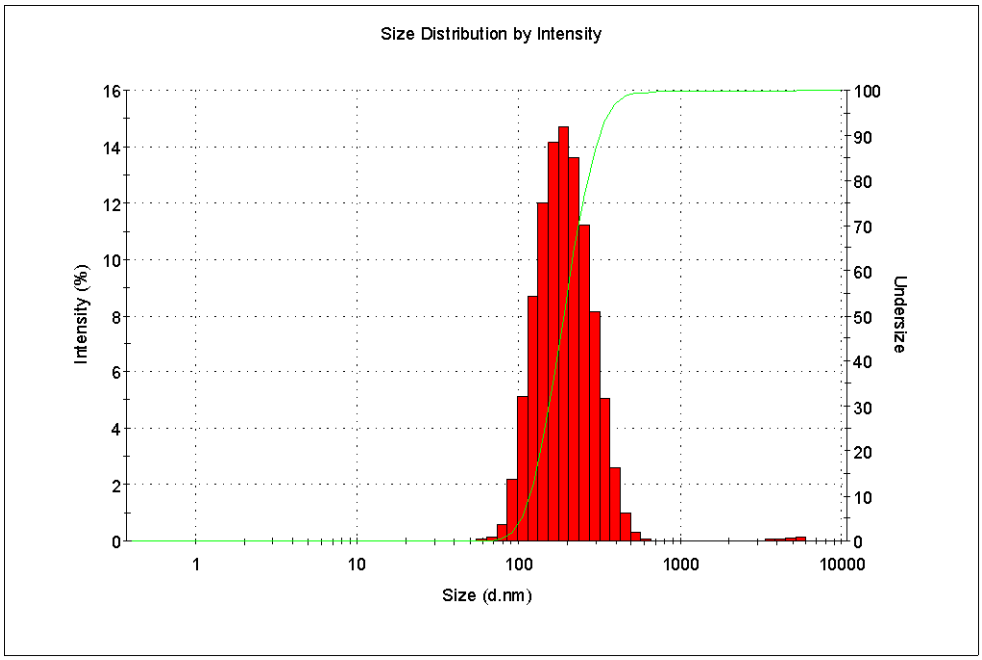

b. Amorphous *n*-boron – pyrolysis temperature 1073 K

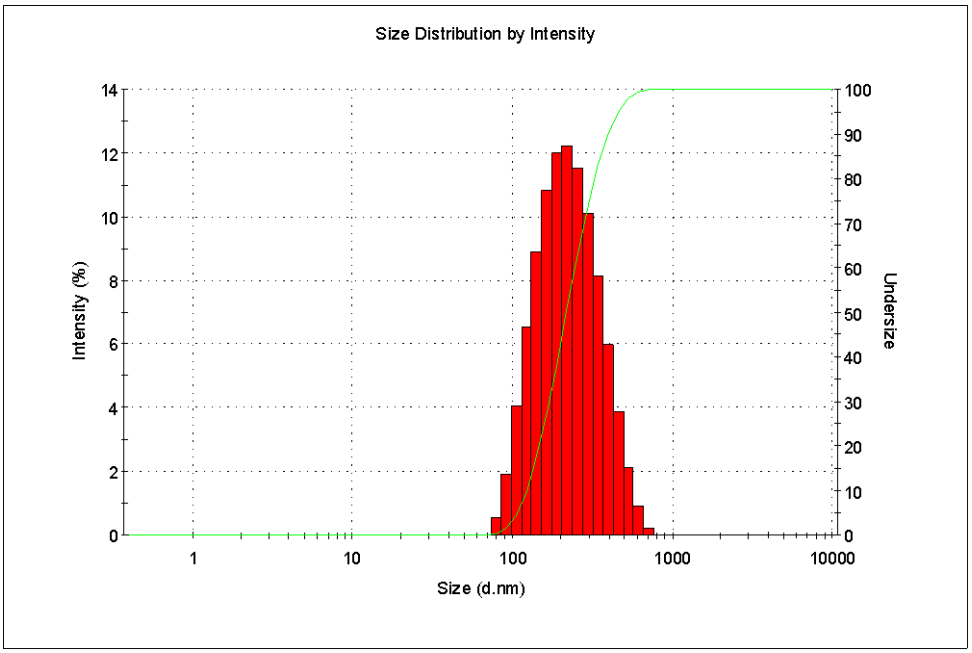

c. Amorphous *n*-boron – pyrolysis temperature 1173 K

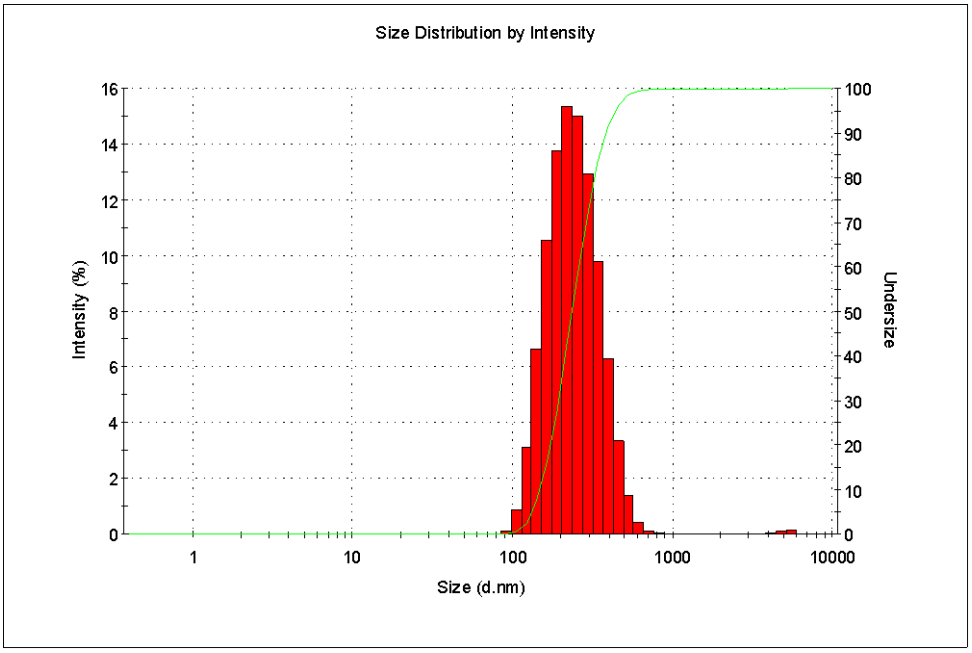

d. Amorphous *n*-boron – pyrolysis temperature 1273 K

Figure 3.18 Size distribution by intensity graphs for amorphous nano boron

The results of Table 3.8 show that there is a trend of increase in the particle size by rising the pyrolysis temperature. The explanation of this average particle size distribution is based on the principles of gas phase nanoparticle synthesis. As our procedure is a gas phase nucleation, once particles are formed in the gaseous phase, they coagulate at a rate which is proportional to the square of their concentration. At sufficiently high temperatures, coalescence (sintering) is thermodynamically more favorable than coagulation and they nucleate to form spherical particles. Once nucleation occurs, particle growth begins rather than further nucleation. At lower temperatures, where sintering is less effective, loose agglomerates with quite open structures are formed [86,87]. According to this explanation, at high pyrolysis temperatures particles were better sintered and nucleated larger spherical cores, whereas at low temperatures the sintering was less effective and smaller particles were formed.

Table 3.8 also shows the polydispersity index value of the particles, which is the measure of how much particle size differ through the sample. As the PDI values are close to 0.1, it means there is a narrow particle size distribution, which indicates that majority of the particles have size close to the average value (intensity mean) and they have identical shapes. Of course, since this measurement give a distribution, it is possible to observe particles smaller than 50 nm and larger than 300 nm. It is known that particle size measurements of DLS may give higher values than the actual diameter due to the formation of hydration layer on the surface of spherical boron particles.

TEM and SEM measurements were taken to observe the particle size distribution and the shape. Figure 3.19 shows the TEM images of amorphous boron samples synthesized at 1173 K.

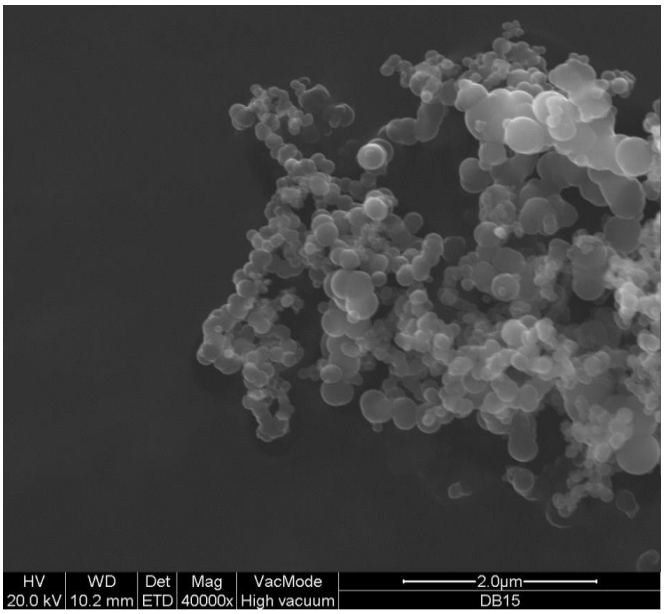
HV
20.0 kV
WD
10.2 mm
Det
ETD
Mag
40000x
VacMode
High vacuum
2.0µm
DB15

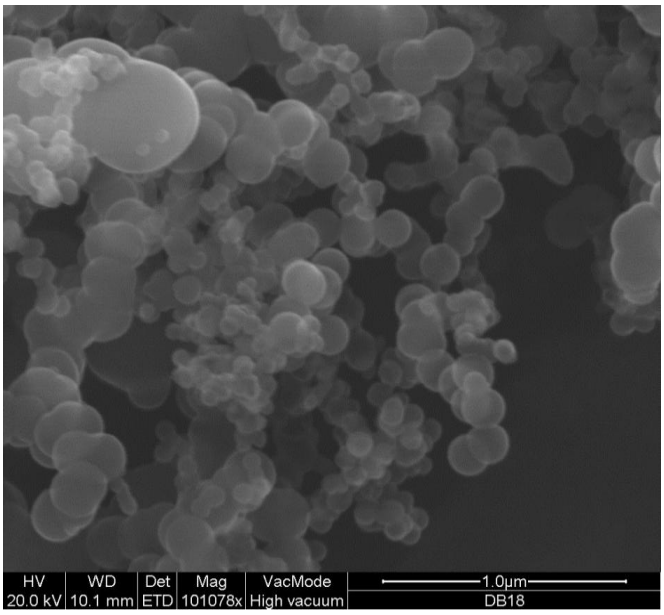
HV
20.0 kV
WD
10.1 mm
Det
ETD
Mag
101078x
VacMode
High vacuum
1.0µm
DB18

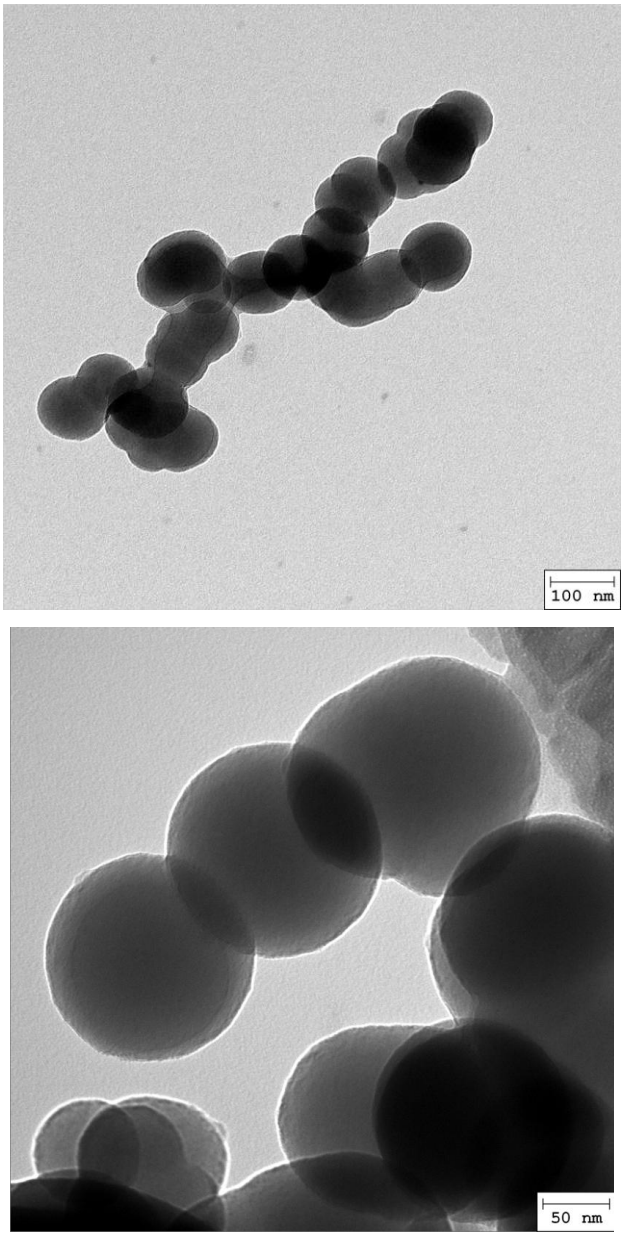

Figure 3.19 TEM images of amorphous boron samples

TEM images revealed that amorphous boron particles are in spherical shape (aspect ratio >0.9) having the size less than 300 nm. To better clarification the particle size

distribution complementary SEM imaging was conducted on the samples that were also used in the DLS measurements. Figure 3.20 to 3.23 show the SEM images of the amorphous boron samples which were synthesized at different temperatures.

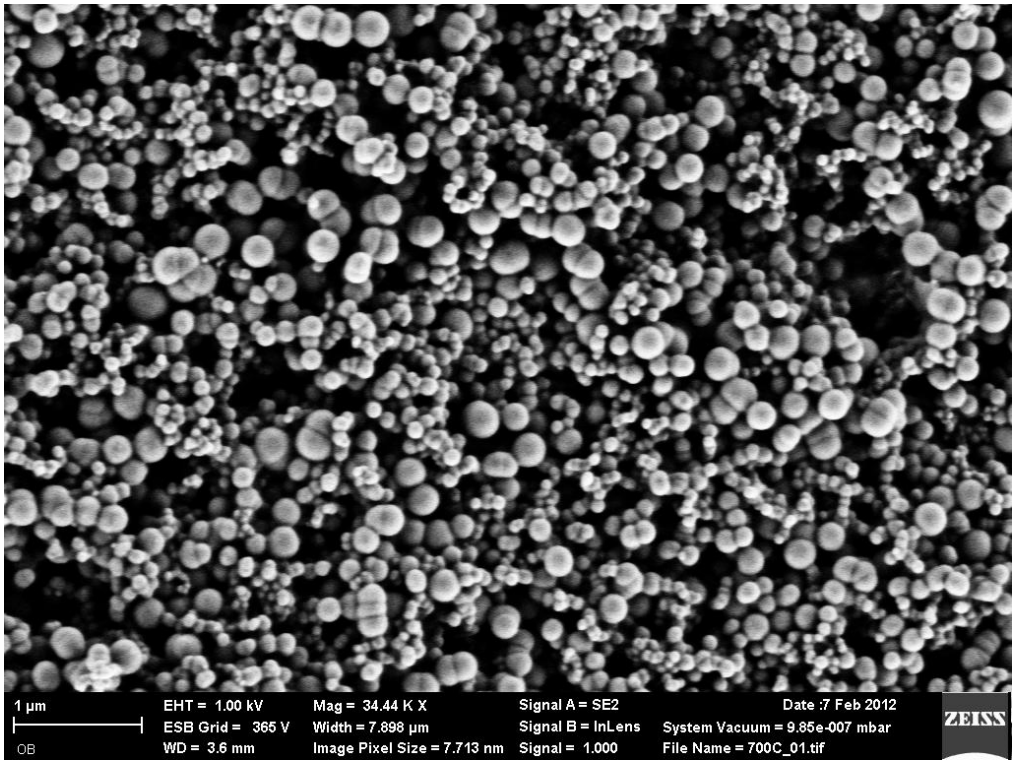

Figure 3.20 SEM image of amorphous boron synthesized at 973 K

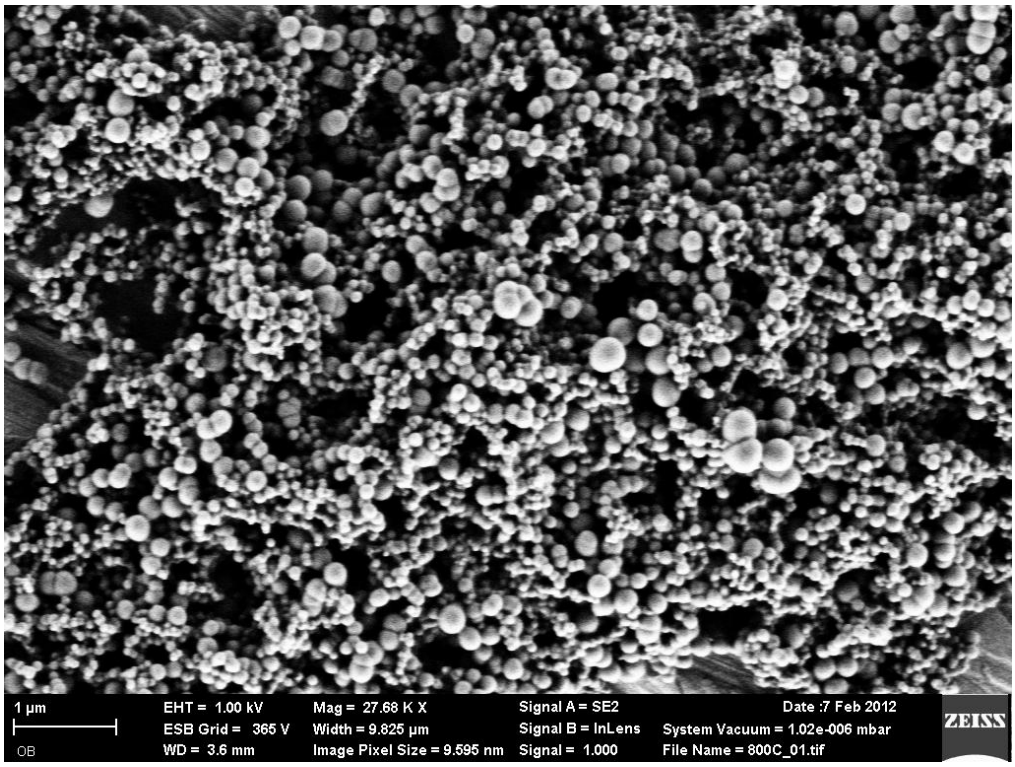

Figure 3.21 SEM image of amorphous boron synthesized at 1073 K

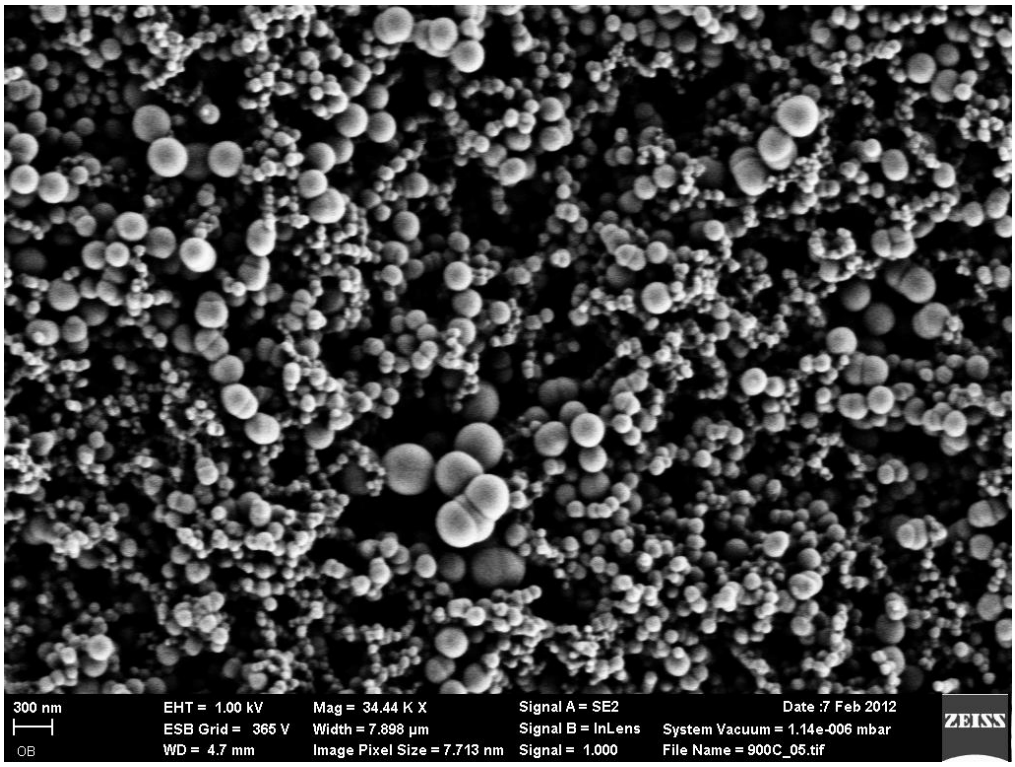

Figure 3.22 SEM image of amorphous boron synthesized at 1173 K

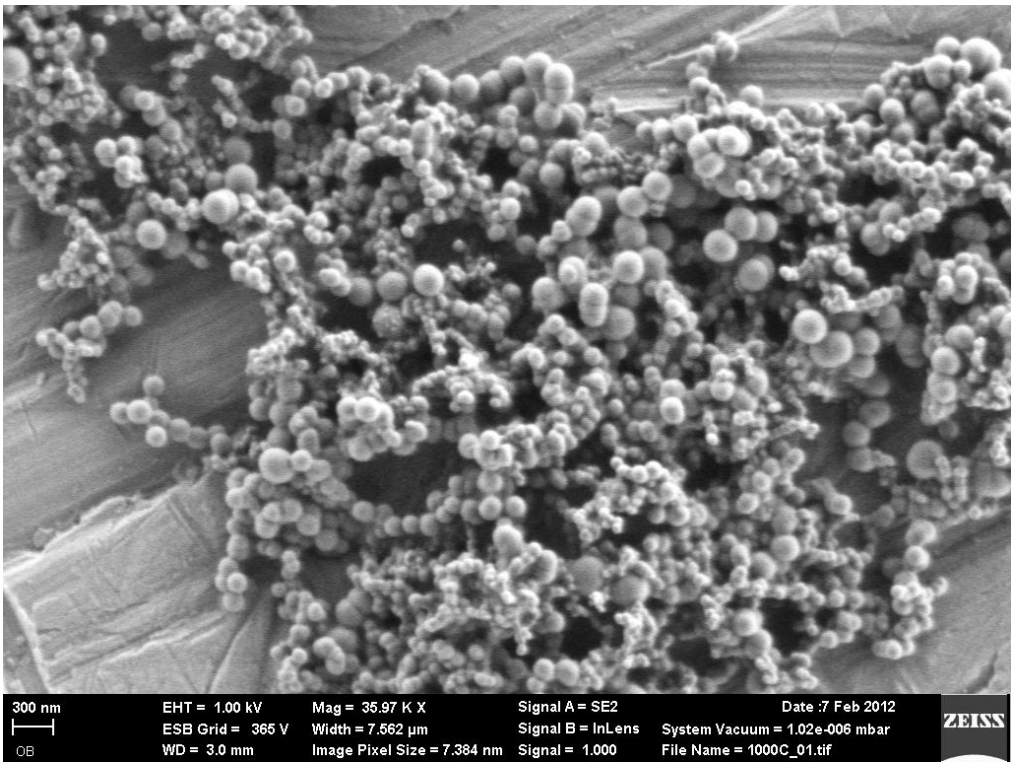

Figure 3.23 SEM image of amorphous boron synthesized at 1273 K

SEM images also show the formation of spherical boron nanoparticles and reveal that there is a distribution in the particle size. Although it is difficult to depict an average size value from the SEM images, it is clear that particles are in the range of 50 – 300 nm for all pyrolysis temperatures which is also in good agreement with the DLS results.

3.5 Surface Area Measurements

Surface area of nano amorphous boron was measured via BET technique in Koç University. The measurement indicates that nano boron (*n*-boron) powder has around 35 m^2/g specific surface area which is almost twice as much as the highest surface area measured for any commercially available amorphous boron. Table 3.9 gives the

comparative particle size and surface area values of nano amorphous boron and commercial amorphous boron.

Table 3.9 Particle size and surface area values of different amorphous boron grades [101]

Material	**Boron (wt%)**	**Magnesium (wt%)**	**Particle Size (nm)**	**Surface area (m^2/g)**
Nano-boron	>98.5	-	50 – 300	>35
Grade 1	95 – 97	<0.8	<1000	>10
Grade 2	90 – 92	<6.0	<800	>18
Grade 3	85 – 86	<12.0	<1400	>5

According to the results given in Table 3.9, amorphous nano boron has the lowest particle size and highest specific surface area among all commercial boron grades. High surface area enhances its reactivity and since it is not containing any magnesium impurities it is easier to control the reaction stoichiometry and obtain higher purity products. The effect of its high purity and high surface area on a commercial product will be given at the end of this chapter on the synthesis and magnetic characterization of superconducting MgB_2 preparation.

DTA analyses were performed to observe the effect of surface area on the thermal properties of amorphous boron samples. The samples were heated under air flow (burned) from room temperature to 1273 K. Figure 3.24 shows the DTA diagram of the experiment.

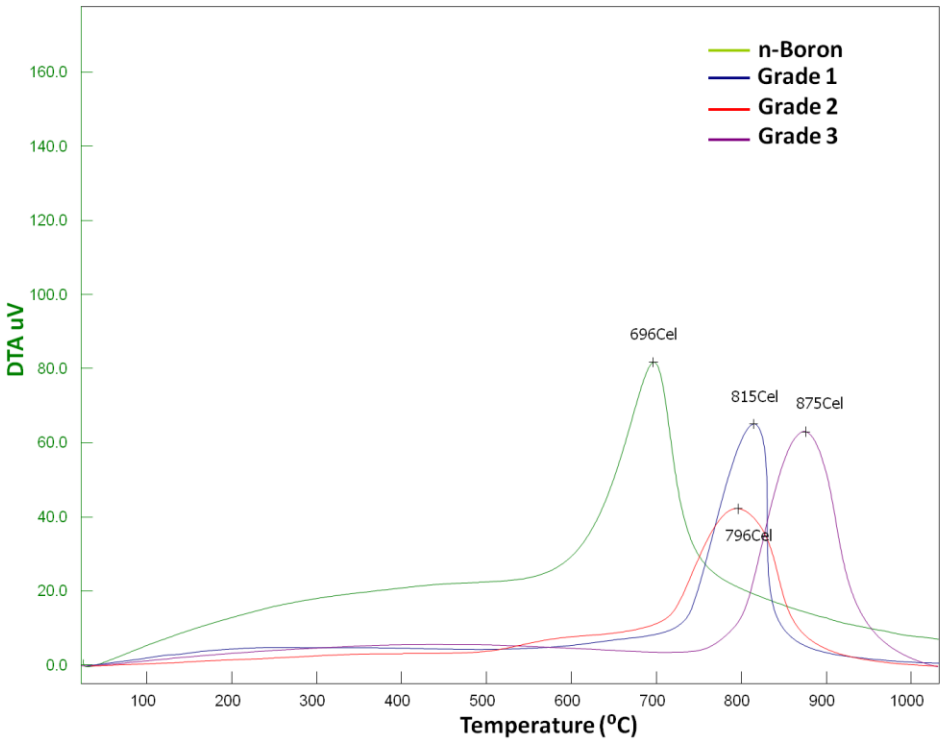

Figure 3.24 DTA diagram of the heating of amorphous boron samples under air flow

DTA analysis supports the findings of surface area and particle size measurements. Since heating under the air flow in DTA is basically the combustion of amorphous boron specimen, the powders with smaller particle size and higher surface area start burning at lower temperatures. The trend in the onset temperatures of burning was as expected, meaning that nano boron started the first and Grade 3 was the last. It is important to note that nano boron starts burning even below 373 K and peaks around 973 K. Area under DTA curve gives the heat of combustion indirectly, so in comparison amorphous nano boron released more energy than commercial grades which can be referred to its high boron content (purity). Table 3.10 gives the calculated energy values by integrating the areas under the DTA curves.

Table 3.10 Comparison of heats of combustion calculated from DTA curves

Material	**n-Boron**	**Grade 1**	**Grade 2**	**Grade 3**
Surface Area (m^2/g)	35	10	18	5
ΔH_{comb} (J/g)	9909	5777	6471	6902

It is important to underline that the above given DTA results do not give the exact heats of combustion. These results are given to verify that nano sized spherical boron powder is highly reactive upon heating. The commercial boron samples do not reveal a direct correlation between surface area and heat of combustion, since the purity of the samples (e.g. boron contents) are different. One should also take into account that commercial boron samples contains up to 12 wt % magnesium. Since the heat of combustion per unit mass for boron is almost 2.5 times higher than for Mg, the results obtained in DTA are clearly affected by the magnesium impurity

3.6 Crystallization of amorphous nano boron

Crystallization experiments were performed by direct heating of amorphous nano boron powders in a tube furnace (<1773 K) and in an induction furnace. Conventional tube furnace was limited to 1773 K and required 4 hours of heating – 6 hours of annealing and presence of inert atmosphere to avoid oxidation of samples. However, induction furnace can operate under vacuum supplying rapid heating up to 2773 K in less than one minute and can be annealed up to one hour. Amorphous nano boron was pressed into a pellet form and filled in a BN crucible and both were placed in a tantalum crucible to obtain highest heating rate, as tantalum can withstand temperatures up to 3273 K prior to its melting point. Figures 3.25 and 3.26 give the XRD patterns of crystallization experiments.

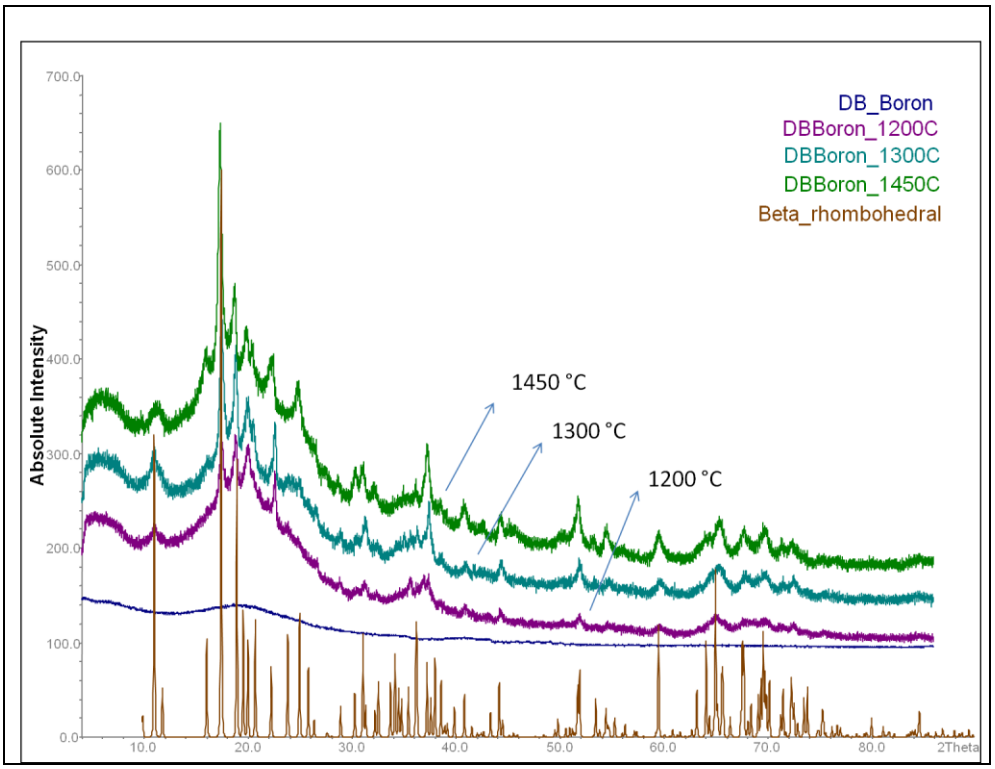

Figure 3.25 Crystallization of n-boron in tube furnace under Ar flow in BN boat

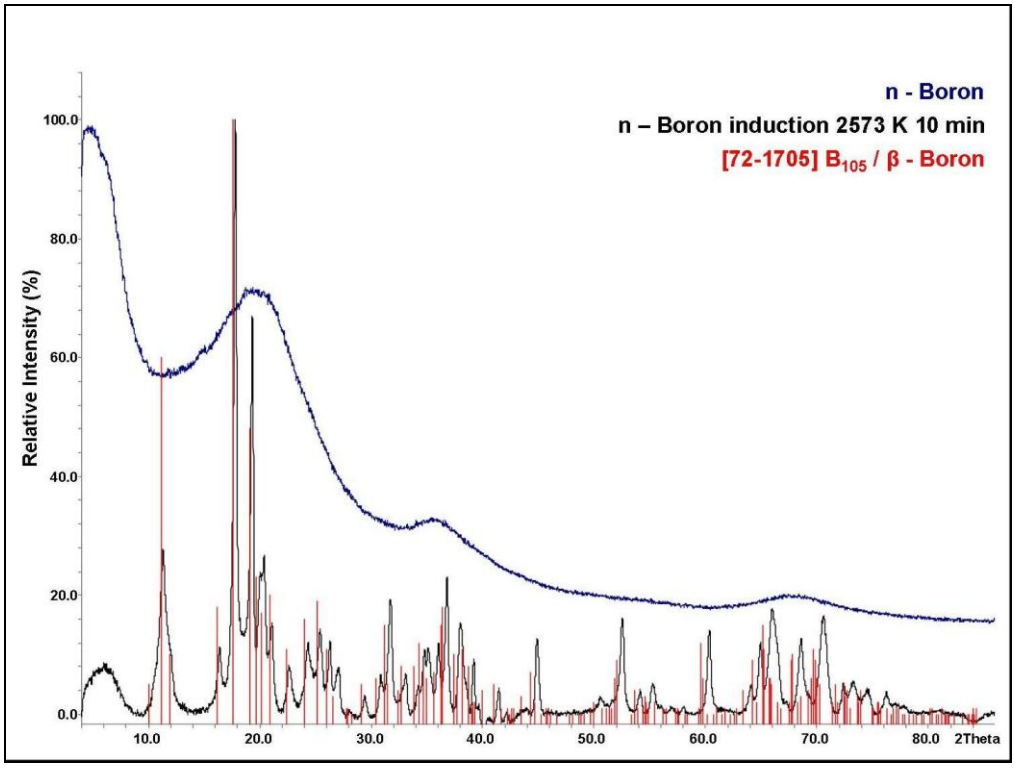

Figure 3.26 Crystallization of n-boron in induction furnace under vacuum

As expected, the crystallization experiments yielded β – rhombohedral form of elemental boron since it is the thermodynamically most stable and favored phase. Peaks of crystalline form were observed above 1473 K which became sharper as the annealing temperature increased (Figure 3.25). High temperature treatment with induction furnace resulted better crystallinity in a shorter heating time with respect to the conventional tube furnace. Moreover, it seems to be a practical way of synthesizing crystalline boron in small scale. Induction furnace experiments were carried out at 2573 K for 10 minutes in a single run. The percent of crystallinity was not investigated here, however, it is known that repetition of the described heat treatments would increase the percentage of crystalline portion of the elemental boron.

The oxygen impurity in the amorphous nano boron samples are originated from thin layer of surface oxide (B_2O_3) which is known to evaporate above 1773 K [28,29]. As induction furnace experiments were conducted under vacuum and above evaporation temperature of the oxide layer, it was possible to remove oxide impurity. Oxygen content of the samples was measured before and after high temperature treatments both with induction under vacuum and tube furnace under argon flow.

Table 3.11 Change of oxygen content after high temperature heat treatment

Sample	Conditions	% Oxygen
n – Boron	-	1.47
DBIC001	2573 K – 1 min	0.85
DBIC002	2573 K – 5 min	0.44
DBIC003	2573 K – 10 min	0.32
DBTC003	1723 K – 360 min	1.35

Oxygen content analysis revealed that high temperature treatment of amorphous nano boron samples decreased the oxygen amount by evaporating the surface oxide layer and causing crystallization of the samples. It is very likely that temperature of the tube furnace was not sufficiently high to remove a considerable amount of oxide layer, while the induction process was run at approximately 800 K higher temperatures and in vacuum.

3.7 Characterization of MWIP

The basic knowledge on microwave induced plasmas is available from the literature [REF]. What was missing was a precise characterization of the species formed in the different gas plasma in dependency of applied power, temperature and gas flow rate. For this purpose, optical emission spectra and temperature measurements of hydrogen and argon plasmas were conducted. The data were quite helpful to develop the current process. Temperature measurements were done employing a K-type (chromel – alumel, 273 to 1273 K temperature ranges) thermocouple and a data acquisition system which were connected to a computer. The present plasma system is defined as “cold plasma”, meaning that it is below or around 2273 K and it was considered that the K-type thermocouple would be appropriate to measure the temperature inside the plasma chamber. To avoid the interference with microwaves, the thermocouple was inserted in a small diameter silica tube and placed into the plasma chamber. By this protection, formation of arcs due to the interaction of metal and microwave field was avoided. Figure 2.10 shows the experimental setup used for temperature sensing. Figures 3.27 and 3.28 show the results of temperature measurements taken for argon and hydrogen plasmas. For each gas 800, 1000 and 1200 W power values were used by varying the gas flow rates and data were recorded.

We investigated and measured gas pressure inside the plasma chamber with respect to flow rates. Pressure values and flow rates are corrected by using gas correction factors (GCF) for argon and hydrogen gases [88]. Table 3.12 gives the GCF coefficients and corrected values for argon and hydrogen.

Table 3.12 GCF corrected pressure and flow rates

Flow rate of x gas Flow rate of N_2 x GCF_{gas} GCF_{Ar} : 1,39 GCF_{H2}: 1,01		**Pressure of x gas** Pressure of N_2 / GCF_{gas} GCF_{Ar} : 1.29 GCF_{H2} : 0.46	
Ar flow	**N_2 flow**	**Ar pressure**	**N_2 pressure**
10	7,2	0,290	0,374
20	14,4	0,423	0,546
30	21,6	0,529	0,683
40	28,8	0,622	0,803
50	36,0	0,706	0,911
60	43,2	0,783	1,01
70	50,4	0,853	1,1
80	57,6	0,922	1,19
90	64,7	0,984	1,27
100	71,9	1,047	1,35
110	79,1	1,109	1,43
H_2 flow	**N_2 flow**	**H_2 pressure**	**N_2 pressure**
10	9,9	1,398	0,643
20	19,8	2,435	1,12
30	29,7	3,435	1,58
40	39,6	4,500	2,07
50	49,5	5,652	2,6
60	59,4	6,870	3,16

70	69,3	8,174	3,76
80	79,2	9,696	4,46
90	89,1	11,370	5,23
100	99,0	13,326	6,13
110	108,9	15,891	7,31

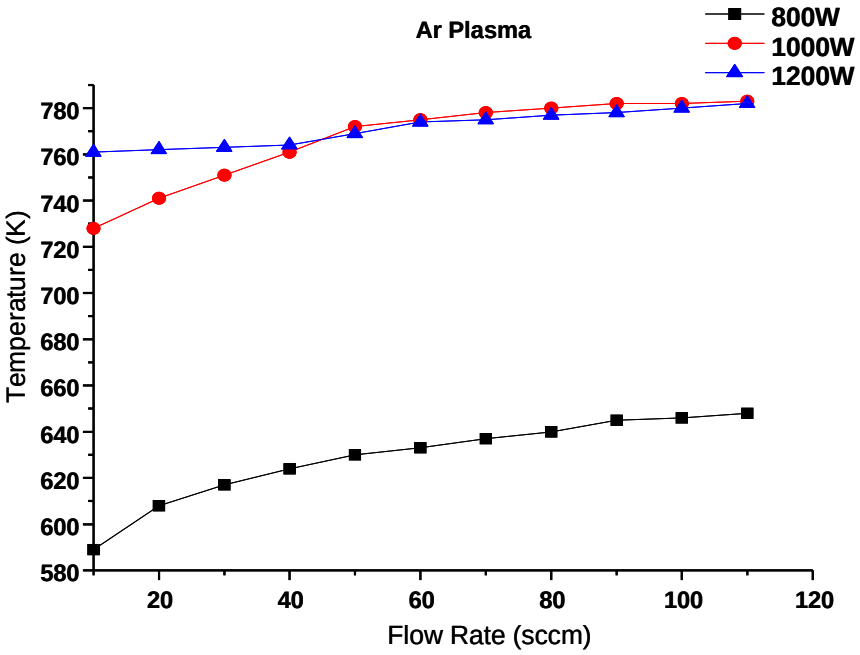

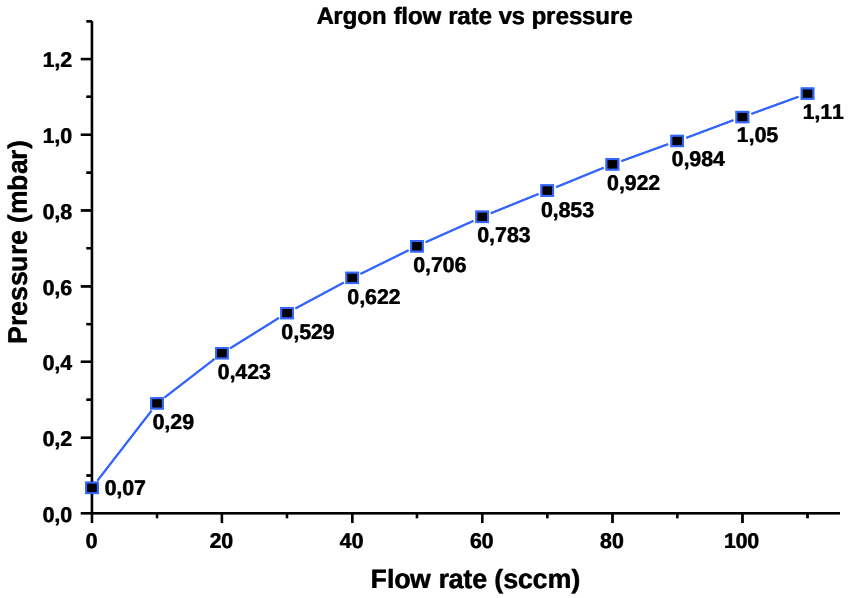

Figure 3.27. Effect of MW power and gas flow rate on the temperature of Argon plasma and flow rate versus gas pressure graph

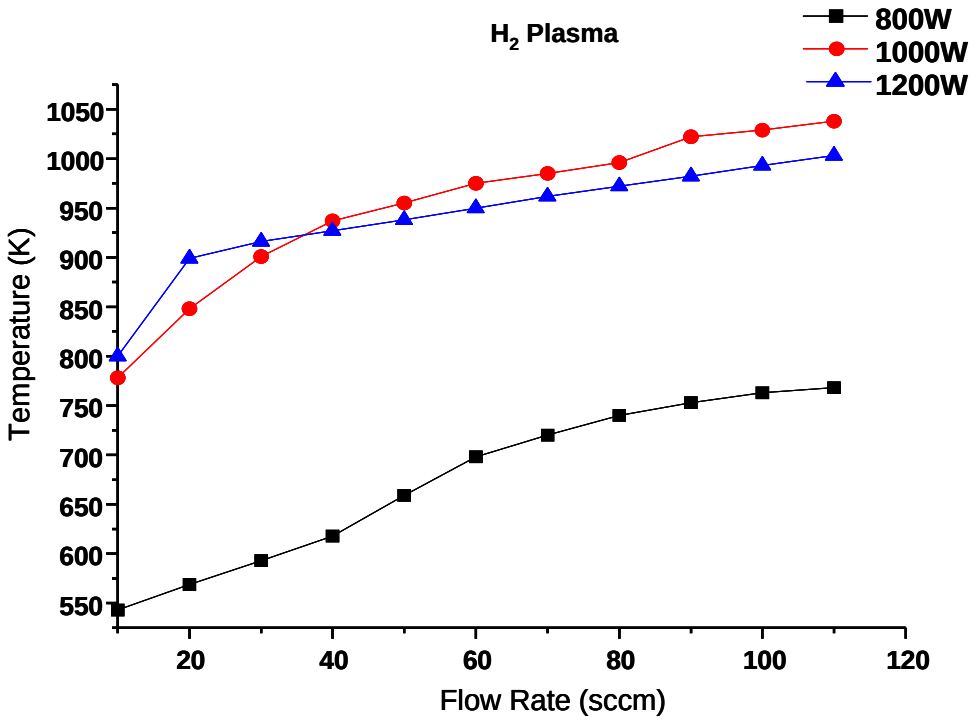

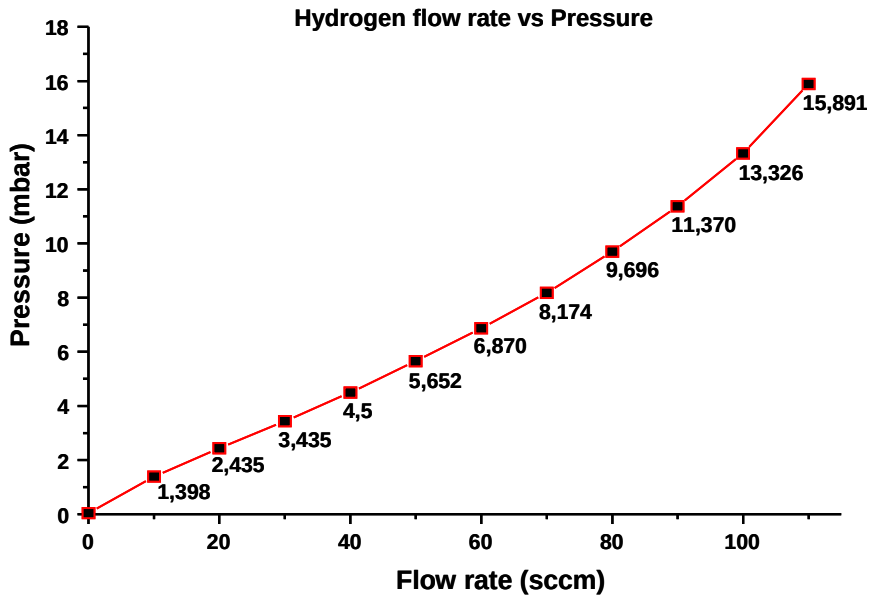

Figure 3.28 Effect of MW power and gas flow rate on the temperature of Hydrogen plasma and flow rate versus gas pressure graph

According to literature reports highly sophisticated instruments were used to measure exact electron and ion temperatures inside a plasma chamber [65-76]. Comparatively, our set up is very simple but quite powerful to allow measuring how plasma parameters affect reaction conditions. The results can be summarized as follow:

- As expected, the hydrogen plasma reaches higher temperature than argon plasma due to the requirement of higher ionization energy for H_2 molecules (splitting of H_2 + ionization)
- There is a distinct temperature difference between 800 W and 1000 W. Thus, we can conclude that when the microwave power is 1000 W or above, ionization is highly progressed and better results can be achieved for oxygen removal from boron samples, as more active species (radicals and ions) are present

- If the temperature curve did not reach a linear region at the given conditions, higher flow rates or gas pressures can be employed to obtain higher ionization and better results for oxygen removal

Optical emission spectrum of hydrogen plasma was investigated to detect which reactive species were present during the plasma process. Ocean optics MAYA 2000 UV-Visible spectrometer was employed for these measurements.

As our spectrometer was sensitive to UV-VIS range, the investigations were focused on the Balmer series of hydrogen. According to Rydberg's and Balmer's formula, atomic hydrogen has 8 spectral lines in the UV – VIS region [89, 90].

$$\frac{1}{\lambda} = R\left(\frac{1}{(n')^2} - \frac{1}{n^2}\right) \qquad \left(R = 1.097373 \times 10^7\ \mathrm{m}^{-1}\right)$$

Transition of *n*	$3 \rightarrow 2$	$4 \rightarrow 2$	$5 \rightarrow 2$	$6 \rightarrow 2$	$7 \rightarrow 2$	$8 \rightarrow 2$	$9 \rightarrow 2$	$\infty \rightarrow 2$
Name	H - α	H - β	H - γ	H - δ	H - ε	H - ζ	H - η	
Wavelength (nm)	656.3	486.1	434.1	410.2	397.0	388.9	383.5	364.6
Color	Red	Blue – Green	Violet	Violet	UV	UV	UV	UV

Figure 3.29 shows the emission spectrum taken for hydrogen plasma with the described experimental setup using an UV – VIS spectrometer.

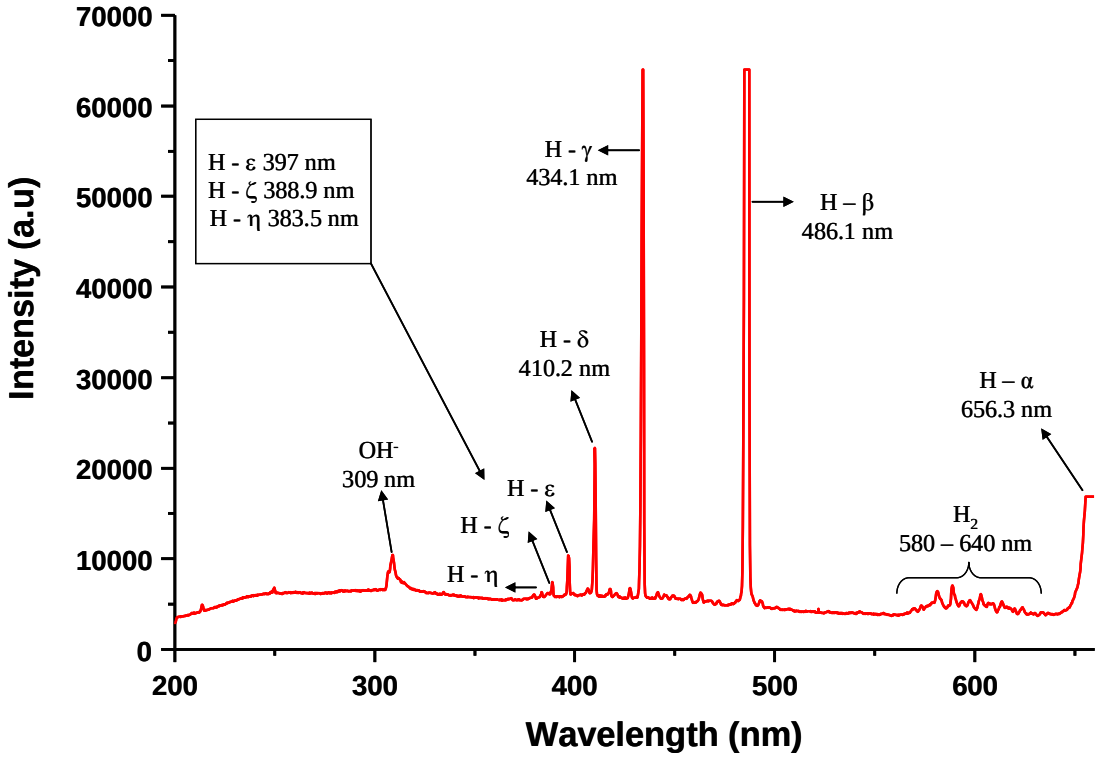

Figure 3.29 Emission spectrum of hydrogen plasma with 1200 W power and 100 sccm hydrogen gas flow

According to Figure 3.29, all spectral lines except 364.6 nm were observed confirming the presence of atomic hydrogen or hydrogen radicals inside the plasma chamber. However, the experiments do not allow a clear quantification with respect to the concentration of radicals or the degree of ionized gas. It is reported that hydrogen plasma radicals and hydrogen ions are always present together but ions are 100 – 1000 times lower in concentration [65-67]. On the other hand, it is impossible to detect hydrogen ions by emission spectroscopy since they do not have any electrons, but observation of the presence of hydrogen radicals is indicating that hydrogen ions are formed in the plasma but with lower concentrations.

The region around 600 nm corresponds to molecular hydrogen [90]. 309 nm is assigned to OH^- which is thought to be the indication of the presence of water inside the plasma chamber. All gas connections and hydrogen gas tank itself are possible water sources as hydrogen gas has 5 ppm water content given in the label.

Observation of the presence of hydrogen radicals and ions suggested how a reasonable oxygen removal mechanism could work:

$$2H^+/2H^\cdot + B_6O + 2e^- \rightarrow 6B + H_2O \quad (5)$$

$$2H^+/2H^\cdot + B_7O + 2e^- \rightarrow 7B + H_2O \quad (6)$$

$$3H^+/3H^\cdot + B_2O_3 \text{ (thin oxide layer) } 6e^- \rightarrow 2B + 3/2\ H_2O \quad (7)$$

According to these reactions, hydrogen active species would combine with oxygen and remove it in the form of H_2O which could be observed in the emission spectrum. Thus, the presence of H_2O or OH^- would confirm the suggested reaction mechanism. Emission spectra of the blank chamber and the one loaded with boron sample were taken with 1 minute intervals for 30 minutes. Figures 3.30 and 3.31 show the results of the experiments.

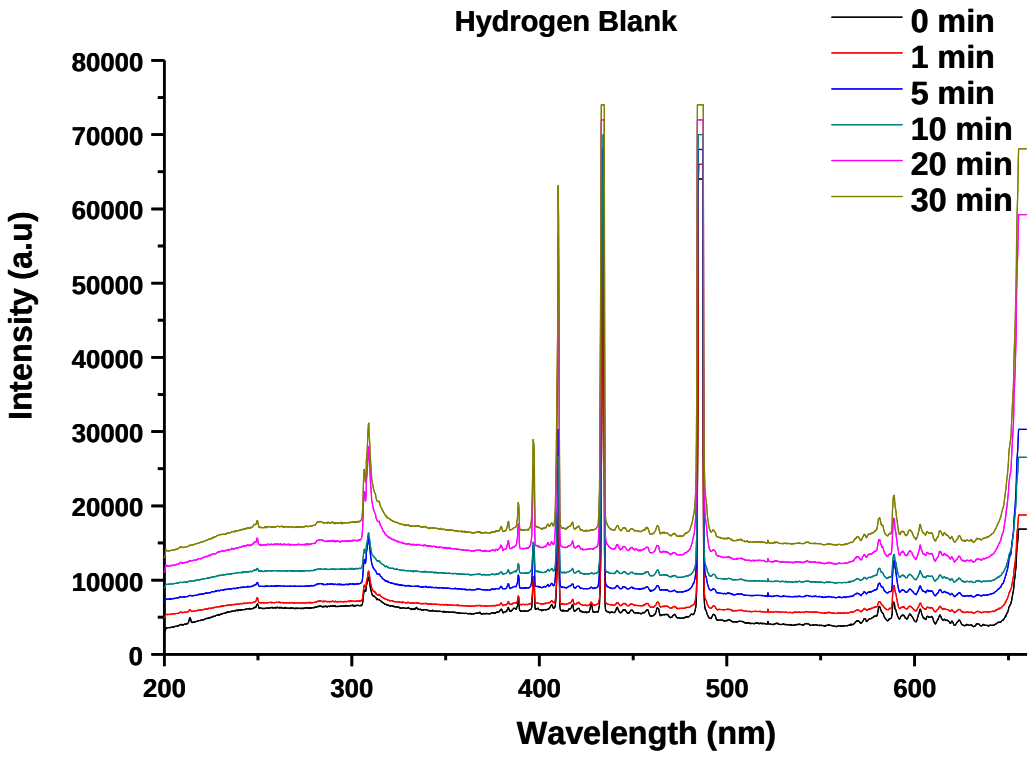

Figure 3.30 Optical emission spectra of blank chamber with hydrogen plasma

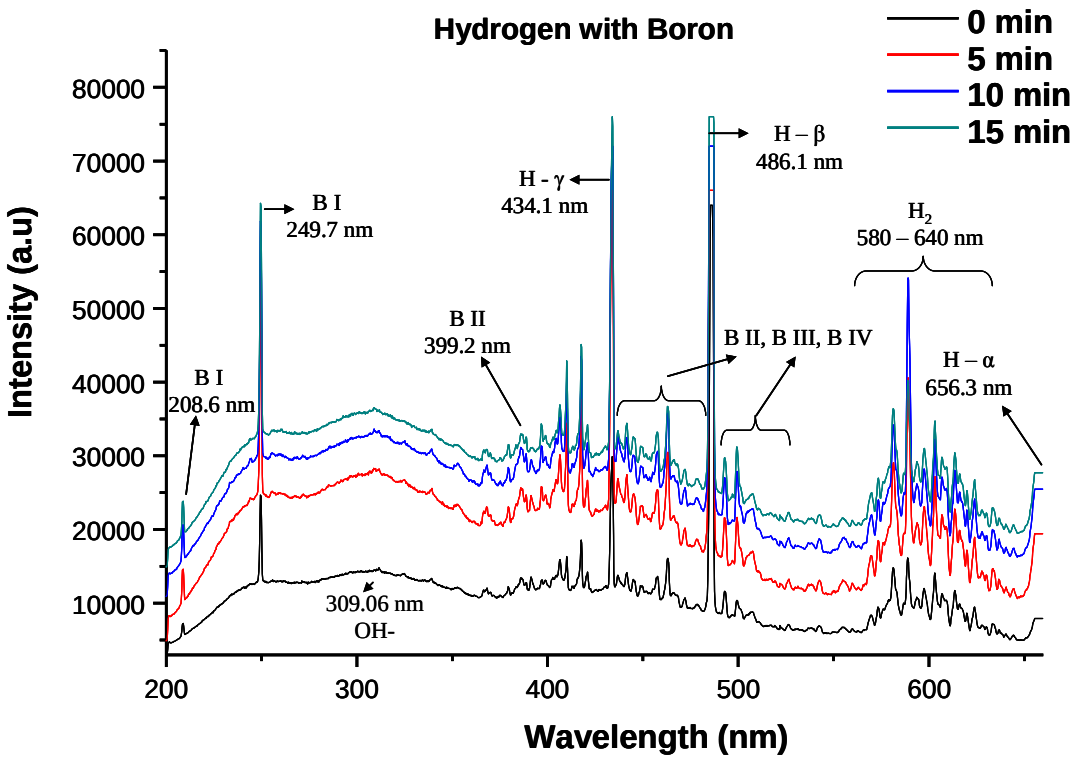

Figure 3.31 Emission spectra of boron sample with hydrogen plasma

Emission lines of boron can be easily determined in Figure 3.31. An interesting detail is that the peak at 309 nm is almost disappeared. This can be referred to a reaction that took place between the boron sample and the water vapor inside the plasma chamber took place, although the latter is known to exist in trace amounts. Several measurements can be taken to avoid the presence of water, such as longer evacuation of the plasma chamber and using water traps or moisture absorbers for the gas line.

The attempt of using the 309 nm OH^- peak in the emission spectrum to clarify the oxygen removal mechanism was, thus, cancelled. The private communications with the authors of the MWIP patent revealed that considerably higher levels of oxygen removal should only be possible when an oxygen getter material was used. Titanium and zirconium

metals are the most well-known and applied oxygen getters undergoing highly exothermic reactions with water at elevated temperatures yielding hydrogen gas and metal oxide. The oxygen removal mechanism with the aid of oxygen getters will be explained in the upcoming sections of this chapter.

In the meanwhile, another remarkable observation was made while recording the emission spectra of hydrogen plasma. At ca. 600 nm peaks of molecular hydrogen were observed, which could be interpreted as the plasma still contained undissociated hydrogen molecules. For a deeper insight, emission spectra were recorded at variable gas flow rates using 1200, 1000 and 800 Watts of microwave power (Fig. 3.32, 3.33 and 3.34).

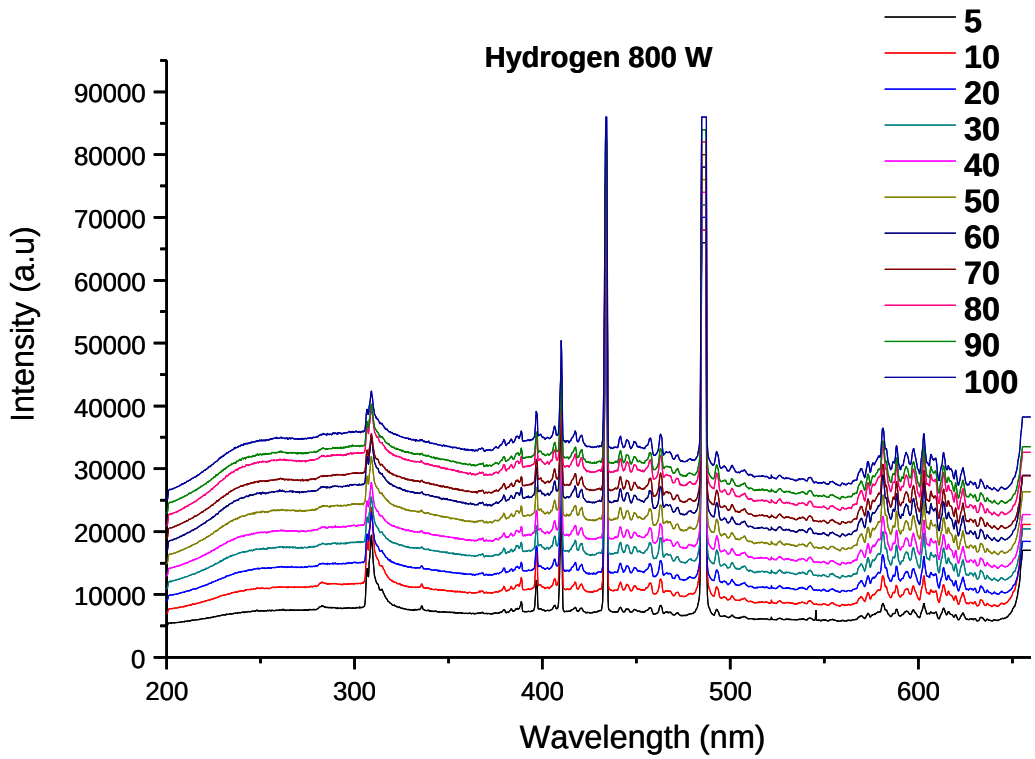

Figure 3.32 Emission spectra of hydrogen plasma at 800 W with different gas flow rates

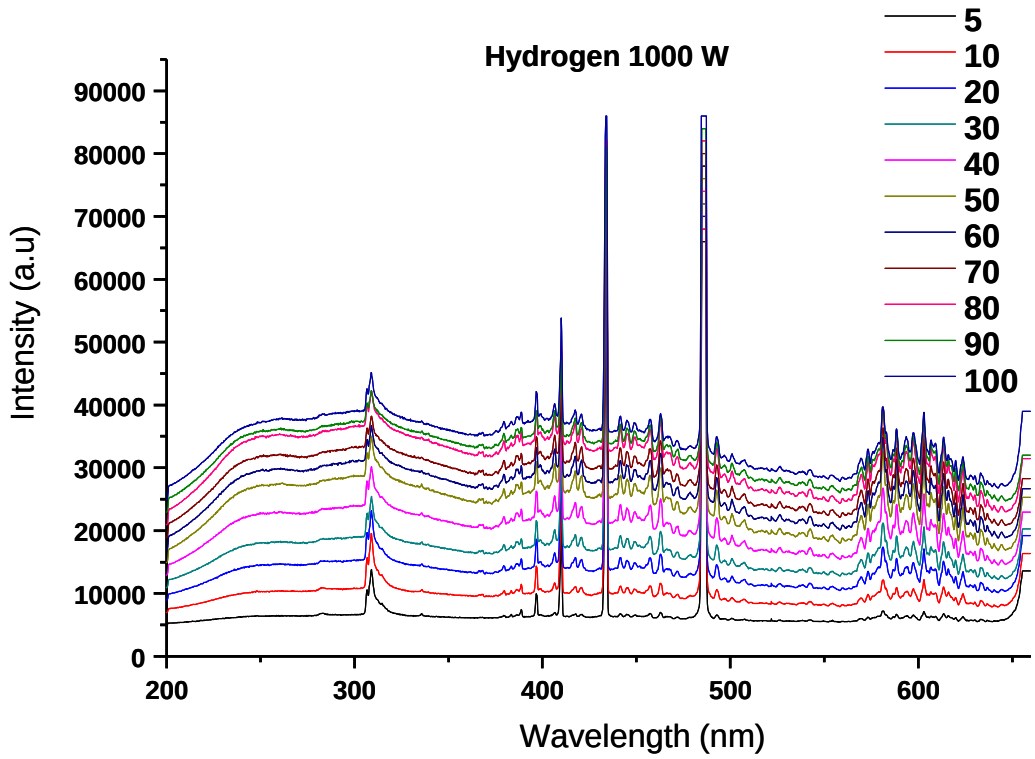

Figure 3.33 Emission spectra of hydrogen plasma at 1000 W with different gas flow rates

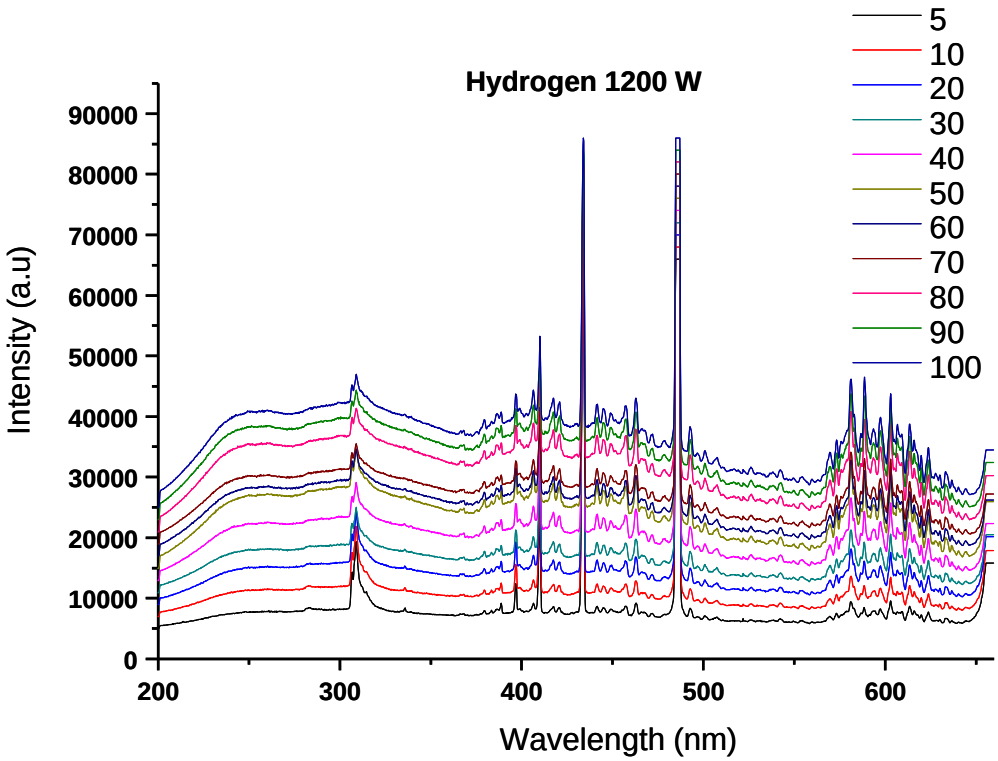

Figure 3.34 Emission spectra of hydrogen plasma at 1200 W with different gas flow rates

The experiments revealed that as the gas flow rate or the gas pressure decreased peaks of molecular hydrogen weakened indicating that a higher ionization rate or higher radical/ion concentrations could be achieved at lower gas flow rates/pressures, yielding to a more efficient oxygen removal. By using optical emission spectra, intensities of hydrogen radicals (H·) and molecular hydrogen are compared. OES measurements were conducted at 1200, 1000 and 800 W of microwave power again by changing gas flow rates. Emission spectra are base lined and one peak is selected for both hydrogen radical and molecular hydrogen (410.3 nm for H·, 581.8 nm for H_2). Figure 3.35 shows the graphs for H_2/ H· ratio versus gas flow rate at different microwave power values. According to Figure 3.35, H_2/ H· ratio is rising with increasing gas flow rate or pressure. It is reasonable to conclude that,

under constant microwave power gain, at low pressures dissociation of molecular hydrogen is higher as there are less amount of molecules present to be converted into radicals and ions. Temperature measurements (Figure 3.28) reveal that raising the pressure increases the temperature of the system, which on the other hand might be an indication for formation of radicals in higher concentrations. More detailed discussions of the effect of plasma gas pressure (flow rate) and microwave power will take place in the sections where oxygen content measurements are described.

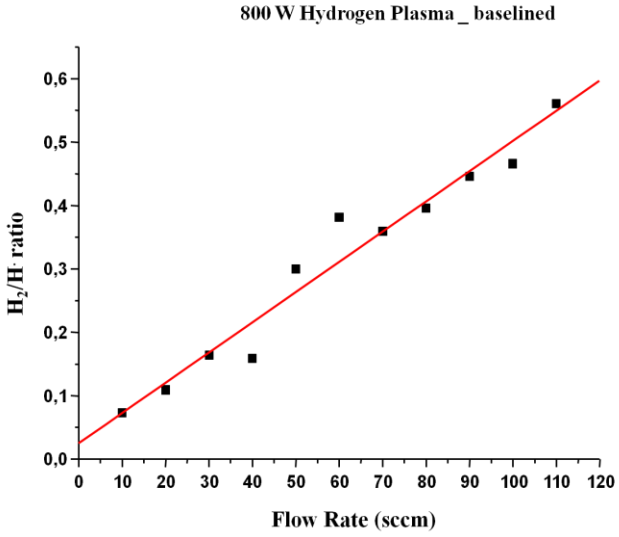
800 W Hydrogen Plasma _ baselined
H2/H- ratio
0,0
0,1
0,2
0,3
0,4
0,5
0,6
0 10 20 30 40 50 60 70 80 90 100 110 120
Flow Rate (sccm)

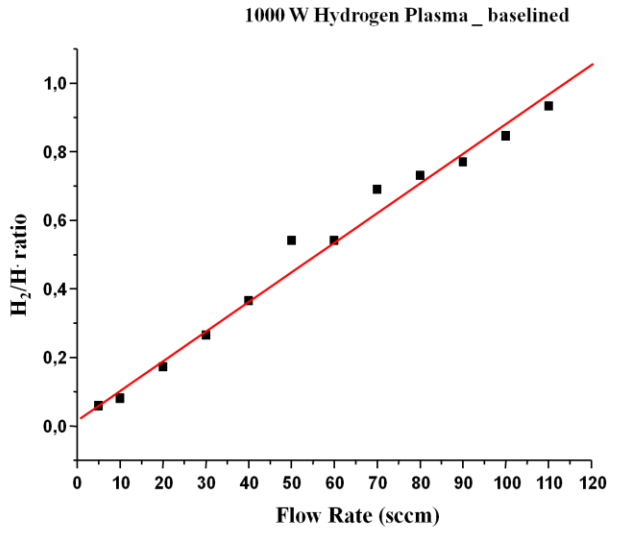
1000 W Hydrogen Plasma _ baselined
H2/H- ratio
0,0
0,2
0,4
0,6
0,8
1,0
0 10 20 30 40 50 60 70 80 90 100 110 120
Flow Rate (sccm)

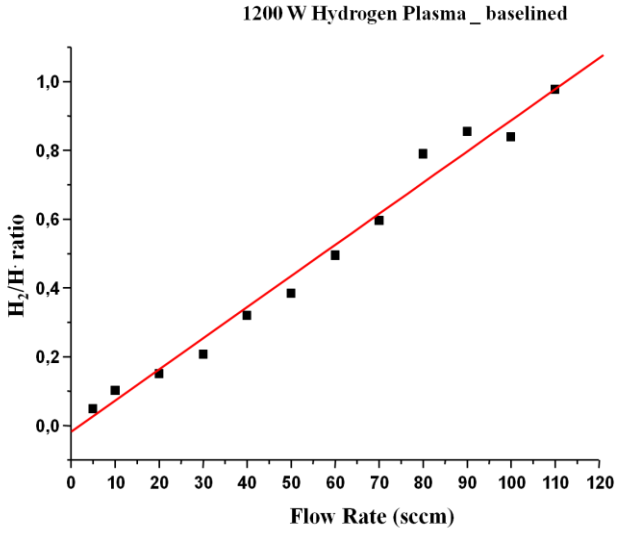

Figure 3.35 $H_2/H^{\cdot}$ ratio versus gas flow rate

3.8 Effect of MWIP procedure on the crystallinity of the samples

Patent authors of MWIP system claimed that, as this is a cold plasma process, hydrogen plasma treatment of the samples would not enhance crystallinity. To investigate the validity of this claim, two sets of experiments were done. In the first set, commercial Grade 1 (>95% Boron) amorphous boron samples were treated up to three hours with hydrogen plasma with maximum power and gas pressure. Figure 3.36 shows the p – XRD diagrams comparing untreated Grade 1 and after three hours of hydrogen plasma treated sample. XRD measurement clearly shows that after three hours of hydrogen plasma treatment no enhancement can be observed in the crystallinity of the sample. The crystallinity of the samples arises from the production conditions and corresponds to rhombohedral boron phases. The results are in agreement with the temperature measurements of hydrogen plasma in which the highest temperature achieved was at around 1000 K, which is,

however, still below the value necessary to initialize the crystallization of the boron samples.

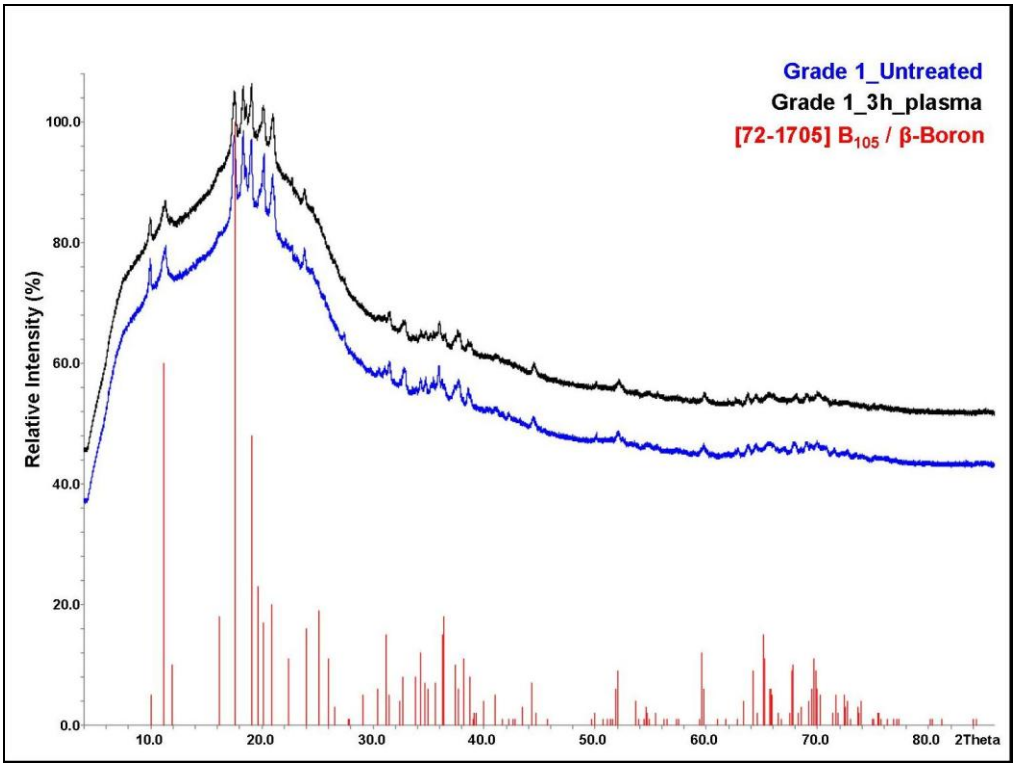

Figure 3.36 p – XRD diagrams of plasma treated (3 h) and untreated G1 amorphous boron samples

The second set of experiment was done with amorphous boron samples obtained from the pyrolysis of B_2H_6. Same plasma treatment was employed for the "nano boron" at maximum microwave power (1200 W) and gas pressure for three hours. Figure 3.37 shows the results of the XRD experiments. Untreated amorphous boron powder after one hour and three hours of hydrogen plasma exposure revealed no peak formation, allowing the conclusion that the specimen was still in amorphous state

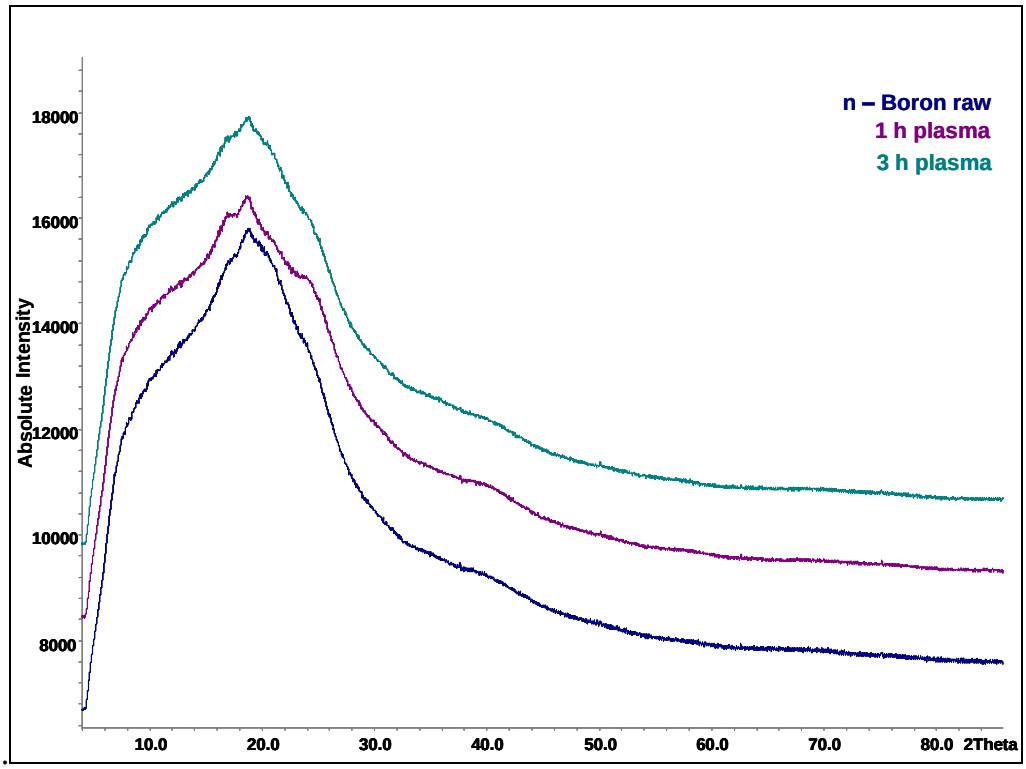

Figure 3.37 p – XRD diagrams of plasma treated (3 h) and untreated nano boron samples

3.9 Oxygen removal experiments

The main goal of the present study was the synthesis of high purity (>99 wt %) amorphous boron. The purity value of over 98.5 wt % boron was reached already in the synthesis part where B_2H_6 was decomposed to its components; solid boron and hydrogen gas. As repeatedly mentioned, the primary contamination in amorphous nano boron is stemming from oxygen, which is present as a surface oxide layer, which is also acting as a native protection to further oxidation of the bulk and non-stoichiometric boron suboxides (B_6O and B_7O). The chemical analyses showed that nitrogen and carbon are the other impurities present as surface nitride and carbide. The method that was used to remove surface oxide layer is based on employing the highly energetic hydrogen plasma and a suitable oxygen getter material combination. The plasma generated here is considered as cold plasma, in which the material was subjected to temperatures below 2000 K. The oxygen removal mechanisms were predicted as follows**:**

$$6H\cdot/6H^+ + B_2O_3 + 6e^- \rightarrow 2B + 3H_2O \qquad (8)$$

$$2\ H\cdot/2H^+ + B_6O + 2e^- \rightarrow 6B + H_2O \qquad (9)$$

$$2\ H\cdot/2H^+ + B_7O + 2e^- \rightarrow 7B + H_2O \qquad (10)$$

The reactions (9) and (10) are valid for the commercial amorphous boron samples. The suboxides are assumed to form during the exothermic reduction of B_2O_3 with magnesium metal. Reaction (8) is the removal mechanism of surface oxide layer with highly energetic hydrogen species that are generated during the plasma treatment of material. It is important to note that the temperature of the plasma medium is above the melting point of surface oxide (B_2O_3), meaning that it is considered to be molten. Although, our temperature

measurements resulted lower temperatures of the plasma medium, as indicated before it may not give the exact values, local temperatures and surface temperatures are assumed to be higher than what was measured.

The patent authors claimed that hydrogen based plasma treatment is suitable for the materials that have melting points above 2000 K removing primarily the surface oxide layer without causing any crystallization in the material. They also reported that oxygen removal was highly enhanced by using suitable oxygen getter materials such as titanium and zirconium according to:

$$Ti_{(s)} + 2H_2O_{(g)} \rightarrow TiO_{2(s)} + 2H_{2(g)} \qquad (11)$$

$$Zr_{(s)} + 2H_2O_{(g)} \rightarrow ZrO_{2(s)} + 2H_{2(g)} \qquad (12)$$

At moderate temperatures, titanium and zirconium do not undergo a direct reaction with oxygen to form metal oxide [7]. However, their reactions with water at elevated temperatures are thermodynamically favored yielding metal oxide and hydrogen gas. Although, boron has a higher affinity to oxygen than titanium and zirconium, the water that is formed after the reaction of B_2O_3, B_6O or B_7O with the hydrogen species will further react with the getter metal. In this manner the oxygen is “trapped” on the surface of the getter material. The resulting metal oxide layer is highly stable with respect to the oxide(s) of boron. Finally, hydrogen plasma acts both as oxide remover and transport medium from boron surface to oxygen getters.

It is important to note that, the plasma treatment described here is not effective on the removal of nitride layer (BN) since boron nitride is stable and inert to the species formed in the hydrogen plasma. The effect of hydrogen plasma on the carbon content is assumed to be in the reducing manner, since it is possible to remove carbon impurity in the form a

carbon – hydrogen compound (CH_4 etc.) in the plasma conditions. Our experiments with pure methane plasma have shown that it can easily be decomposed to generate a layer of soot (carbon) and hydrogen on the glass surface. However, when the sooth gets in contact with the hydrogen plasma, the soot layer is converted very likely to methane which leaves the system through the vacuum line. However, the lack of an analytical device to measure carbon content during the experiments is limiting the possibility of further discussions.

After plasma conditions were determined and optimized for the use of amorphous nano boron samples, an experimental matrix was established as depicted in the below tables. Based on this, effects of plasma treatment parameters, which were time, gas pressure and microwave power, etc, were investigated. The results obtained from these experiments clarified the mechanism of oxygen removal via hydrogen based plasma treatment of amorphous boron samples. Commercial amorphous boron of Grade 1 (>95 % B) and amorphous nano boron synthesized in the present study were used in the oxygen removal experiments. The main goal was the detection of the change in oxygen content of the samples and to correlate it with the experimental parameters. The following tables and figures summarize the experiments, as well as the change in oxygen content of samples which was measured using a LECO TCH600 elemental analysis device.

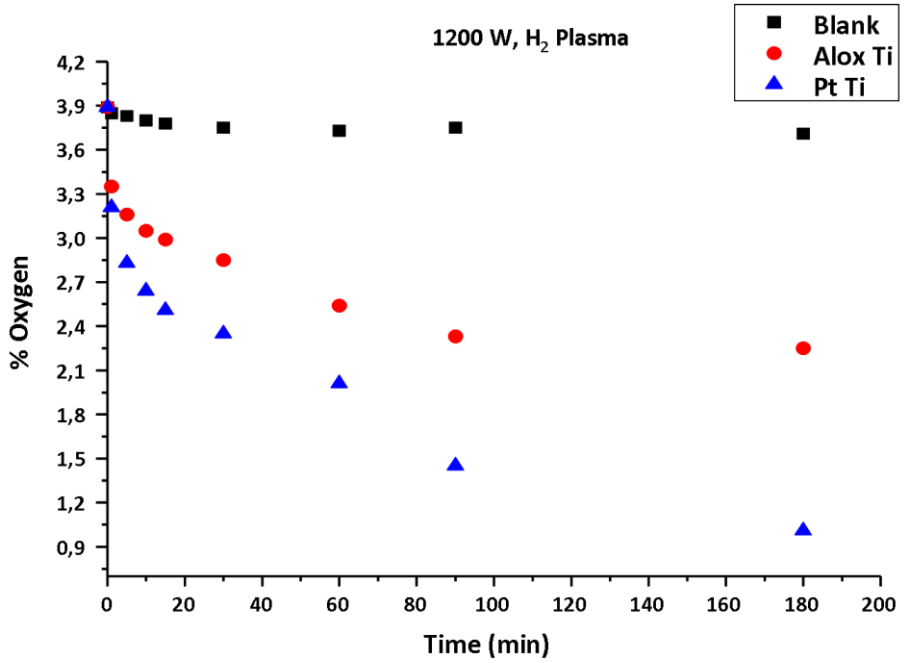

Figure 3.38 Effect of plasma treatment time on oxygen content (Grade 1 boron)

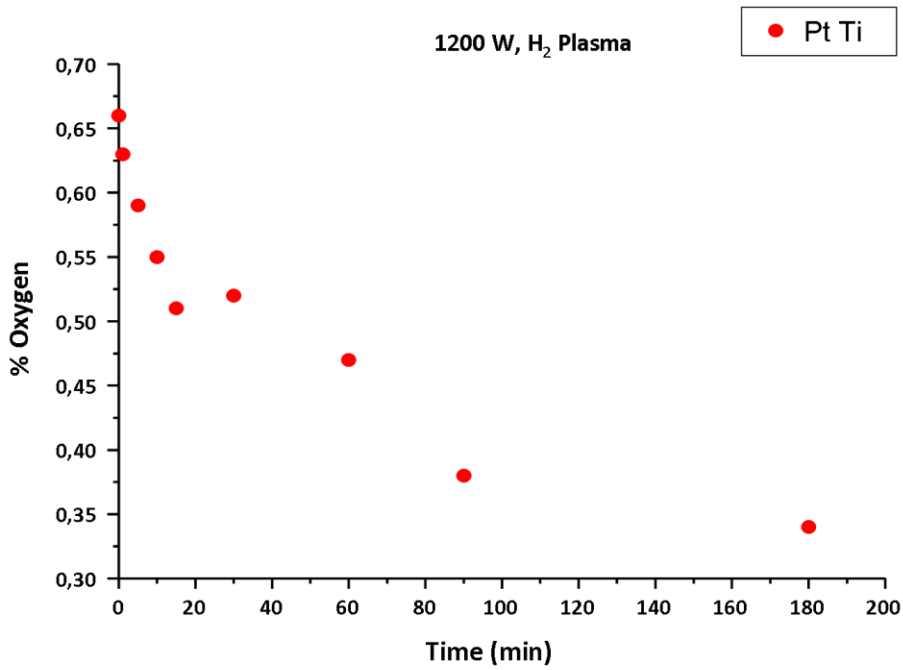

Figure 3.39 Effect of plasma treatment time on oxygen content (*n* – Boron)

Table 3.13 Effect of plasma treatment time on oxygen content

Sample	**MW Power (Watts)**	**Time (sec)**	**Oxygen Getter**	**Crucible**	**Gas Pressure (mbar)**	**% Oxygen**
Grade 1	-	-	-	-	-	3.89
Grade 1	1200	60	1 g Ti	Pt	15.9 H_2	3.21
Grade 1	1200	300	1 g Ti	Pt	15.9 H_2	2.83
Grade 1	1200	600	1 g Ti	Pt	15.9 H_2	2.64
Grade 1	1200	900	1 g Ti	Pt	15.9 H_2	2.51
Grade 1	1200	1800	1 g Ti	Pt	15.9 H_2	2.35
Grade 1	1200	3600	1 g Ti	Pt	15.9 H_2	2.01
Grade 1	1200	10800	1 g Ti	Pt	15.9 H_2	1.01
n - Boron	-	-	-	-	-	0.66
n - Boron	1200	60	1 g Ti	Pt	15.9 H_2	0.63
n - Boron	1200	300	1 g Ti	Pt	15.9 H_2	0.59
n - Boron	1200	600	1 g Ti	Pt	15.9 H_2	0.55
n - Boron	1200	900	1 g Ti	Pt	15.9 H_2	0.51
n - Boron	1200	1800	1 g Ti	Pt	15.9 H_2	0.52
n - Boron	1200	3600	1 g Ti	Pt	15.9 H_2	0.47
n - Boron	1200	10800	1 g Ti	Pt	15.9 H_2	0.34

Table 3.14 Effect of plasma gas type on oxygen content

Sample	MW Power (Watts)	Time (sec)	Oxygen Getter	Crucible	Gas Pressure (mbar)	% Oxygen
Grade 1	-	-	-	-	-	3.89
Grade 1	1200	300	1 g Ti	Pt	15.9 H_2	2.83
Grade 1	1200	600	1 g Ti	Pt	15.9 H_2	2.64
Grade 1	1200	300	1 g Ti	Pt	1.1 Ar	3.87
Grade 1	1200	600	1 g Ti	Pt	1.1 Ar	3.93

Table 3.15 Effect of plasma gas pressure on oxygen content

Sample	MW Power (Watts)	Time (sec)	Oxygen Getter	Crucible	Gas Pressure (mbar)	% Oxygen
Grade 1	-	-	-	-	-	3.89
Grade 1	1200	300	1 g Ti	Pt	15.9 H_2	2.83
Grade 1	1200	300	1 g Ti	Pt	13.3 H_2	2.95
Grade 1	1200	300	1 g Ti	Pt	5.7 H_2	3.01
Grade 1	1200	300	1 g Ti	Pt	1.4 H_2	3.05

Table 3.16 Effect of crucible material on oxygen content

Sample	MW Power (Watts)	Time (sec)	Oxygen Getter	Crucible	Gas Pressure (mbar)	% Oxygen
Grade 1	-	-	-	-	-	3.89
Grade 1	1200	300	1 g Ti	Alox	15.9 H_2	3.35
Grade 1	1200	300	1 g Ti	Pt	15.9 H_2	2.83
n – Boron	-	-	-	-	-	0.66
n – Boron	1200	300	1 g Ti	Alox	15.9 H_2	0.94
n – Boron	1200	300	1 g Ti	Pt	15.9 H_2	0.59

Table 3.17 Effect of oxygen getter on oxygen content

Sample	MW Power (Watts)	Time (sec)	Oxygen Getter	Crucible	Gas Pressure (mbar)	% Oxygen
Grade 1	1200	300	-	Pt	15.9 H_2	3.81
Grade 1	1200	300	1 g Ti	Pt	15.9 H_2	2.83
n – Boron	1200	300	-	Pt	15.9 H_2	0.67
n – Boron	1200	300	1 g Ti	Pt	15.9 H_2	0.59
n – Boron	1200	300	5 g Ti	Pt	15.9 H_2	0.61

Table 3.18 Effect of microwave power on oxygen content

Sample	MW Power (Watts)	Time (sec)	Oxygen Getter	Crucible	Gas Pressure (mbar)	% Oxygen
Grade 1	-	-	-	-	-	3.89
Grade 1	800	300	1 g Ti	Pt	15.9 H_2	3.21
Grade 1	1000	300	1 g Ti	Pt	15.9 H_2	2.91
Grade 1	1200	300	1 g Ti	Pt	15.9 H_2	2.83
n – Boron	-	-	-	-	-	0.66
n – Boron	800	300	1 g Ti	Pt	15.9 H_2	0.63
n – Boron	1000	300	1 g Ti	Pt	15.9 H_2	0.62
n – Boron	1200	300	1 g Ti	Pt	15.9 H_2	0.59

The results of oxygen removal experiments and the effects of experimental variables on the oxygen content of boron samples can be summarized as follows:

- Higher microwave power and higher gas pressure gave better oxygen removal results, since the system could be operated at higher temperatures.
- Platinum crucible was more effective in plasma treatment since boron powders and particularly n – boron act as strong reducing agent at elevated temperatures even towards Al_2O_3.
- Usage of oxygen getter material considerably enhanced the oxygen removal from boron samples.
- Longer plasma treatment time on the boron samples resulted in a higher loss of oxygen content.

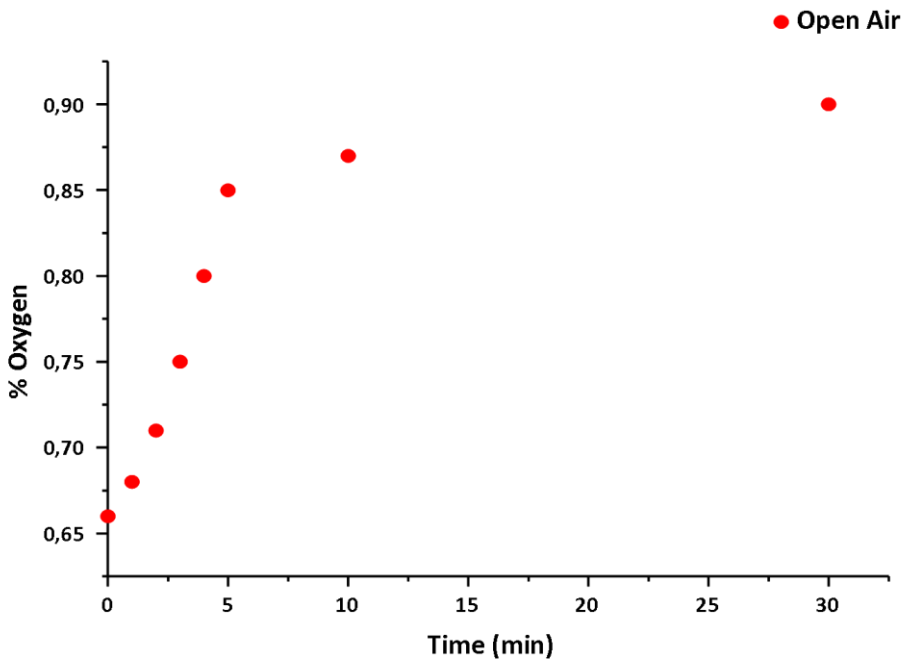

Figure 3.40 Oxidation of n – Boron in open air

Figure 3.40 shows the oxidation of n – Boron in open air with respect to time. It is obvious that the material has a very high oxidation tendency and should be kept under inert atmosphere for further uses after the synthesis.

3.10 Continuous MWIP Experiments

The hydrogen plasma based oxygen removal is a batch process and is limited to 100 mg/hour. Another important aim of this study was to increase the amount of plasma treated boron up to 50 – 100 g/day by converting the present system into a continuous one. The working principle of the c-MWIP system was described in the previous chapter. During our studies the c-MWIP system was optimized to obtain a vacuum tight plasma generation while amorphous boron powder was fed to the plasma chamber through a powder dosing device which was assembled on top of the microwave furnace. The capacity of powder dosing device was 1 liter and could be filled with ca. 300 grams of amorphous boron at a time. The preliminary attempts showed that by adjusting the dosing speed of powder, 100 grams could be easily fed to the plasma chamber with 20 to 50 mg/minute feed rate. The results of the experiments proved that amorphous boron powder could be treated in hydrogen plasma after performing a series of modifications on the system. Table 3.19 shows the results of c-MWIP experiments by monitoring the change in oxygen content of amorphous boron samples at different plasma generation conditions.

Table 3.19 Results of c-MWIP experiments

Sample	Plasma Conditions	% Oxygen(±0.05)
CMW000	Raw sample (commercial Grade 1)	3.41
CMW001	1200 W, 15.9 mbar H_2, 20 mg/min feed rate	3.39
CMW002	1200 W, 15.9 mbar H_2, 30 mg/min feed rate	3.40
CMW003	1200 W, 15.9 mbar H_2, 50 mg/min feed rate	3.35
CMW004	1000 W, 15.9 mbar H_2, 20 mg/min feed rate	3.42

However, as described in the previous section, the oxygen removal efficiency of hydrogen plasma was highly enhanced by the usage of an oxygen getter material. The c-MWIP system could not be modified to incorporate the oxygen getter material inside the plasma chamber without having a direct contact with the sample powder. The solution of this technical problem was indeed not impossible, but required an extensive and time consuming research time which would exceed the scope the present thesis.

3.11 Storage of Diborane

The aim of storing diborane in a lecture bottle was partially achieved. As afore mentioned, very little amount of diborane could be kept in the lecture bottle with the described procedure. The worldwide applications of diborane show, however, that instead of storing diborane “on-demand” production should be the method of choice.

The guidebooks of main diborane producers claim that the transportation of diborane (maximum 100 g) is achieved in thermally isolated containers where diborane tank is kept at dry ice temperature to avoid decomposition during the transfer [91]. In addition, diborane is highly toxic (lethal dose: 2.5 ppm) and explosive, requiring several safety precautions. Most probably these are the main reasons why diborane is an extremely expensive gas.

3.12 Application of nano boron in Superconducting MgB_2 synthesis

Magnesium diboride (MgB_2), a simple ionic binary boride, was discovered 50 years ago, but the discovery of its superconducting behavior (K_c = 39 K) in 2001 [92,93], made it a promising material for many high technology applications, like NMR, MRI, super conducting magnets and magnetic levitation trains etc. The simplest synthesis method is the direct combination of boron and magnesium in stoichiometric amounts and heating the mixture above 923 K where MgB_2 formation starts. Since, magnesium melts at 925 K, the reaction mechanism is considered to be moderated by the diffusion of magnesium vapor across boron grain boundaries [94]. Commercial applications employ, “in situ” and “ex situ” production methods for MgB_2 where powder is filled inside a nickel - copper coating and drown in a wire form [92,94]. Studies showed that, doping of MgB_2 with suitable materials, mostly carbon and transition metals, enhanced the magnetic properties.

The important parameters of superconducting materials are; the critical temperature (T_c) below which the superconductivity occurs, critical current (J_c) the maximum value of current that can pass through the material before breakdown, and coherence length (L), which describes the distance between pinning centers that are responsible for the transferring of current through the material. The values of these parameters for MgB_2 are as follows:

- T_c = 39 K and below
- J_c = 10^9 A/m^2 at 5 Tesla
- Coherence Length = 40 – 50 Å

According to literature reports, magnetic properties of MgB_2 are directly affected by the doping element and purity of boron [95,96]. MgB_2 synthesis was performed with amorphous nano boron in this manner and several characterizations were made. Amorphous nano boron sample was sent to Prof. René Flükiger at University of Geneva, where MgB_2 was synthesized, transformed to wire and measured J_c versus magnetic field. Figure 3.41 shows the result of magnetic measurement in which, the properties of our nano boron is compared with commercial boron samples.

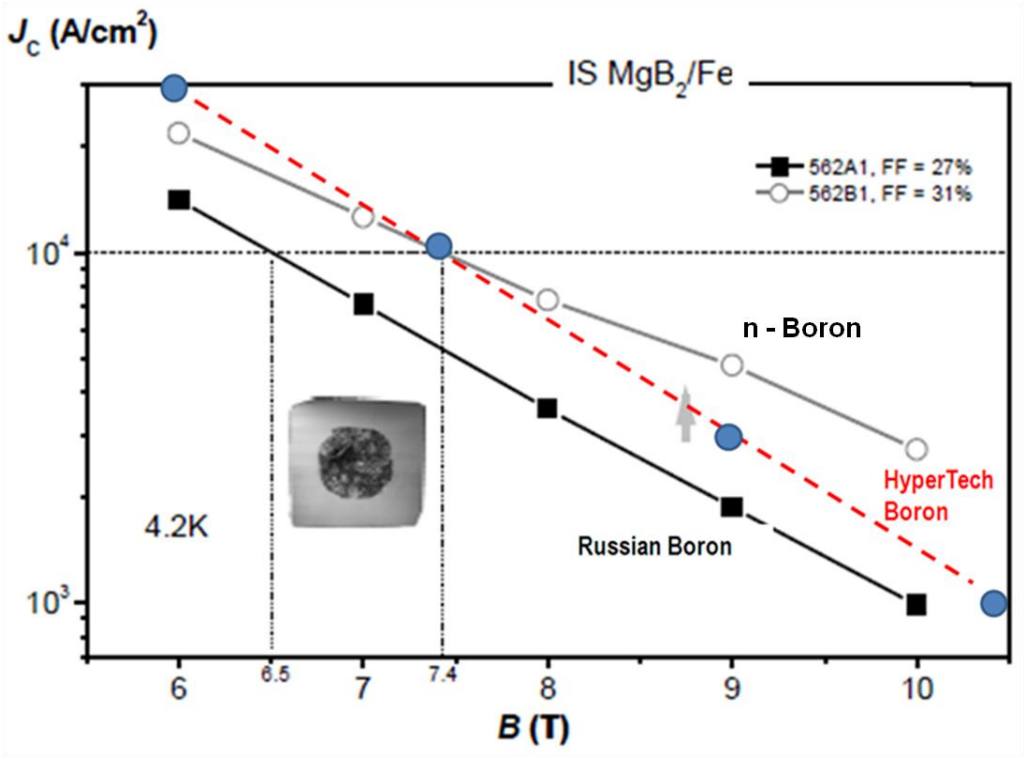

Figure 3.41 J_c versus magnetic field graph

The results clearly prove that our boron sample showed better J_c value at higher magnetic fields, which makes it a very promising material for magnet applications. The better performance of the MgB_2 samples prepared from the nano-boron with respect to commercial ones is considered to have two main reasons:

- High purity of nano boron avoided impurities which may disturb the current transfer and increase the resistance of materials, since other boron samples contained 95 – 97 % pure amorphous boron
- Nano size particles provided low temperature synthesis and avoided crystallization that might occur at higher temperatures and kept the material in amorphous form, which is desirable in superconductor applications [97].

In another experiment, different MgB_2 specimens were synthesized using both commercial boron and nano boron. For this purpose blends of the constituent Mg and B powders were mixed (molar ratio 2 : 1) and filled into steel tubes, sealed and heated to 923 K and annealed for ½ hour. Figure 3.42 shows the XRD diagrams of the products (MgB_2).

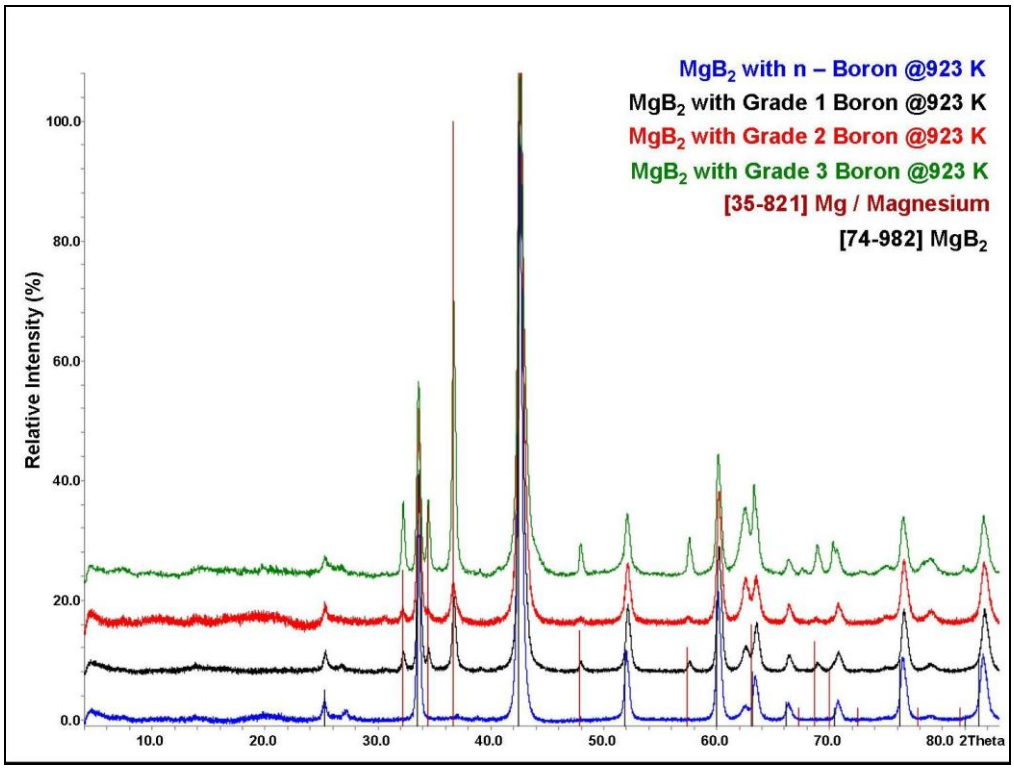

Figure 3.42 XRD diagrams of MgB_2 samples

The powder patterns confirm that, except for nano boron, all MgB_2 samples contain unreacted magnesium. The reason is the high reactivity of amorphous nano boron, due to its spherically shaped nano sized powder structure and the high purity.

Recent studies showed that, carbon doping of MgB_2 increases the J_c value at higher magnetic fields dramatically [95,96]. This phenomenon is basically originated from two reasons:

- Carbon atoms are substituting the boron vacancies in the crystal lattice of MgB_2 and enhance the conductivity
- Carbon coating avoids the agglomeration of boron particles and increase the contact of boron and magnesium during the diffusion reaction

As the chemical analysis of the amorphous nano boron revealed (Table 3.7), the material contains ca. 0.15 % carbon, whose origin is assumed to be organic contaminations from the commercial $NaBH_4$ production.

Prof. Flükiger suggested that in addition to the afore mentioned two effects which could enhance the remarkable magnetic behavior of the MgB_2 samples synthesized from amorphous nano boron, the carbon content of the boron powder might play also an important role. To verify it nano boron specimen with different carbon contents were prepared. The carbon doping experiment was conducted in that manner that high purity (>99.995 %) CH_4 was purged into the gas stream before the pyrolysis step of B_2H_6. The carbon content of the sample was measured to be 1.5 %, and while the present thesis was written the magnetic measurements were ongoing. The result of the last experiment proved that carbon doping was possible via CH_4 purging during the pyrolysis. Preparation of samples with controllable carbon content and the investigation of the effect of carbon doping on the magnetic behavior of the MgB_2 are in process.

Chapter 4

CONCLUSIONS

In this study, we mainly focused on the synthesis of high purity elemental boron both in the crystalline and amorphous forms. As described in the previous chapters, several methods are given in the literature for elemental boron synthesis. The most widely used commercial production route is known as Moissan method, in which B_2O_3 is reduced with magnesium and followed by several purification steps including acid leaching which results in 97 % pure elemental amorphous boron. Moissan method is suitable for large scale elemental boron production, however, the presence of impurities in the final product is inevitable due to the formation of magnesium – boron and magnesium – boron – oxygen compounds which cannot be eliminated via chemical methods. High temperature (>1500 K) treatments of this boron samples can be a solution to get rid of magnesium impurities, in which amorphous material is transformed into the inert crystalline form.

According to literature, the most suitable production method for high purity and magnesium free elemental boron is the pyrolysis of diborane gas (B_2H_6). As diborane consists of only boron and hydrogen, its thermal decomposition yields only boron in solid form and hydrogen gas. The main disadvantages of diborane gas, however, are its availability, price and toxicity. High purity (>99.99%) diborane is commercially available for 1500 € (28 g gas per tank) and requires 6 months for shipping. In addition, diborane is extremely toxic and explosive when exposed to atmospheric air and must be kept at dry ice temperature (195 K). It burns rapidly when combined with oxygen and water forming boric acid. Thus, it is not safe or feasible to store large amounts of diborane due to its unstable nature and toxicity.

The novelty in our approach in obtaining high purity amorphous boron is the development of a synthesis technique for "*on-demand diborane*" which can be *in situ* pyrolyzed to its elements at T>573 K. Several methods for the preparation of B_2H_6 are reported in the literature. A great majority of them are solvent based reactions requiring further purifications and removal of solvents. Solid state reactions are easier to handle and do not mostly need additional refining. In the last ten years new B_2H_6 production methods were introduced one of which is the metathesis reaction of metal chlorides with alkaline metal boron hydrides via ball-milling.

In the present study, mixtures of $SnCl_2$, $ZnCl_2$, $CuCl_2$ and $NiCl_2$ with alkaline metal borohydrides (Li/Na/KBH_4) were chosen as candidate reactants for the formation of complex metal borohydrides. These complex metal borohydrides are thermodynamically unstable compounds and via moderate heating they decompose to form diborane, hydrogen gas and chloride of the metal. The mixtures given above were investigated in details with respect to their diborane release behaviors. $Sn(BH_4)_2$ and $Zn(BH_4)_2$ were found to be the appropriate candidates for practical applications. Between those two, $Sn(BH_4)_2$ was the better one according to the amount of diborane release on weight percentage and ease of preparation of the starting mixtures. According to our final experimental studies, 96% of the theoretical diborane content of $SnCl_2$ – $NaBH_4$ mixtures was released with the conditions given in the experimental procedures chapter. In the rest of the experimental studies, "on-demand" diborane production was done by thermal decomposition of $Sn(BH_4)_2$.

In the next step of the experimental studies, a pyrolysis setup was built and finalized after five versions, in which diborane is produced "on-demand" and pyrolyzed "in situ" by passing through a hot silica glass tube result in the formation of solid amorphous elemental boron. Our studies showed that diborane can be dissociated to its constituents with ca. 88%

efficiency. The overall efficiency of the whole pyrolysis setup, including the formation of diborane from $Sn(BH_4)_2$ (96%), was calculated as 85%.

The solid products were characterized with several analytical methods. Chemical analyses were performed to quantify the boron, oxygen, nitrogen and carbon content of the material. Since, boron has high affinity to oxygen and easily form surface oxide layer, samples were kept in the argon filled glove box. Up to 98.5 % pure amorphous elemental boron was synthesized in our studies. The rest were assigned to mainly oxygen, nitrogen and carbon according to our analyses.

SEM – TEM analyses revealed that the pyrolysis of diborane resulted in amorphous elemental boron with sub-micron (<300 nm) and spherical particles. The effect of synthesis conditions on the particle size distribution was also studied with DLS. It was observed that particle size was getting larger with the increase of the pyrolysis temperature.

As described in the previous chapters, oxygen was the main impurity in our samples. Since, our material has a high specific surface area (~35 m^2/g) and consists of spherical nano-sized particles, it was easily oxidized to form a protective oxide layer. Oxidation caused an indirect decrease in the boron content of the material. Microwave Induced Plasma Furnace (MWIPF) system was employed to remove this surface oxide layer and obtain the highest purity elemental boron in amorphous form. MWIPF is based on the utilization of hydrogen gas plasma to remove thin layers of surface oxides by reacting with highly energetic hydrogen species. The results of the MWIPF experiments were monitored by an elemental analysis device in which oxygen and nitrogen contents were measured in wt %. Effects of MWIPF parameters on the oxygen content of amorphous boron samples were investigated and tabulated. The results showed that, MWIPF method was not effective on the removal of surface oxide layer of amorphous elemental boron by itself only. The addition of oxygen getter materials enhanced the oxygen removal dramatically. As MWIPF technique was patented by Max Planck Institute CPfS – Dresden, we did not have

all the details of experimental procedures. According to the original patent, authors claimed that they had achieved to reduce oxygen content of amorphous boron samples (Grade 1, 97 % pure) below 0.1 wt %. In our studies the lowest value of oxygen was 0.34 wt %. Since we did not know the exact conditions of the original experiments, in our studies we could not reduce the oxygen content below 0.3 wt %. Also, one should take into account that, MWIPF patent authors used commercial amorphous boron powder which has lower surface area and higher particle size that has lower affinity to oxygen with respect to nano – boron. However, our trials can be accepted as successful, which showed that MWIPF was applicable for amorphous nano boron samples.

When the effect of the oxygen getter materials were understood in our experiments, the continuous MWIPF project was stopped due to the technical difficulties explained before. However, c-MWIPF system is still assumed to be feasible if the problem of feeding the oxygen getter material into the plasma chamber is solved, and is a feasible way to produce higher amount (50 – 100 g/day) and higher purity (>99.9 wt %) amorphous nano boron.
According to the material characterizations, it was clear that, amorphous nano boron was highly reactive and we decided to observe its performance in applications. Samples of MgB_2 were synthesized with commercial amorphous boron samples and n-boron. Among others, the sample which contained n-boron showed very interesting and promising magnetic properties. Later on, our collaborators suggested that carbon content of the boron had an important effect on the magnetic properties of the final product. Since our material had ca. 0.15 wt % carbon, a new study was started to investigate if carbon content of the n-boron could be controlled. That study is still on-going and a carbon analyzer should be purchased to better monitor the carbon doping experiments.

In conclusion, high purity amorphous nano boron was synthesized, the reaction conditions and experimental procedures were investigated in details. The pyrolysis of diborane at elevated temperatures on silica glass tube was the route for obtaining solid

product. Diborane was produced via the metathesis reaction of metal chlorides and alkaline metal borohydrides. The product was characterized as high purity (>98.5 wt %) amorphous elemental boron with sub-micron particle size, which made us call it nano – boron. The product was highly reactive itself and showed interesting results in several applications that make it a promising candidate in high – tech applications like superconducting materials fabrication.

BIBLIOGRAPHY

1. Giunchi, G., *THE REACTIVE Mg-LIQUID INFILTRATION TO OBTAIN LONG SUPERCONDUCTING MgB2 CABLES*, 2009, EDISON SpA: Milano.
2. J. Kortus, I.I.M., K. D. Belashchenko, V. P. Antropov, L. L. Boyer, *Superconductivity of Metallic Boron in MgB2.* PHYSICAL REVIEW LETTERS, 2001. **86**(20): p. 4656-4659.
3. Eberhard Amberger, W.S., *Gmelin Handbook of Inorganic Chemistry, Boron Volume 2*1981, Berlin: Springer-Verlag.
4. Thomas Onak, L.B., *Gmelin Handbook of Inorganic Chemistry, Boron Compounds Volume3-1*. 8 ed, ed. K.-C. Bushbeck. Vol. 3-1. 1987, Berlin: Springer-Verlag.
5. JANSEN, L.H., *BORON, ELEMENTAL,* in *Kirk-Othmer Encyclopedia of Chemical Technology*2001. p. 132-138.
6. Mikhailov, B.M., *THE CHEMISTRY OF DIBORANE.* RUSSIAN CHEMICAL REVIEWS, 1962. **31**(4).
7. Shriver, D., *Inorganic chemistry*1999, Oxford: Oxford University Press.
8. Karl Beeker, M.K.D., *Gmelin Handbuch der Anorganishen Chemie, Bor-Halogen-Verbindungen*, ed. K. Niedenzu1978, Berlin: Springer-Verlag.
9. Lawrence Barton, T.O., *Gmelin Handbook of Inorganic and Organometallic Chemistry, Boron Compounds Volume 4-1a*. 8 ed, ed. J. Faust. Vol. 4-1a. 1994, Berlin: Springer-Verlag.
10. Vladimir V. Volkov, K.G.M., *Mechanochemical reactions in the chemistry of boranes.* Inorganica Chimica Acta, 1999. **289**: p. 51–57.
11. Vladimir V. Volkov, K.G.M., *Mechanochemical Technology of Borane Compounds and Their Applications.* Chemistry for Sustainable Development, 2002. **10**: p. 221-233.

12. Eun Jeon, Y.C., *Mechanochemical synthesis and thermal decomposition of zinc borohydride.* Journal of Alloys and Compounds, 2006. **422**: p. 273–275.
13. Barbara Albert, H.H., *Boron: Elementary Challenge for Experimenters and Theoreticians.* Angew. Chem. Int. Ed., 2009. **48**: p. 8640 – 8668.
14. BALL, P., *Why is boron so hard?* Nature Materials, 2010. **9**.
15. Matthew Davidson, A.K.H., Todd B. Marder, Ken Wade, *Contemporary Boron Chemistry*2000, Cambridge: The Royal Society of Chemistry. 558.
16. Luis Bolaños a, Krystyna Lukaszewski b, Ildefonso Bonilla a, Dale Blevins, *Why boron?* 2004. Plant Physiology and Biochemistry(42): p. 907–912.
17. A. R. Oganov, V.L.S., *Boron: a Hunt for Superhard Polymorphs.* Journal of Superhard Materials, 2009. **31**(5): p. 285–291.
18. HELVACI, C., *Bor mineralerinin işletme, zenginleştirme ve pazarlama sorunları*, 2006, Dokuz Eylül Üniversitesi Mühendislik Fakültesi Jeoloji Mühendisliği Bölümü: İzmir.
19. Woods, W.G., *An Introduction to Boron: History, Sources, Uses, and Chemistry*, 2000, Office of Environmental Health and Safety, University of California: Riverside, California.
20. Report, R.I., *Boron: global industry markets & outlook*, 2010, Roskill: London.
21. Salih Ugur BAYÇA, K.K., Turan BATAR, *Bor mineral ve bilesiklerinin endüstride baslıca kullanım alanları*, 2003, Dokuz Eylül Üniversitesi, Maden Mühendisligi Bölümü: İzmir.
22. TAVMAN, A., *BOR ESASLI YAKIT HÜCRESİ VE BATARYALAR.* Mühendislik ve Fen Bilimleri Dergisi Sigma, 2004. **2004-2**: p. 40-45.
23. Uslu, T. *BOR MADENİNİN ENERJİ KAYNAĞI OLARAK KULLANILMASI*. in *TMMOB TÜRKİYE VI. ENERJİ SEMPOZYUMU - KÜRESEL ENERJİ POLİTİKALARI VE TÜRKİYE GERÇEĞİ*. 2008.

24. Ş G. ÖZKAN, H.Ç., S. DELİCE, M. DOĞAN. *Bor Minerallerinin Özellikleri ve Madenciliği*. in *2 Endüstriyel Hammaddeler Sempozyumu*. 1997. izmir, Türkiye.
25. Ataman, O.Y., *Bor, Analitik Kimya ve İnsan Sağlığı*, METU, Editor 2005.
26. Acarkan, N., *Boron Products and Their Uses*, 2001, İTÜ. Maden Fakültesi, Cevher ve Kömür Hazırlama Anabilim Dalı: İstanbul.
27. GmbH, H.C.S., *Boron – from eye drops to rocket propellants*, 2001, H.C. Starck GmbH.
28. Brian Van Devener, J.P.L.P., Joseph Jankovich, and Scott L. Anderson, *Air-stable, unoxidized, hydrocarbon dispersible boron nanoparticles.* Journal of materials research, 2009. **24**(11): p. 3462-3464.
29. Brian Van Devener, J.P.L.P., Joseph Jankovich, and Scott L. Anderson, *Oxide-Free, Catalyst-Coated, Fuel-Soluble, Air-Stable Boron Nanopowder as Combined Combustion Catalyst and High Energy Density Fuel.* Energy and Fuels, 2009. **10**.
30. Moissan, H., Ann. Chim. Phys, 1895. **6**: p. 296-304.
31. Tadashi Ogitsu, F.G., John Reed, Yukitoshi Motome, Eric Schwegler, and Giulia Galli, *Imperfect Crystal and Unusual Semiconductor: Boron, a Frustrated Element.* J. Am. Chem. Soc., 2009. **131**(5): p. 1903-1909.
32. JR., R.H.W., *REFRACTORY BORON COMPOUNDS*, in *Kirk-Othmer Encyclopedia of Chemical Technology*2000.
33. Artem R. Oganov, J.C., Carlo Gatti, Yanzhang Ma, Yanming Ma, Colin W. Glass, Zhenxian Liu,Tony Yu, Oleksandr O. Kurakevych & Vladimir L. Solozhenko, *Ionic high-pressure form of elemental boron.* Nature, 2009. **457**: p. 863-867.
34. Lipscomb, W.N., *Three-Center Bonds in Electron-Deficient Compounds.* ACCOUNTS OF CHEMICAL RESEARCH, 1973. **6**(8).
35. Wang, L., *ELECTRONIC STRUCTURE OF ELEMENTAL BORON*, in *Physics*2010, University of Missouri: Kansas.

36. Volker Adasch, K.-U.H., Thilo Ludwig, Natascha Vojteer, Harald Hillebrecht, *Synthesis, crystal growth and structure of Mg containing b-rhombohedral boron: MgB17.4.* Journal of Solid State Chemistry, 2006. **179**: p. 2900–2907.
37. Herve´ Hubert, B.D., Laurence A. J. Garvie, Michael O'Keeffe, Peter R. Buseck,William T. Petuskey, Paul F. McMillan, *Icosahedral packing of B12 icosahedra in boron suboxide (B6O).* Nature, 1998. **391**: p. 376-378.
38. Vitalij K. Pecharsky, P.Y.Z., *Fundamentals of Powder Diffraction and Structural Characterization of Materials*2005, New York: Springer.
39. Masayoshi Kobayashi, I.H., and Michio Takami, *Fundamental Structure of Amorphous Boron.* JOURNAL OF SOLID STATE CHEMISTRY, 1997. **133**: p. 211Ð214.
40. SCHUBERT, D.M., *BORON HYDRIDES, HETEROBORANES, AND THEIR METALLA DERIVATIVES (COMMERCIAL ASPECTS)*, in *Kirk-Othmer Encyclopedia of Chemical Technology*2001. p. 169-232.
41. Brown, R.N.S.a.P.H., *Boron Determination—A Review of Analytical Methods.* MICROCHEMICAL JOURNAL, 1997. **56**: p. 285–304.
42. Laszlo, P., *A Diborane Story.* Angew. Chem. Int. Ed., 2000. **39**(12).
43. LANE, C.F., *Reduction of Organic Compounds with Diborane*, 1975, Aldrich-Boranes, Inc: Milwaukee, Wisconsin.
44. H. I. SCHLESINGER, H.C.B., *New Developments in the Chemistry of Diborane and the Borohydrides*, 1952, GEORGE HERBERT JONES LABORATORY: Chicago.
45. H. I. SCHLESINGER, H.C.B., *Reactions of Diborane with Alkali Metal Hydrides and Their Addition Compounds. New Syntheses of Borohydrides. Sodium and Potassium Borohydrides*, 1952, GEORGE HERBERT JONES LABORATORY: Chicago.

46. Joyce Barrett, C.L., *Guide to Safe Handling of Compressed Gases*1982, New York: Matheson Gas Products.
47. MULLIKEN, R.S., *THE STRUCTURE OF DIBORANE AND RELATED MOLECULES*, 1947, Ryerson Physical Laboratory: Illinois.
48. HEDBERG, K., *A Reinvestigation of the Structures of Diborane and Ethane by Electron Diffraction*, 1950, GATES AND CRELLIN LABORATORIES OF CHEMlSTRY: California.
49. Harrison, W.A., *Theory of the two-center bond.* PHYSICAL REVIEW B, 1983. **27**(6).
50. Ohwada, K.L.a.T., *Three-Center, Two-Electron Systems. Origin of the Tilting of Their Substituents.* JACS, 1996. **118**(31).
51. Vicenzo Barone, L.O., *Density Functional Study of Diborane, Dialane, and Digallane.* J. Phys. Chem. , 1994. **98**: p. 13185-13188.
52. Thomas Onak, L.B., *Gmelin Handbook of Inorganic Chemistry*. Boron Compounds 3rd supplement, ed. K.C. Buschbeck. Vol. 1. 1987, Berlin: Springer - Verlag.
53. Lawrence Barton, T.O., Jürgen Faust, *Gmelin Handbook of Inorganic and Organometallic Chemistry*. Boron Compounds 4th supplement, ed. K.N. Jürgen Faust. Vol. 1a. 1994, Berlin: Springer - Verlag.
54. Eberhard Amberger, W.S., *Gmelin Handbook of Inorganic Chemistry*. Boron Supplement ed. K.C. Buschbeck. Vol. 2. 1981, Berlin: Springer - Verlag.
55. Vladimir V. Volkov, K.G.M., *Mechanochemical Technology of Borane Compounds and Their Application.* Chemistry for sustainable development, 2002. **10**: p. 221-233.
56. K. Miwa, N.O., S. Towata, Y. Nakamori, *Correlation between thermodynamical stabilities of metal borohydrides and cation electronegativities: First principles calculations and experiments.* Physical Review B, 2006. **74**(045126).

57. McKee, M.L., *Ab Initio Study of Diborane Hydrolysis.* J. Phys. Chem, 1996. **100**(10): p. 8261-8267.
58. STUARRT . Gunn, L.G.G., *THE HEATS OF HYDROLYSIS OF DIBORANE AND BORON TRICHLORIDE*, 1959, Lawrence Radiation Laboratory: Livermore, California.
59. Moldebuck, E., *US Patent 2658815, Preperation of diborane*, G.E. Company, Editor 1953.
60. Bronaugh, H., *US Patent 2967761, Process of preparing diborane*, T.C. Company, Editor 1961.
61. Smith, C., *US Patent 2983582, Production of diborane*, M.C. Company, Editor 1961.
62. Dean, L., *US Patent 3024091 Diborane Manufacture*, D.C. Company, Editor 1962.
63. Schultz, R.D., *US Patent 3,069,237 Method for the preperation of diborane*, A.-G. Corporation, Editor 1962: USA.
64. SHAPIRO, H.G.W.A.I., *Diborane from the Sodium Borohydride-Sulfuric Acid Reaction.* 1959.
65. M.Y.A. Mollah, R.S., J. Patscheider, S. Promreuk , D.L. Cocke, *Plasma chemistry as a tool for green chemistry, environmental analysis and waste management.* Journal of Hazardous Materials B, 2000. **79**: p. 301–320.
66. Jitai Niu, W.G., Mianhuan Guo, Shixiong Lu, *Plasma application in thermal processing of materials.* Vacuum, 2002. **65**: p. 263–266.
67. Annemie Bogaertsa, E.N., Renaat Gijbelsa, Joost van der Mullen, *Gas discharge plasmas and their applications.* Spectrochimica Acta Part B, 2002. **57**: p. 609-658.
68. Fridman, A., *Plasma Chemistry*2008, Cambridge: Cambridge University Press.
69. Mozetic, M., *Discharge cleaning with hydrogen plasma.* Vacuum, 2001. **61**(367-371).

70. Fridman, A., *Plasma Chemistry*2008, New YOrk: Cambridge University Press. 1022.
71. M.Y.A. Mollah, R.S., J. Patscheider,S. Promreuk b, D.L. Cocke, *Plasma chemistry as a tool for green chemistry, environmental analysis and waste management.* Journal of Hazardous Materials, 2000. **B79**: p. 301-320.
72. H.M. Kingston, S.J.H., *Microwave Enhanced Chemistry*1997, Washington: ACS.
73. Grill, A., *Cold Plasma in Materials Fabrication*, ed. W. Perkins1994, New York: IEEE Press. 256.
74. Annemie Bogaerts, E.N., Renaat Gijbels, Joost van der Mullen, *Gas discharge plasmas and their applications.* Spectrochimica Acta Part B, 2002. **57**: p. 609-658.
75. G. Bonizzoni, E.V., *Plasma physics and technology; industrial applications.* Vacuum, 2002. **64**: p. 327-336.
76. Michel Moisan, J.P., *Microwave Excited Plasmas*. Plasma Technology, ed. L. Holland. Vol. 4. 1992, Amsterdam: Elsevier. 518.
77. Kasap, S., *Principles of Electronic Materials and Devices*2006, Boston: McGraw Hill.
78. Mozetic, M., *Discharge cleaning with hydrogen plasma.* Vacuum, 2001. **61**: p. 367-371.
79. S.R. Wylie, A.I.A.-S.a., J. Lucas, R.A. Stuart, *An atmospheric microwave plasma jet for ceramic material processing.* Journal of Materials Processing Technology 2004. **153**: p. 288-293.
80. Glossop, D.C.L.a.M., *The SLAN - A New Microwave Plasma Source.* Microelectronics Journal, 2003. **28**(3).
81. M. Balat-Pichelin a, L. Bedra a, O. Gerasimova a, P. Boubert, *Recombination of atomic oxygen on a-Al2O3 at high temperature under air microwave-induced plasma.* Chemical Physics, 2007. **340**: p. 217–226.

82. http://en.wikipedia.org/wiki/Induction_furnace

83. LECO TCH600 User's Manual, LECO Corporation 2011

84. Woollins, J. D. (2006). Inorganic experiments. Weinheim, Wiley-VCH.

85. http://chemdata.nist.gov/

86. Mark T. Swihart, Vapor-phase synthesis of nanoparticles, Current Opinion in Colloid and Interface Science 8 (2003) 127–133

87. F. Einar Kruis, Heinz Fissan and Aaron Peled, SYNTHESIS OF NANOPARTICLES IN THE GAS PHASE FOR ELECTRONIC, OPTICAL AND MAGNETIC APPLICATIONS - A REVIEW, *J. Aerosol Sci*. Vol. 29 (1998), No. 5/6, pp. 511-535

88. http://www.mksinst.com/docs/ur/MFCGasCorrection.aspx

89. http://en.wikipedia.org/wiki/Balmer_series

90. S Darwiche, M Nikravech, Optical emission spectroscopic investigation of hydrogen plasma used for modification of electrical properties of multi-crystalline silicon, J. Phys. D: Appl. Phys. 40 (2007) 1030–1036

91. Carl Yaws, Matheson Gas Data Book, 7th Edition, McGraw Hill Professionals, 2001

92. K Vinod, R G Abhilash Kumar and U Syamaprasad, Prospects for MgB_2 superconductors for magnet application, Supercond. Sci. Technol. 20 (2007) R1–R13

93. Paul C. Canfield, Magnesium Diboride: Better Late than never, Physics Today, March 2003

94. Cristina Buzea, Review of the superconducting properties of MgB2, Supercond. Sci. Technol. 14 (2001) R115–R146

95. J. H. Kim, S. Zhou, M. S. Hossain, Carbohydrate doping to enhance electromagnetic properties of MgB_2 superconductors, Appl. Phys. Lett. 89, 142505 (2006)

96. M A Susner, Y Yang, M D Sumption, E W Collings, M A Rindfleisch, M J Tomsic and J V Marzik, Enhanced critical fields and superconducting properties of pre-doped B powder-type MgB2 strands, Supercond. Sci. Technol. 24 (2011) 012001 (5pp)

97. J. V. Marzik, R. C. Lewis, M. R. Nickles, D. K. Finnemore, J. Yue, PLASMA SYNTHESIZED BORON NANOSIZED POWDER FOR MgB2 WIRES, AIP Conf. Proc. 1219, 295 (2010)

98. http://en.wikipedia.org/wiki/File:Diborane-2D.png

99. Findit - Visualizer Program 2011 - Diborane 3D Sketch

100. www.plasmas.org/E-4thstate.jpg

101. HC Starck Materials Pamphlet

VITA

Selçuk Acar was born in Balıkesir, Turkey, in 1982. He graduated from Balıkesir Sırrı Yırcalı Anatolian High School in 2001. He received his B.S. degree in Chemical Engineering from Yıldız Technical University, İstanbul, in 2005. The same year, he started his graduate studies in the program of Materials Science and Engineering at Koç University. His research interests are hydrogen storage materials, renewable and sustainable energy systems and boron related technologies.